TECHNISCHE UNIVERSITÄT
ILMENAU

Analyse und Synthese von Konzepten für hybride leistungselektronische Erdschlusskompensatoren für Mittelspannungsnetze

Dissertation zur Erlangung des akademischen Grades
Doktor-Ingenieur (Dr.-Ing.)

vorgelegt der Fakultät für Elektrotechnik und Informationstechnik
der Technischen Universität Ilmenau

von M.Sc. Pavel Smirnov

1. Gutachter: PD Dr.-Ing. habil. Thomas Ellinger
2. Gutachter: Univ.-Prof. Dr.-Ing. Dirk Westermann
3. Gutachter: Univ.-Prof. Dr.-Ing. habil. Sergey Kharitonov

Tag der Einreichung: 09.04.2019
Tag der wissenschaftlichen Aussprache: 05.06.2020

urn:nbn:de:gbv:ilm1-2020000510

Erklärung

Ich versichere, dass ich die vorliegende Arbeit ohne unzulässige Hilfe Dritter und ohne Benutzung anderer als der angegebenen Hilfsmittel angefertigt habe. Die aus anderen Quellen direkt oder indirekt übernommenen Daten und Konzepte sind unter Angabe der Quelle gekennzeichnet.

Bei der Auswahl und Auswertung folgenden Materials haben mir die nachstehend aufgeführten Personen in der jeweils beschriebenen Weise unentgeltlich geholfen:

1. Dr.-Ing. habil. Thomas Ellinger – sprachliche Korrektur der Formulierungen und Ausdrücke.
2. Prof. Sergey Kharitinov – universitäre Betreuung in Russland.

Weitere Personen waren an der inhaltlich-materiellen Erstellung der vorliegenden Arbeit nicht beteiligt. Insbesondere habe ich hierfür nicht die entgeltliche Hilfe von Vermittlungs- bzw. Beratungsdiensten (Promotionsberater oder anderer Personen) in Anspruch genommen. Niemand hat von mir unmittelbar oder mittelbar geldwerte Leistungen für Arbeiten enthalten, die im Zusammenhang mit dem Inhalt der vorgelegten Dissertation stehen.

Die Arbeit wurde bisher weder im In- noch im Ausland in gleicher oder ähnlicher Form einer Prüfungsbehörde vorgelegt.

Ich bin darauf hingewiesen worden, dass die Unrichtigkeit der vorstehenden Erklärung als Täuschungsversuch bewertet wird und gemäß §7 Abs. 10 der Promotionsordnung den Abbruch des Promotionsverfahrens zur Folge hat.

Ilmenau, den

_____

Pavel Smirnov

Vorwort

Die vorliegende Arbeit entstand während meiner Tätigkeit als wissenschaftlichen Mitarbeiter an der Staatlichen Technische Universität Novosibirsk ab 06/2015 bis 07/2017 und als Promotionsstudent an der Technischen Universität Ilmenau seit 10/2017, in dem Fachgebiet „Leistungselektronik und Steuerungen in der Elektroenergietechnik “ der Fakultät für Elektrotechnik und Informationstechnik.

Hiermit möchte ich mich insbesondere bei all denjenigen bedanken, die mich fachlich und privat beim Gelingen der Arbeit unterstützt haben.

Mein besonderer Dank gilt natürlich Prof. Sergey Kharitonov, dem Leiter des Fachgebiets der Staatlichen Technische Universität Novosibirsk, für die universitäre Betreuung, sein Interesse am Fortgang der Arbeit und die wohlwollende Unterstützung.

Besonders möchte ich mich bei meinem Doktorvater Dr. Thomas Ellinger bedanken, für die universitäre Betreuung an der Technischen Universität Ilmenau, für die anregenden Diskussionen in entspannter Atmosphäre und die Unterstützung während meines Aufenthalts in Ilmenau.

Bei allen Freunden, die ich in der Universitätsstadt kennengelernt habe, möchte ich mich für ihre Unterstützung recht herzlich bedanken. Nicht zuletzt gilt mein besonderer Dank meinen Eltern und meiner Familie, die mich an meinen Promotionsanliegen ständig unterstützt haben.

Ilmenau, April 2019

Kurzfassung

In den vergangenen Jahren ist das Energieübertragungssystem mit der Zunahme der Produktion angewachsen. Jedes Jahr werden daher neue Übertragungsnetze in Betrieb genommen und die bereits bestehenden Übertragungsnetzwerke werden erweitert. In der Vergangenheit wurde der Strom in großen Kraftwerken zentral erzeugt und vom Hochspannungsnetz übertragen. Jetzt werden jedoch zunehmend auch große Mengen der elektrischen Energie vom Nieder- und Mittelspannungsnetz übertragen. Die Anlagen zur Nutzung der erneuerbaren Energien sind grundsätzlich auf der Mittelspannungseben angeschlossen. Die modernen Netze müssen somit nicht nur mit einer schwankenden Stromerzeugung sondern auch mit verschiedenen Fehlern umgehen können. Mit wachsender Netzausdehnung steigt auch die Wahrscheinlichkeit für einen Fehlereintritt. Folglich müssen neue Verfahren entwickelt werden, um die Zuverlässigkeit und Stabilität der Netze auch im Fehlermodus zu verbessern.

Derzeit werden oft kompensierte Mittelspannungsnetze zum Schutz vor einphasigen Erdfehlern verwendet, wobei der Neutralleiter entweder über eine Drossel oder einen Widerstand mit der Erde verbunden ist. Damit kann der Fehlerstrom begrenzt und die Netze im Fehlerfall weiter betrieben werden. Gleichwohl haben auch die modernen passiven Kompensationsanlagen Probleme mit der Abstimmgenauigkeit, den Abmessungen sowie aufgrund der Komplexität des Antriebssystems. Moderne leistungselektronisch basierte Kompensationsanlagen werden zunehmend in MS-Netzen eingesetzt, um die Blindleistung (STATCOMs) zu kompensieren und nichtlineare Lastströme zu filtern. Sie können außerdem verwendet werden, um den Fehlerstrom zu kompensieren und eine optimale Ausnutzung der Übertragungskapazitäten der Leitungen zu ermöglichen. Da diese innovativen leistungselektronischen Kompensationsanlagen bei relativ hohen Frequenzen arbeiten, können außerdem wertvolle Materialien wie Kupfer und Stahl, die für die 50-Hz-Drosseln notwendig sind, eingespart werden.

Diese Arbeit widmet sich der Entwicklung eines Hochleistungs-Mittelspannungswechselrichters sowie dessen zur Kompensation notwendigen Steuerungssystems. Der Kompensator dient dabei zur Eliminierung des einpoligen Erdfehlerstromes (Grund- und Oberschwingungskomponenten) und kann daher im Übertragungssystem als Äquivalent der Petersonspule oder des Widerstands betrachtet werden. Der auf der Hilbert-Transformation basierende Steueralgorithmus wird ebenfalls erörtert.

Kapitel 1 enthält Informationen zu vorhandenen Erdungsmethoden und Kompensationstechniken. Darüber hinaus werden ihre Vor- und Nachteile diskutiert. Es werden verschiedene Konfigurationen für Spannungswechselrichter untersucht, die für Anwendungen bis in Bereiche der höheren Mittelspannung geeignet sind.

In Kapitel 2 wird die vereinfachte Ersatzschaltung eines Netzwerks betrachtet. Anschließend werden die analytischen Gleichungen in $\alpha\beta$-Koordinaten für die verschiedenen

Moden abgeleitet. Basierend auf diesen Erkenntnissen wird die symmetrische Komponentenmethode zur Steuerung des Umrichters vorgeschlagen. Eine verallgemeinerte Methode der symmetrischen Komponenten, die auf der Hilbert-Transformation basiert, wird vorgestellt. Darüber hinaus sind die Algorithmen zur Hilbert-Filtersynthese angegeben.

Kapitel 3 verwendet eine Wechselrichter-Ersatzschaltung, um die Regelungsstruktur zu entwickeln und deren Parameter zu bestimmen. Ein Betriebsartenregler wird entworfen, um den Fehlerbeginn und das Fehlerende (Löschen oder Selbstlöschen) detektieren zu können. Darüber hinaus wird ein Algorithmus zur Bestimmung der Erdkapazität des Netzes vorgeschlagen, um den notwendigen Erdfehlerstromsollwert zu bestimmen. Zum Schluss werden komplexere Verteilnetzstrukturen betrachtet. Die Struktur der Oberschwingungskomponentenregler wird abgeleitet und deren Besonderheiten bezüglich der betrachteten Netzkonfiguration diskutiert.

Die Simulationsergebnisse sind in Kapitel 4 zusammengefasst. Die Simulation erfolgte unter Nutzung des Programmsystems Matlab/Simulink. Durch die Simulationsergebnisse für die jeweiligen Netzwerkmodi konnten die zuvor abgeleiteten Algorithmen verifiziert werden.

Abstract

In the last years, the power generation systems have increased constantly with the increase in production. Every year new distribution networks are put into operation. The already existing networks are expanded. Moreover, in the past the power had been generated centrally in large power plants and transmitted by the high-voltage transmission grid, now vast amounts of the electric energy are handled by the low- and medium-voltage grid. The renewable energy sources are basically united in medium voltage grids. The modern grids has to be able to handle the fluctuating power generation and various sort of faults. With the growing grids the fault chance increases. Consequently, the new methods have to be developed to improve the reliability and stability of the grids in fault modes.

Currently, to protect from one-phase ground faults the compensated networks are used with the neutral connected with the ground through the reactor or resistor. It allows to limit the fault current and the networks be able to be operated. Nevertheless, the modern compensation devices have the problems with the tuning accuracy, dimensions and the complexity due to the drive system. The modern power electronic devices are used in MV grids to compensate the reactive power (STATCOMs) and to filter the non-linear loads currents. They could be used to compensate the fault current and to allow the optimal utilization of lines as well. Moreover, since these converters operate at relatively high frequencies, valuable materials like copper and steal, used for 50 Hz reactors, can be saved.

This work is dedicated to the development of a high-power medium-voltage power converter and its control system. This converter is used to compensate the one-phase ground fault current (main and high frequency components) and therefore is considered as the equivalent of the reactor or resistor in the classical system. The control algorithm based on the Hilbert transformation is proposed as well.

Chapter 1 gives the information about existing grounding methods and compensation techniques. Moreover, their advantages and disadvantages are discussed. Different dc-ac converter configurations suitable for high-power medium-voltage applications are considered.

In chapter 2, simplified equivalent circuit of a network is considered. The analytical equations in $\alpha\beta$-coordinates for the different modes are being obtained. Based on the findings, the symmetrical components method is proposed to control the converter. The generalized symmetrical components method based on the Hilbert transform is introduced. Moreover, the Hilbert filter synthesis techniques are given.

Chapter 3 examines the converter equivalent circuit to develop the control structure and to determine the controller parameters. The modes controller is introduced being able to define the fault start and the fault finish (extinguishing or self-extinguishing). Moreover, the network capacitance measure technique is proposed to determine the possible ground fault current value.

Finally, the complex distribution grids are considered. The high-frequency components controllers are introduced and compared in terms of grid configuration.

The simulation results are given in chapter 4. The simulations are carried out in Matlab Simulink. The simulation results in different network modes are examined to confirm the obtained algorithms.

Contents

CHAPTER 1. NEUTRAL GROUNDING OF POWER DISTRIBUTION SYSTEMS AND CAPACITIVE CURRENT COMPENSATION METHODS IN MEDIUM VOLTAGE NETWORKS.

This chapter gives the short overview of the existing alternating current (AC) systems neutral treatment techniques. The overview includes advantages and challenges of the methods concerning AC networks grounding. The motivation of the active converter medium voltage alternating current (MVAC) system grounding is given. The different converter topologies are considered.

This chapter closes with the aims and objectives of the thesis.

Neutral grounding classification

The method of a neutral-point treatment is not important during the normal operation of a grid. However, the neutral grounding methods have a wide effect on the system behavior in the fault modes. As well as a lot of technical and economical network features (short circuit capacity, surge and overvoltage protection, insulation types, protective relaying etc.) depend on the neutral grounding modes. The grounding modes directly affect the system behavior and the maximum levels of the earth-faults currents. Many papers and standards have discussed the grounding of electrical distribution systems [1, 2]. Currently the neutral grounding method of power systems can be classified as follows [3]:

- Solidly (effective) grounded system (Figure 1.1);
- Neutral ungrounded system (Figure 1.2);
- Arc-suppression coil neutral grounded system (Figure 1.3);
- Resistive neutral grounded system (Figure 1.4).

In the solidly grounded system all the transformers installed at substations belonging to the same rated voltage are solidly neutral grounded (Figure 1.1). Overhead transmission lines are usually solidly grounded. The high value one-phase ground fault (GF) current is the distinctive feature of the solid grounding. The GF current may exceed the 3-phase fault current in a solidly grounded system. Nevertheless, the high value fault current is cleared quickly by the relay protection devices. In Europa, AC distribution networks in excess of 110 kV are solidly grounded (high voltage alternating current (HVAC) networks), mainly because of the insulation costs rise. Almost all the medium voltage (2 – 35 kV) networks are operated as the neutral ungrounded systems with the three-phase connection of the feeders (Figure 1.2).

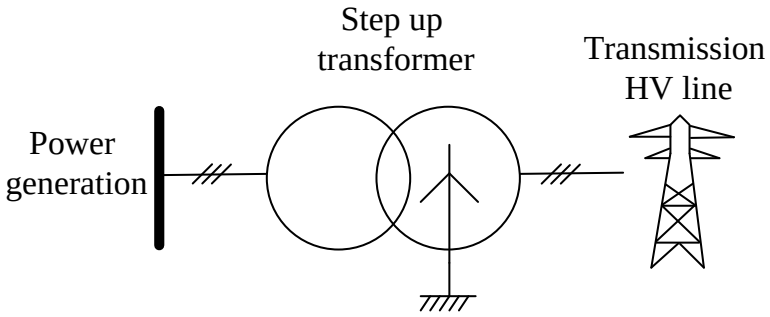

Figure 1.1 Solidly grounded system

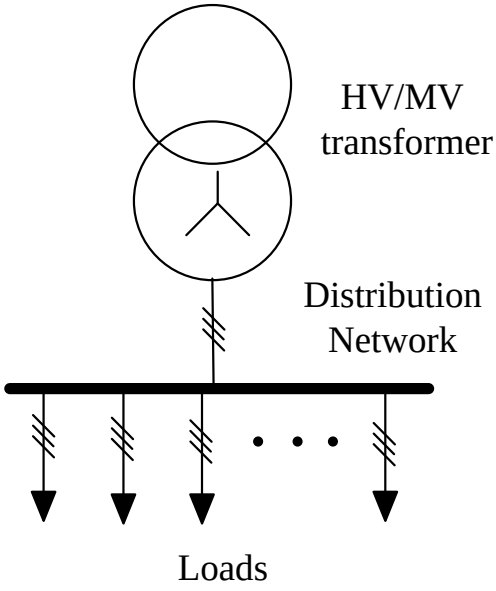

Figure 1.2 Neutral ungrounded system

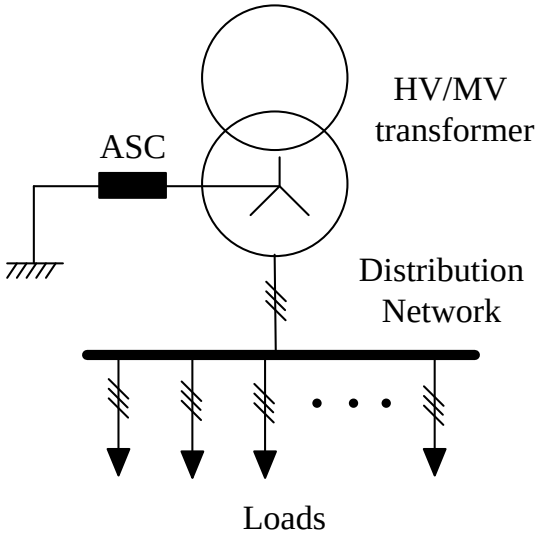

Figure 1.3 Arc suppression coil (ASC) neutral grounded system

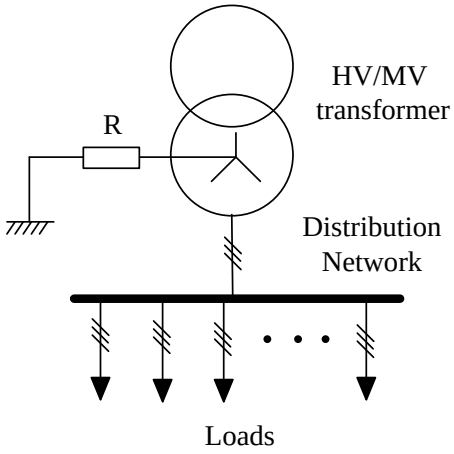

Figure 1.4 Resistor neutral grounded system

By far, distribution systems around the world have evolved into different forms. And different approaches in the system grounding are used. For example, in North America the four-wire multiground medium voltage systems predominate [4]. A phase and the neutral supply single-phase loads connected to the phase-to-ground voltage. Each load is supplied by the single-phase step-down transformer (Figure 1.5). Distribution overhead lines are divided into several circuits by the automated switches or reclosers. The recloser is the specialty distribution protective device which is capable of automatically reclosing and interrupting fault current [5, 6].

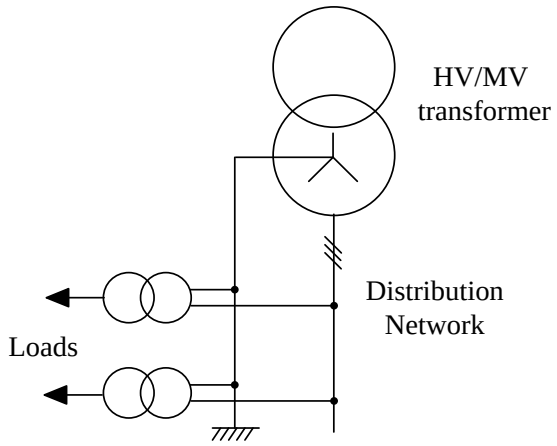

Figure 1.5 Four-wire multigrounded system

One-phase ground fault and neutral ungrounded system

The one-phase GF is the most frequent accident likely to take place in medium voltage systems. The relationship between fault causes and the fault type was surveyed for example in [7, 8] and is shown in Table 1.1.

Table 1.1

Fault	Percentage
One phase to neutral	63%
Phase to phase	11%
Two phase to neutral	2%
Three phase	2%
One phase on the ground	15%
Two phase on the ground	2%
Three phase on the ground	1%

This statistic cannot fully demonstrate the situation, but the predomination of the one-phase faults can be seen.

The intentional neutral grounding connections do not exist in the neutral ungrounded system. These networks have the advantage to be able to be operated with the sustained fault until the fault is cleared. The absence of the neutral connection results in low values of the one-phase GF current equal to the system capacitance current. It happens because there is no return path available for the earth fault current to flow. However, the current still flows from a faulted phase conductor to the ground through the phase-to-ground disturbed capacitance (Figure 1.6).

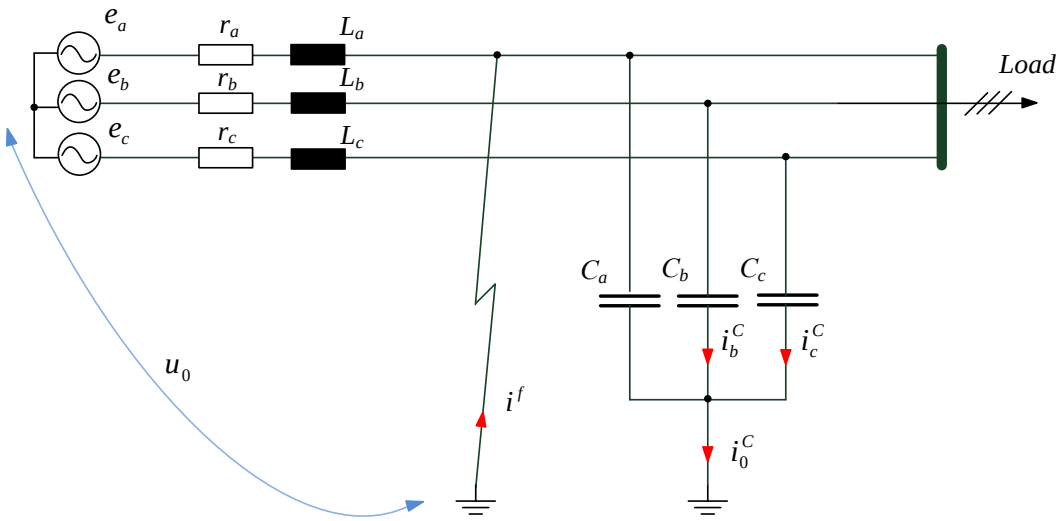

Figure 1.6 Equivalent circuit of the faulted isolated neutral system

When the one-phase GF occurs, the fault current mainly returns in the two healthy phases through the phase-to-ground capacitances. Nevertheless, three-phase load transformers are supplied by the line voltages and the GF does not affect the feeders. It can be seen in Figure 1.7 keeping the line voltages without any changes. The vector diagram in Figure 1.7 (a) is supposed without existence of the negative voltage sequence. Therefore, the faulted line can be operated in the presence of the earth-fault. However, the earth-fault has to be eliminated due to the following reasons:

- Whenever the GF occurs, the unfaulted phase voltages increase and become approximately $\sqrt{3}$ times nominal phase voltages. The decreasing of the unfaulted phase insulation could result the two-phase fault with more damage as well;

- There is a chance that line workers and public would be subjected to touch and step voltages with the GF current flowing through the pole;

- Sometimes the voltage of the faulted phase can fluctuate creating significant overvoltages due to the arcing GF [9, 10]. The arc is an electrical phenomenon in which the voltage of the faulted phase would have been fluctuating due to the capacitive charging current.

According to electrical installation rules (EIR) [11] 6 – 35 kV networks can be operated with the isolated neutral. However, there is the current threshold above which the network must be grounded (compensated) through a reactor or a resistor [12]. In Russian Federation the isolated neutral system must be equipped with the arc suppression coil or the resistor with level of the earth-fault current more than 10 A (RMS).

In Germany [13] the residual GF current should be less than 60 A (RMS).

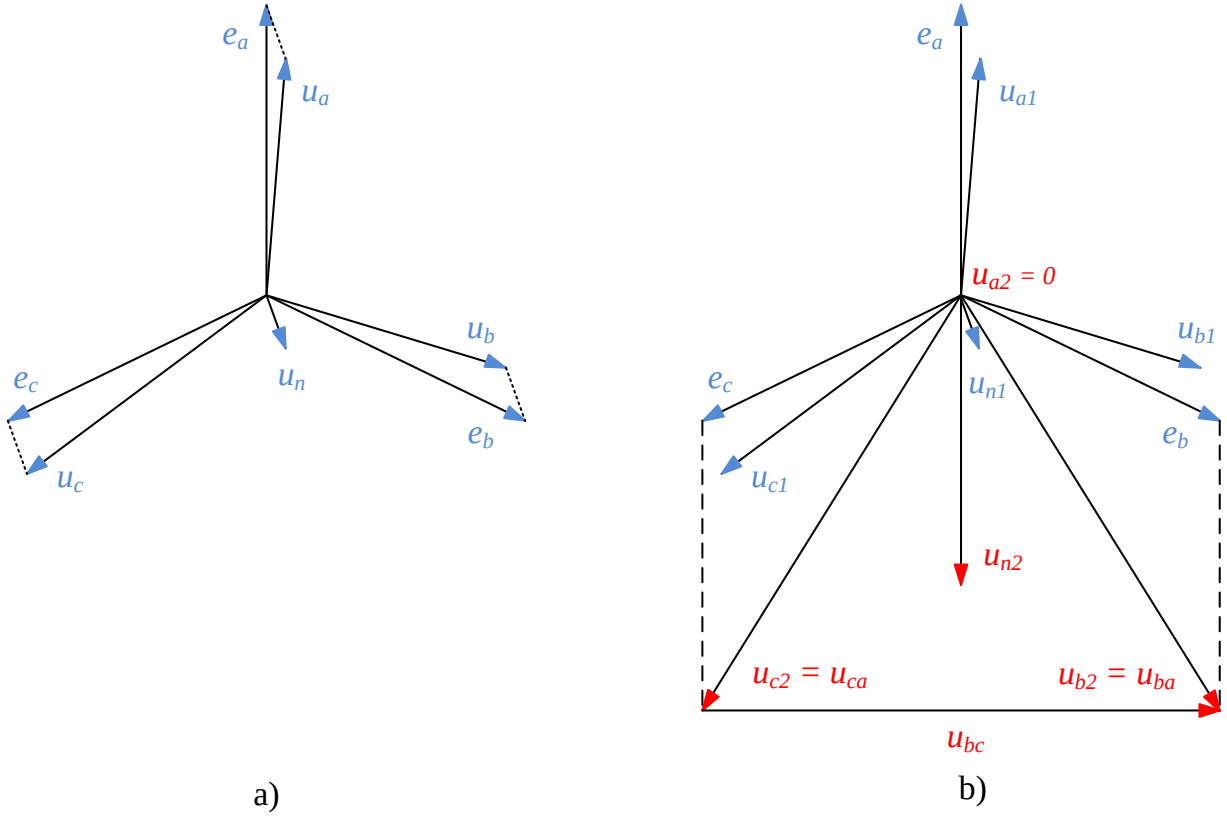

Figure 1.7 Vector diagram before (a) and after (b) the phase a one-phase GF

The existing of the high frequency components in the ground fault current is one of the important problems as well [14]. In [12] the ground fault current of the 10 kV substation was measured and the harmonic composition is shown in Figure 1.8.

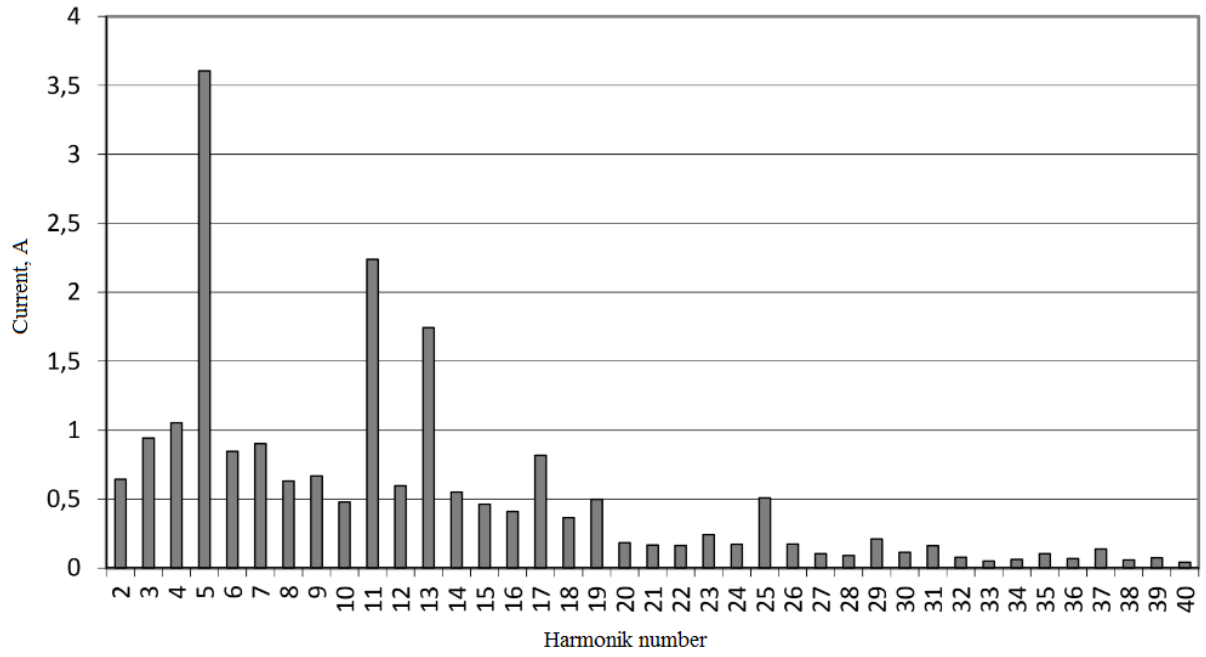

Figure 1.8 Effective ground fault current values for 10 kV substation

The high frequency components can be generated by the voltage sources or by nonlinear loads. In the Chapter 3 this case will be considered in details.

Thus, there are following neutral ungrounded system disadvantages:

- Overvoltages during ground fault transient process;
- The arcing faults likely to occur;
- Phase-to-ground insulation have to resist to the line voltages (or even higher voltages);
- Complexity to locate a fault;
- Dangerous for the general public and operational staff;
- Protective devices failure to operate.

Arc suppression coil neutral grounded system

In order to reduce the GF current the reactor connected between the substation transformer and the ground is used. The reactor was suggested in 1916 by Petersen [15] and currently is called arc suppression coil (ASC) or Petersen coil.

The reactor inductance can be adjusted to match closely the network phase-earth capacitance. Consequently, the result fault current is resistive and low in magnitude depending on the accuracy of the adjustment. But, during the arcing fault the voltages of the unfaulted phases can be even higher due to the departing from the ideal tuning. It can stress the insulation and convert the one-phase GF into phase-to-phase fault. Whenever the earth fault occurs, the earth fault current flowing through the fault place causes the line-to-neutral voltage across the ASC (Figure 1.9).

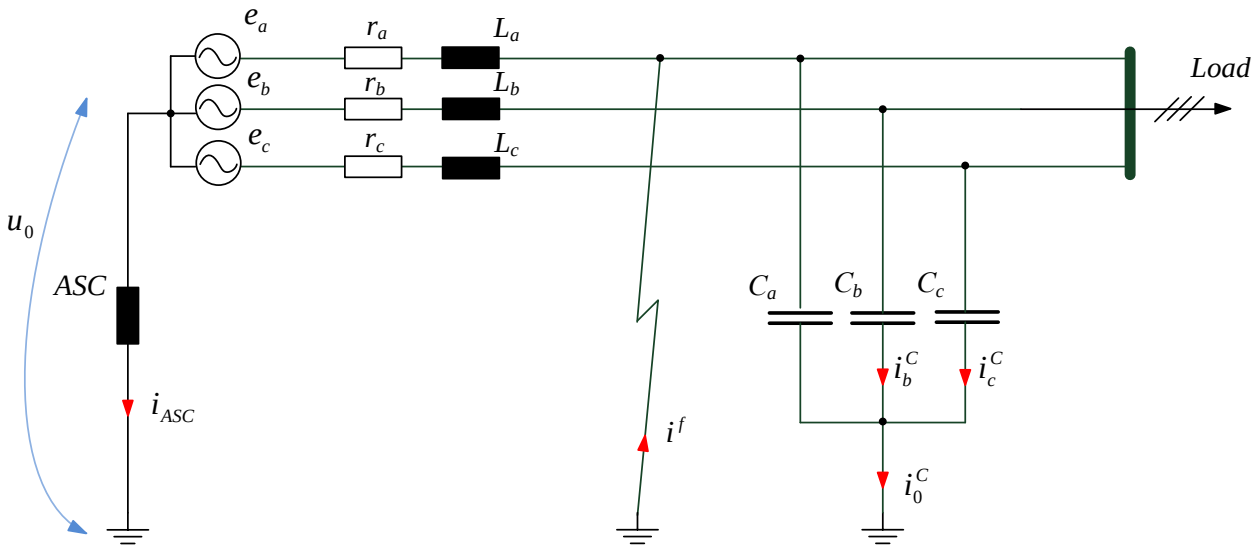

Figure 1.9 Equivalent circuit of an ASC grounded faulted system

This produces the lagging inductive (compensating) ASC current that flows from the reactor to the ground. At the same time the leading capacitive current flows from the two unfaulted lines through the capacitance to the ground and to the fault. The lagging current from the reactor and the leading current from the disturbed capacitance are 180° out of phase. By the properly reactor tuning, the inductive and the capacitive component can compensate each other, leaving only the small resistive current component [16]. Thus, with the sustained fault the network can operate until the fault can be cleared. If the ground fault is in the air, it may be self-extinguishing. The selection of the ASC impedance should be performed for example by the methods [17, 18]. At the same time the suppression of the arc can be possible by the ASC tuning within limits described in [19, 20]. Departing from the ideal tuning can cause the hazard overvoltages.

Nowadays, there are regulated and unregulated ASCs and they can be classified according to the following features:

1. Uncontrolled reactors.
2. Drive-controlled reactors.

Uncontrolled reactors have a fixed impedance (calculated by the standards) to decrease the ground fault current to an acceptable value. In fact it is inductance connected between the neutral and the ground.

Drive-controlled reactors can be tuned in resonance with the total system capacitance to eliminate the ground fault current. It can be done by the variation of the winding turns, the air gap adjustment or the magnetic flux adjustment.

There are some thyristor controlled coils [21] as well. In series with the coil the thyristor switch is connected controlling mean value of the coil current. Thyristor controlled coils overcome above drawbacks. However, they generate the low order harmonics. The thyristor commutation can result the network interference as well.

The following types of control principles are used [22]:

1. Artificial earth fault;
2. Residual neutral voltage analysis;
3. 50 Hz current injection;
4. Double frequency current injection.

The artificial earth fault method is based on the searching of the GF current minimum by the ASC adjusting. It leads to the compensation in case of the fault. But it is not used to control ASCs but only to check the quality of the control algorithm.

The next method supposes the system to have the natural asymmetry. However, the symmetrical system is likely not to generate the residual voltage. At the same time, when the system generates the residual voltage, the 50 Hz current injection method could probably lead to the wrong measurement result.

The double frequency current injection method does not have the disadvantages of the previous techniques. However, in ASC grounded systems it is supposed to have an additional equipment to generate the double frequency current. It will be discussed in the Chapter 3.2 applied to the active power converter.

There are following advantages of the ASC neutral grounded system:

- Ability of the continuous operation with the sustained fault;
- Low fault current in magnitude (resonance tuning);
- Self-extinguishing capability of the one-phase GF (only in overhead lines).

Despite the active using all types of ASCs in the modern medium voltage systems it still has the following drawbacks:

- Arc overvoltage possibility under departing from the ideal tuning;
- Transformation possibility into two-phase fault under departing from the ideal tuning;
- Large weight and dimensions;
- Precise mechanical drive system requirement;
- Inability to compensate high frequency components (the complex passive structures should be used).

Resistive neutral grounded system

The resistive neutral grounding method is wide used as well (Figure 1.10). It can be an alternative to the ASC neutral grounded system. It was also proposed by Petersen in 1916.

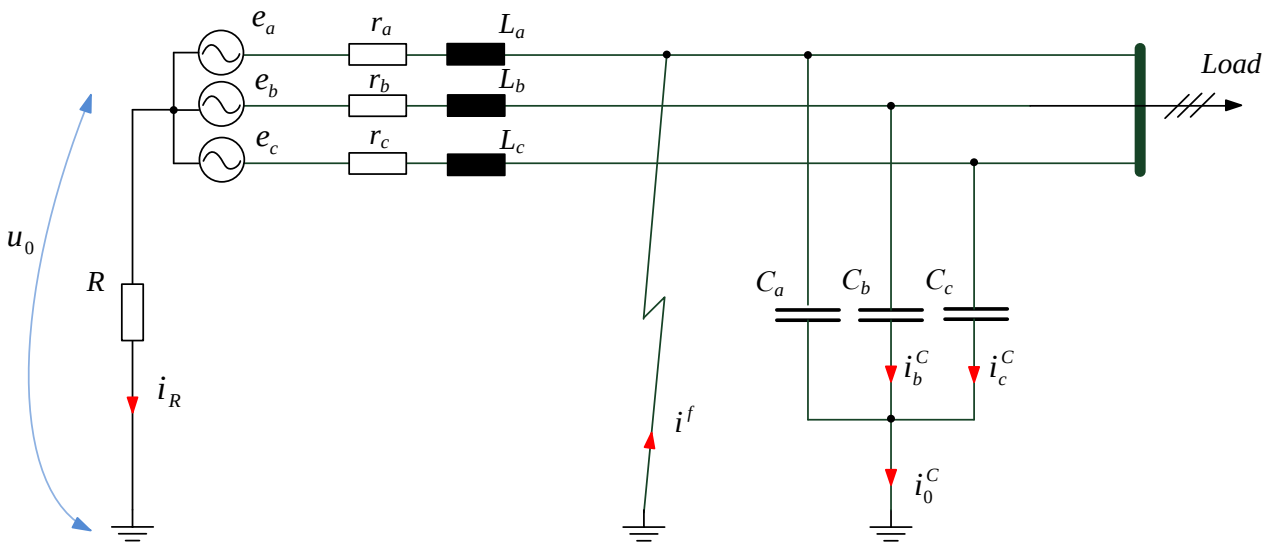

Figure 1.10 Equivalent circuit of a resistor grounded faulted system

According to [16] there are two neutral grounding methods through the resistance: the high resistance grounding and the low-resistance grounding. Although there are no recognized standards for the levels of the ground fault current that define these two classes, in practice there is the clear difference. The high-resistance-grounded system is designed to limit the GF current to the value that could be allowed to flow for an extended period of time, maintaining the service continuity. The transient voltages from the arcing GFs are also reduced. Usually, the GF current is limited to 10 A or less.

High-resistance grounding method has the following advantages:

- Transient overvoltage is decreased due to the ground fault current value restricting;
- Service continuity is maintained;
- Public safety.

However, there are following drawbacks:

- Electrical system growth restriction due to the finite resistance value;
- Necessity of the resistance thermal protection.

The low-resistance grounded system is designed to obtain the sufficient ground fault current for the selective relay operation. Typically the GF current is between 100 A and 1000 A. The low-resistance grounding has the advantage of contribution the direct and selective disconnection of the faulted circuit. It requires the GF current to be large enough to actuate the GF relay protection. The low-resistance grounding method has the following advantages:

- Direct and selective disconnection of a faulted circuit;
- Transient overvoltage decrease.

However, there are following drawbacks:

- The electrical system growth restriction due to the finite resistance value;
- Service continuity is not maintained;

- Necessity of the resistance thermal protection;
- Ground fault current value increase.

In some cases for the both classes the neutral point has to be provided by the special auxiliary transformers (star-interstar or zigzag).

Lately, many articles about the ASC with the parallel resistance grounding have been published [23, 24]. Authors point out the following advantages:

- Simultaneous capacitive current compensation with improving the decay rate of overvoltage;
- Increase the arc self-extinguish probability.

However, this grounding method is demand more thorough research and experiments. According to the articles [25 – 27] there are no advantages compared to the classic methods (ASC and resistance grounding).

The listed drawbacks showed that the issue about the grounding methods remains open. Currently, the continuous power and length growth of the networks can be observed. And more and more new resistors and arc suppression coils need to be installed. At the same time, the active power converters are more and more used in the distribution networks and feasible topologies for a wide variety of applications aroused in the last decades. A relatively young research field is the use of active power converters for the neutral grounding. Recently some publications about active converter grounding have been published e.g. [28 – 31]. Modern power electronic devices allow to be used in medium voltage networks to protect from GFs and to control the neutral grounding. In the GF mode such device is able to compensate the capacitive fault current by injecting the zero-sequence current.

Active power converter grounded system

As stated in the previous section, the active power converter grounding can be used as the alternative to the existing neutral treatment techniques. Furthermore, the active earth fault current compensator (AEFCC) has more advantages compared to the ASC or the resistor. It can be utilizable for different purposes. However, depending on the task the different features can be required. The following section presents the different converter topologies regarding the application purpose.

The converter topologies mainly differ in their functionality, galvanic isolation, voltage level and number of phases. The converter can complement the existing neutral grounding method as well.

The first topology depicted in Figure 1.11(a) represents the one-phase converter connected between the neutral and the ground. The converter can operate with the ASC in parallel as well (Figure 1.11 (b)). By controlling the neutral (zero) current, the proper ground fault current compensation is ensured. Regarding to the converter, any topology of multilevel ones can be

used. The applicability of this topology is limited by being able to control only zero sequence. The application with the step-up transformer is permitted to allow higher voltage levels.

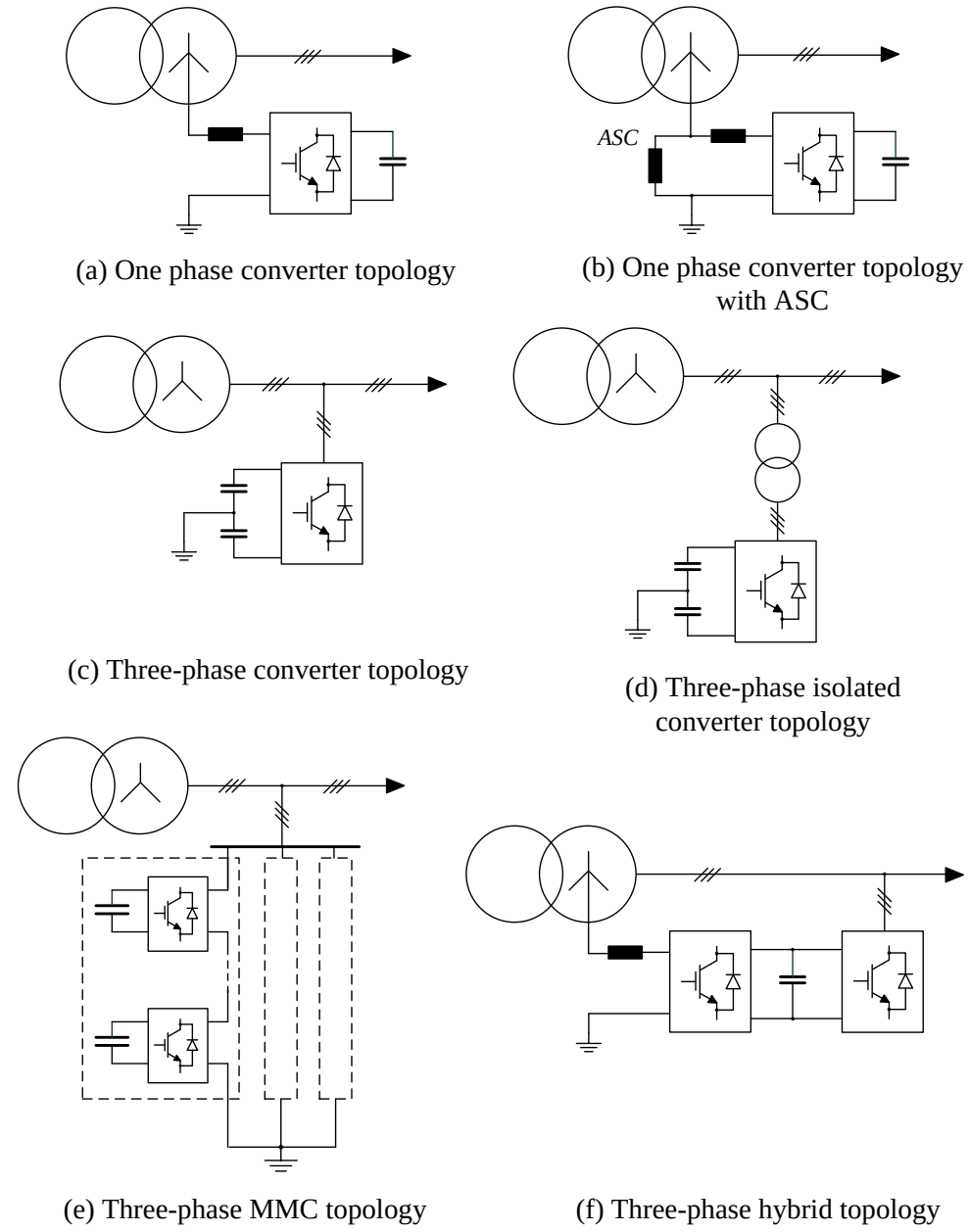

(a) One phase converter topology

(b) One phase converter topology with ASC

(c) Three-phase converter topology

(d) Three-phase isolated converter topology

(e) Three-phase MMC topology

(f) Three-phase hybrid topology

Figure 1.11 Power stage topologies

The three-phase topologies are depicted in Figure 1.11(c), (d), and (e). The three phase topologies expand the converter functionality. The GF current compensation is ensured as well by splitting DC capacitors to create the neutral. The 4-leg converter can be used but it has larger number of switching devices. Furthermore, the positive and negative sequences can be controlled. Thus, the converter acquires the features of the active power filter. For the proper GF current compensation the negative sequence control is required as well. It will be shown in the next chapters. Thus, there is one more drawback of the one-phase topology.

To achieve the required voltage level the additional step-up transformer should be used in some cases (Figure 1.11(d)). It should be noticed that the transformer has to be five-limbed to allow the zero sequence magnetic flux to flow. At this point of view the modular multilevel converter (MMC) structure (Figure 1.11(e)) has the advantage allowing very high voltage levels by the series connection of the bridge or half-bridge modules.

Regarding to the converter, any topology of multilevel ones can be used as well as four leg multilevel ones. The disadvantage is only the control range while using the converter as the ground fault compensator and the active power filter at the same time.

To avoid the disadvantage of the three phase topology the hybrid converter depicted in Figure 1.11(f) can be used. It consists of two converters with the common DC link. The one-phase converter is intended to control the zero current and to create the neutral connection. The second one has to control the negative sequence, to eliminate the high frequency components and to maintain the DC capacitor voltage.

The ability of the joint operation of the all topologies with the ASCs or grounding resistors is supposed.

Summarizing, the active power converter grounding has the following advantages:

- High accuracy;
- Hast response time compared to arc suppression coil;
- Decreasing weight and dimensions;
- Increasing efficiency;
- Autonomous operation capacity;
- Ground fault current value determination ability algorithmically without additional equipment;

This work focuses on the three-phase multilevel neutral-point clamped converter. This topology is universal for the all kind of networks. The proposed algorithms can be demonstrated to control zero and negative sequences.

Sections conclusions

1) The literature analysis has showed the current state of research. The comparison of grounding methods is performed as well as GF current compensation methods. The main advantages and drawbacks have been specified.

2) Despite widespread using there is still the scientific problem to provide the service continuity and the sustainable network operation. The existing grounding methods not in all cases are able to manage with the tasks.

3) The use of active power converter as the grounding device contributes significant improvement of the network operation whenever the fault occurs.

4) Power converter grounding device is not investigated enough to be used as the protective compensation device. The main problems to be solved to develop the AEFCC are presented in the aim and objectives of the thesis.

Aim and objectives of the thesis

The aim is to develop the AEFCC and its control system to be applied to compensate ground fault capacitive current and high frequency components. The control algorithm can be used in the already existing active filters or reactive compensators as an additional option.

Objectives of the thesis to be solved:

1) To perform the analytical review and to develop an average mathematical model of the AEFCC grounded network.

2) To develop the suitable control strategy for the proposed AEFCC to adjust independently the positive, the negative and the zero sequence current as well as high-frequency components.

3) To verify both the proposed grounding method and the control strategies by the simulation.

3) To perform the comparison of the obtained control strategies to be suitable to provide the required compensation and the adjustment quality. The various techniques are to be compared with respect to features, advantages, drawbacks.

4) To develop the algorithm to determine the ground fault current value, the ground fault presence, the ground fault self-extinguishing. The algorithm should be adjusted to every mode and to switch between them.

5) To select the suitable power converter topology to be able to operate with the medium voltage.

6) To simulate the selected power converter topology with the developed control algorithms to confirm the results obtained in every mode.

CHAPTER 2. MATHEMATICAL MODEL OF THE GRID

This chapter describes the mathematical model of the network in modal coordinates to realize the compensation principle. Based on the model, some transient processes with the converter are considered and the converter influence on the ground fault current value is investigated. Both the isolated neutral system and the ASC grounded neutral system are considered.

Furthermore, to design the control system two different techniques to decompose the system into symmetrical components are considered and compared.

2.1. Three phase coordinate model

The three-phase system can be represented as it is shown in Figure 2.1.1.

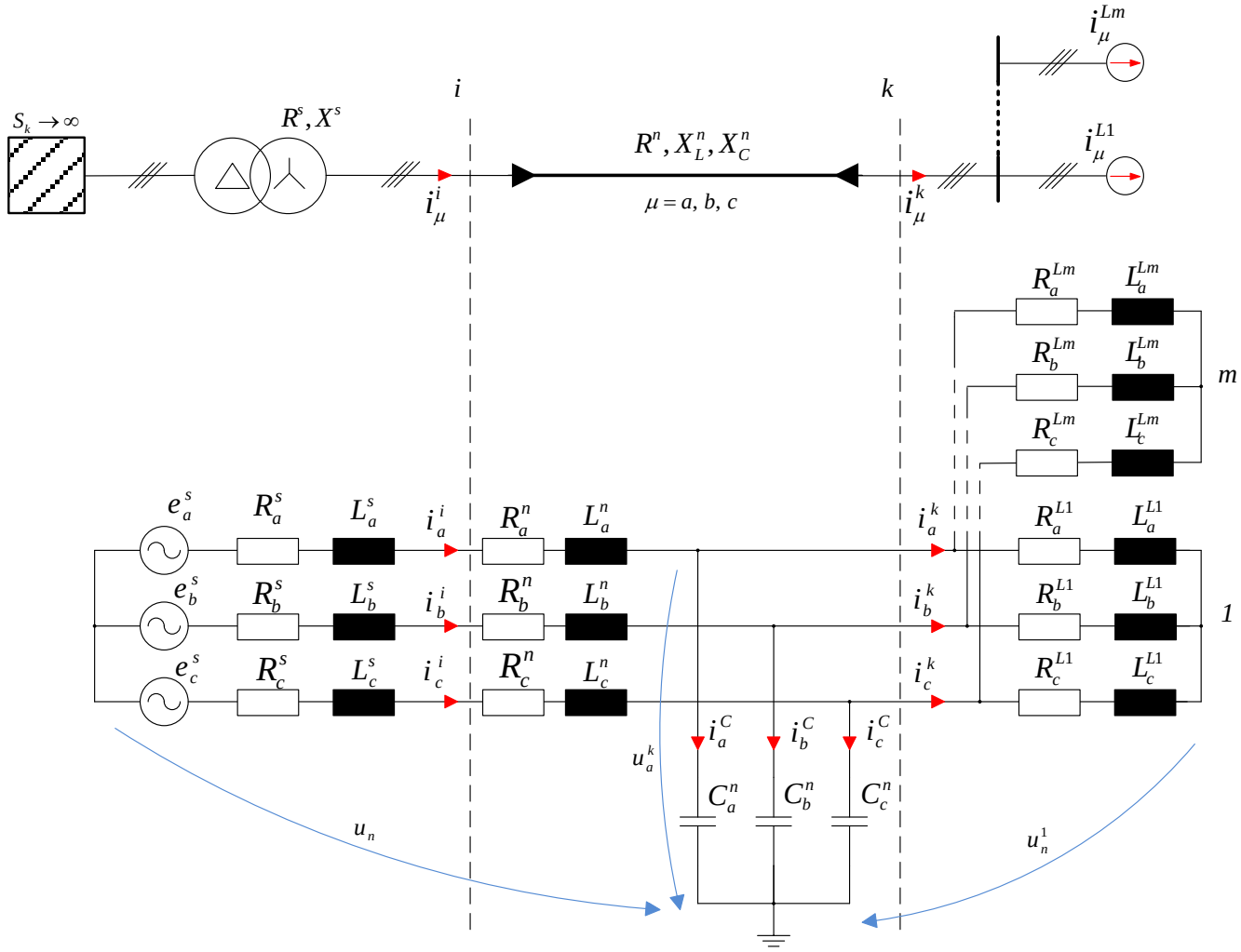

Figure 2.1.1 Equivalent circuit of a neutral ungrounded system

As it mentioned before, there is no connection between the system conductors and the ground. Nevertheless, there is always the capacitive coupling between each phase and the ground due to the disturbed phase-to-ground capacitance. The capacitance between the phases exists as well, but it has little effect on the system characteristics and is disregarded. The network can be considered as the linear and symmetrical system. Since, the parameters distribution has no contribution on the processes considered, all capacitance and inductance are assumed to be equal. The case when the network parameters should be considered disturbed or lumped will be considered in Chapter 3.3. In general case, any number of RL loads L_{aL}, L_{bL}, L_{cL} , R_{aL}, R_{bL}, R_{cL} are supplied by the system.

The mathematical model can be expressed in the basis of phase variables $\vec{F} = \left[\vec{a} \quad \vec{b} \quad \vec{c} \right]$. Referring to Figure 2.1.1, the following equations can be obtained in matrix notation:

$$\begin{cases} \boldsymbol{e} = \boldsymbol{i}^{\boldsymbol{i}} \cdot \left[\boldsymbol{R}^{\boldsymbol{s}}\right] + \left[\boldsymbol{L}^{\boldsymbol{s}}\right]\dfrac{\boldsymbol{di}^{\boldsymbol{i}}}{\boldsymbol{dt}} + \boldsymbol{i}^{\boldsymbol{i}} \cdot \left[\boldsymbol{R}^{\boldsymbol{n}}\right] + \left[\boldsymbol{L}^{\boldsymbol{n}}\right]\dfrac{\boldsymbol{di}^{\boldsymbol{i}}}{\boldsymbol{dt}} + \boldsymbol{u}^{\boldsymbol{k}} - \boldsymbol{u}_n \\ \boldsymbol{i}^{\boldsymbol{k1}} \cdot \left[\boldsymbol{R}^{\boldsymbol{L1}}\right] + \left[\boldsymbol{L}^{\boldsymbol{L1}}\right]\dfrac{\boldsymbol{di}^{\boldsymbol{k1}}}{\boldsymbol{dt}} - \boldsymbol{u}^{\boldsymbol{k}} + \boldsymbol{u}_n^{\boldsymbol{1}} = \boldsymbol{0} \\ \boldsymbol{i}^{\boldsymbol{i}} = \boldsymbol{i}^{\boldsymbol{C}} + \boldsymbol{i}^{\boldsymbol{k}} = \boldsymbol{i}^{\boldsymbol{C}} + \boldsymbol{i}^{\boldsymbol{k1}} + \boldsymbol{...} + \boldsymbol{i}^{\boldsymbol{km}} \\ \boldsymbol{....} \\ \boldsymbol{i}^{\boldsymbol{km}} \cdot \left[\boldsymbol{R}^{\boldsymbol{Lm}}\right] + \left[\boldsymbol{L}^{\boldsymbol{Lm}}\right]\dfrac{\boldsymbol{di}^{\boldsymbol{km}}}{\boldsymbol{dt}} - \boldsymbol{u}^{\boldsymbol{k}} + \boldsymbol{u}_n^{\boldsymbol{m}} = \boldsymbol{0} \\ \boldsymbol{i}^{\boldsymbol{C}} = \left[\boldsymbol{C}^{\boldsymbol{n}}\right]\dfrac{\boldsymbol{du}^{\boldsymbol{k}}}{\boldsymbol{dt}} \end{cases} \tag{2.1.1}$$

As one can see from the equation 2.1.1, the three phase circuit is very complicated to solve it directly. For a better overview, the Clarke transformation is more conveniently to describe transmission lines. One can obtain three one phase equivalent circuit which can be solved easier. The symmetrical coordinate method can be applied as well. However, regarding the GF the Clarke components method is more convenient.

$$\boldsymbol{e} = \begin{bmatrix} e_a^s \\ e_b^s \\ e_c^s \end{bmatrix}, \quad \boldsymbol{i}^{\boldsymbol{i}} = \begin{bmatrix} i_a^i \\ i_b^i \\ i_c^i \end{bmatrix}, \quad \boldsymbol{i}^{\boldsymbol{C}} = \begin{bmatrix} i_a^C \\ i_b^C \\ i_c^C \end{bmatrix}, \quad \boldsymbol{i}^{\boldsymbol{k}} = \begin{bmatrix} i_a^k \\ i_b^k \\ i_c^k \end{bmatrix}, \quad \boldsymbol{i}^{\boldsymbol{k1}} = \begin{bmatrix} i_a^{k1} \\ i_b^{k1} \\ i_c^{k1} \end{bmatrix}, \quad \boldsymbol{i}^{\boldsymbol{km}} = \begin{bmatrix} i_a^{km} \\ i_b^{km} \\ i_c^{km} \end{bmatrix}$$

$$\boldsymbol{u}^{\boldsymbol{k}} = \begin{bmatrix} u_a^k \\ u_b^k \\ u_c^k \end{bmatrix}, \quad \boldsymbol{u}_n = \begin{bmatrix} u_n \\ u_n \\ u_n \end{bmatrix}, \quad \boldsymbol{u}_n^{\boldsymbol{1}} = \begin{bmatrix} u_n^1 \\ u_n^1 \\ u_n^1 \end{bmatrix}, \quad \boldsymbol{u}_n^{\boldsymbol{m}} = \begin{bmatrix} u_n^m \\ u_n^m \\ u_n^m \end{bmatrix}$$

$$\left[\boldsymbol{R}^{\boldsymbol{s}}\right] = \begin{bmatrix} R_a^s & 0 & 0 \\ 0 & R_b^s & 0 \\ 0 & 0 & R_c^s \end{bmatrix}, \quad \left[\boldsymbol{L}^{\boldsymbol{s}}\right] = \begin{bmatrix} L_a^s & 0 & 0 \\ 0 & L_b^s & 0 \\ 0 & 0 & L_c^s \end{bmatrix}, \quad \left[\boldsymbol{R}^{\boldsymbol{s}}\right] = \begin{bmatrix} R_a^n & 0 & 0 \\ 0 & R_b^n & 0 \\ 0 & 0 & R_c^n \end{bmatrix}$$

$$\left[\boldsymbol{L}^{n}\right] = \begin{bmatrix} L_a^n & 0 & 0 \\ 0 & L_b^n & 0 \\ 0 & 0 & L_c^n \end{bmatrix}, \quad \left[\boldsymbol{C}^{\boldsymbol{n}}\right] = \begin{bmatrix} C_a^n & 0 & 0 \\ 0 & C_b^n & 0 \\ 0 & 0 & C_c^n \end{bmatrix}, \quad \left[\boldsymbol{R}^{L1}\right] = \begin{bmatrix} R_a^{L1} & 0 & 0 \\ 0 & R_b^{L1} & 0 \\ 0 & 0 & R_c^{L1} \end{bmatrix}$$

$$\left[\boldsymbol{R}^{Lm}\right] = \begin{bmatrix} R_a^{Lm} & 0 & 0 \\ 0 & R_b^{Lm} & 0 \\ 0 & 0 & R_c^{Lm} \end{bmatrix}, \quad \left[\boldsymbol{L}^{L1}\right] = \begin{bmatrix} L_a^{L1} & 0 & 0 \\ 0 & L_b^{L1} & 0 \\ 0 & 0 & L_c^{L1} \end{bmatrix}, \quad \left[\boldsymbol{L}^{Lm}\right] = \begin{bmatrix} L_a^{Lm} & 0 & 0 \\ 0 & L_b^{Lm} & 0 \\ 0 & 0 & L_c^{Lm} \end{bmatrix} \tag{2.1.2}$$

Clarke components model

According to the *α-β-0* coordinate method currents and voltages can be defined by the following equations:

$$\begin{bmatrix} u_\alpha \\ u_\beta \\ u_0 \end{bmatrix} = \frac{1}{3}\begin{bmatrix} 2 & -1 & -1 \\ 0 & \sqrt{3} & -\sqrt{3} \\ 1 & 1 & 1 \end{bmatrix} \cdot \begin{bmatrix} u_a \\ u_b \\ u_c \end{bmatrix} \Rightarrow \boldsymbol{u}_{\alpha\beta 0} = \left[\boldsymbol{T}_{\alpha\beta 0}\right] \cdot \boldsymbol{u}_{abc}$$
$$\begin{bmatrix} i_\alpha \\ i_\beta \\ i_0 \end{bmatrix} = \frac{1}{3}\begin{bmatrix} 2 & -1 & -1 \\ 0 & \sqrt{3} & -\sqrt{3} \\ 1 & 1 & 1 \end{bmatrix} \cdot \begin{bmatrix} i_a \\ i_b \\ i_c \end{bmatrix} \Rightarrow \boldsymbol{i}_{\alpha\beta 0} = \left[\boldsymbol{T}_{\alpha\beta 0}\right] \cdot \boldsymbol{i}_{abc} \quad (2.1.3)$$

And respectively the inverse transform ($\left[\boldsymbol{T}_{\alpha\beta 0}\right]^{-1}$ is the inverse matrix):

$$\boldsymbol{u}_{abc} = \left[\boldsymbol{T}_{\alpha\beta 0}\right]^{-1} \cdot \boldsymbol{u}_{\alpha\beta 0}, \quad \boldsymbol{i}_{abc} = \left[\boldsymbol{T}_{\alpha\beta 0}\right]^{-1} \cdot \boldsymbol{i}_{\alpha\beta 0}, \left[\boldsymbol{T}_{\alpha\beta 0}\right]^{-1} = \begin{bmatrix} 1 & 0 & 1 \\ -1/2 & \sqrt{3}/2 & 1 \\ -1/2 & -\sqrt{3}/2 & 1 \end{bmatrix} \quad (2.1.4)$$

For simplicity the equivalent circuit (Figure 2.1.1) involves only one load. The definition of *α-β-0* components from the equation 2.1.1 is:

$$\begin{cases} \boldsymbol{e}_{\alpha\beta 0} = \boldsymbol{e} \cdot \left[\boldsymbol{T}_{\alpha\beta 0}\right] \\ \boldsymbol{i}^{i}_{\alpha\beta 0} = \boldsymbol{i}^{i} \cdot \left[\boldsymbol{T}_{\alpha\beta 0}\right] \\ \boldsymbol{i}^{C}_{\alpha\beta 0} = \boldsymbol{i}^{C} \cdot \left[\boldsymbol{T}_{\alpha\beta 0}\right] \\ \boldsymbol{i}^{k}_{\alpha\beta 0} = \boldsymbol{i}^{k} \cdot \left[\boldsymbol{T}_{\alpha\beta 0}\right] \\ \boldsymbol{u}^{k}_{\alpha\beta 0} = \boldsymbol{u}^{k} \cdot \left[\boldsymbol{T}_{\alpha\beta 0}\right] \\ \boldsymbol{u}^{n}_{\alpha\beta} = \boldsymbol{u}_{n} \cdot \left[\boldsymbol{T}_{\alpha\beta 0}\right] \\ \boldsymbol{u}^{n1}_{\alpha\beta} = \boldsymbol{u}_{n}{}^{1} \cdot \left[\boldsymbol{T}_{\alpha\beta 0}\right] \end{cases} \quad \begin{cases} \boldsymbol{e}^{F} = \boldsymbol{e}_{\alpha\beta 0} \cdot \left[\boldsymbol{T}_{\alpha\beta 0}\right]^{-1} \\ \boldsymbol{i}^{i} = \boldsymbol{i}^{i}_{\alpha\beta 0} \cdot \left[\boldsymbol{T}_{\alpha\beta 0}\right]^{-1} \\ \boldsymbol{i}^{C} = \boldsymbol{i}^{C}_{\alpha\beta 0} \cdot \left[\boldsymbol{T}_{\alpha\beta 0}\right]^{-1} \\ \boldsymbol{i}^{k} = \boldsymbol{i}^{k}_{\alpha\beta 0} \cdot \left[\boldsymbol{T}_{\alpha\beta 0}\right]^{-1} \\ \boldsymbol{u}^{k} = \boldsymbol{u}^{k}_{\alpha\beta 0} \cdot \left[\boldsymbol{T}_{\alpha\beta 0}\right]^{-1} \\ \boldsymbol{u}_{n} = \boldsymbol{u}^{n}_{\alpha\beta} \cdot \left[\boldsymbol{T}_{\alpha\beta 0}\right]^{-1} \\ \boldsymbol{u}_{n}{}^{1} = \boldsymbol{u}^{n1}_{\alpha\beta} \cdot \left[\boldsymbol{T}_{\alpha\beta 0}\right]^{-1} \end{cases} \quad (2.1.5)$$

Substituting the equation 2.1.5 into 2.1.1:

$$\begin{cases} \boldsymbol{e}_{\alpha\beta 0}\cdot\left[\boldsymbol{T}_{\alpha\beta 0}\right]^{-1}=\boldsymbol{i}^{i}_{\alpha\beta 0}\cdot\left[\boldsymbol{T}_{\alpha\beta 0}\right]^{-1}\cdot\left(\left[\boldsymbol{R}^{s}\right]+\left[\boldsymbol{R}^{n}\right]\right)+\dot{\boldsymbol{i}}^{i}_{\alpha\beta 0}\cdot\left[\boldsymbol{T}_{\alpha\beta 0}\right]^{-1}\cdot\left(\left[\boldsymbol{L}^{s}\right]+\left[\boldsymbol{L}^{n}\right]\right)+.. \\ +\boldsymbol{u}^{k}_{\alpha\beta 0}\cdot\left[\boldsymbol{T}_{\alpha\beta 0}\right]^{-1}-\boldsymbol{u}^{n}_{\alpha\beta 0}\cdot\left[\boldsymbol{T}_{\alpha\beta 0}\right]^{-1} \\ \boldsymbol{i}^{k}_{\alpha\beta 0}\cdot\left[\boldsymbol{T}_{\alpha\beta 0}\right]^{-1}\cdot\left[\boldsymbol{R}^{L}\right]+\dot{\boldsymbol{i}}^{k}_{\alpha\beta 0}\cdot\left[\boldsymbol{T}_{\alpha\beta 0}\right]^{-1}\cdot\left[\boldsymbol{L}^{L}\right]-\boldsymbol{u}^{k}_{\alpha\beta 0}\cdot\left[\boldsymbol{T}_{\alpha\beta 0}\right]^{-1}=\boldsymbol{u}^{n1}_{\alpha\beta 0}\cdot\left[\boldsymbol{T}_{\alpha\beta 0}\right]^{-1} \\ \boldsymbol{i}^{i}_{\alpha\beta 0}\cdot\left[\boldsymbol{T}_{\alpha\beta 0}\right]^{-1}=\boldsymbol{i}^{C}_{\alpha\beta 0}\cdot\left[\boldsymbol{T}_{\alpha\beta 0}\right]^{-1}+\boldsymbol{i}^{k}_{\alpha\beta 0}\cdot\left[\boldsymbol{T}_{\alpha\beta 0}\right]^{-1} \end{cases} \tag{2.1.6}$$

Multiplying by $\left[\boldsymbol{T}_{\alpha\beta 0}\right]$ and considering that $\left[\boldsymbol{T}_{\alpha\beta 0}\right]\cdot\left[\boldsymbol{T}_{\alpha\beta 0}\right]^{-1}=1$:

$$\begin{cases} \boldsymbol{e}_{\alpha\beta 0}=\boldsymbol{i}^{i}_{\alpha\beta 0}\cdot\left[\boldsymbol{T}_{\alpha\beta 0}\right]^{-1}\cdot\left[\boldsymbol{T}_{\alpha\beta 0}\right]\cdot\left(\left[\boldsymbol{R}^{s}\right]+\left[\boldsymbol{R}^{n}\right]\right)+\dot{\boldsymbol{i}}^{i}_{\alpha\beta 0}\cdot\left[\boldsymbol{T}_{\alpha\beta 0}\right]^{-1}\cdot\left[\boldsymbol{T}_{\alpha\beta 0}\right]\cdot\left(\left[\boldsymbol{L}^{s}\right]+\left[\boldsymbol{L}^{n}\right]\right)+.. \\ +\boldsymbol{u}^{k}_{\alpha\beta 0}-\boldsymbol{u}^{n}_{\alpha\beta 0} \\ \boldsymbol{i}^{k}_{\alpha\beta 0}\cdot\left[\boldsymbol{T}_{\alpha\beta 0}\right]^{-1}\cdot\left[\boldsymbol{T}_{\alpha\beta 0}\right]\cdot\left[\boldsymbol{R}^{L}\right]+\dot{\boldsymbol{i}}^{k}_{\alpha\beta 0}\cdot\left[\boldsymbol{T}_{\alpha\beta 0}\right]^{-1}\cdot\left[\boldsymbol{T}_{\alpha\beta 0}\right]\cdot\left[\boldsymbol{L}^{L}\right]-\boldsymbol{u}^{k}_{\alpha\beta 0}=\boldsymbol{u}^{n1}_{\alpha\beta 0} \\ \boldsymbol{i}^{i}_{\alpha\beta 0}=\boldsymbol{i}^{C}_{\alpha\beta 0}+\boldsymbol{i}^{k}_{\alpha\beta 0} \end{cases} \tag{2.1.7}$$

Multiplying and extracting impedances one can see that $\left[\boldsymbol{R}^{s}_{\alpha\beta 0}\right]=\left[\boldsymbol{T}_{\alpha\beta 0}\right]^{-1}\left[\boldsymbol{T}_{\alpha\beta 0}\right]\left[\boldsymbol{R}^{s}\right]$. And finally, the equation for the circuit in *α-β-0* domain is:

$$\begin{cases} \boldsymbol{e}_{\alpha\beta 0}=\boldsymbol{i}^{i}_{\alpha\beta 0}\cdot\left(\left[\boldsymbol{R}^{s}_{\alpha\beta 0}\right]+\left[\boldsymbol{R}^{n}_{\alpha\beta 0}\right]\right)+\dot{\boldsymbol{i}}^{i}_{\alpha\beta 0}\cdot\left(\left[\boldsymbol{L}^{s}_{\alpha\beta 0}\right]+\left[\boldsymbol{L}^{n}_{\alpha\beta 0}\right]\right)+\boldsymbol{u}^{k}_{\alpha\beta 0}-\boldsymbol{u}^{n}_{\alpha\beta 0} \\ \boldsymbol{i}^{k}_{\alpha\beta 0}\cdot\left[\boldsymbol{R}^{L}_{\alpha\beta 0}\right]+\dot{\boldsymbol{i}}^{k}_{\alpha\beta 0}\cdot\left[\boldsymbol{L}^{L}_{\alpha\beta 0}\right]-\boldsymbol{u}^{k}_{\alpha\beta 0}=\boldsymbol{u}^{n1}_{\alpha\beta 0} \\ \boldsymbol{i}^{i}_{\alpha\beta 0}=\boldsymbol{i}^{C}_{\alpha\beta 0}+\boldsymbol{i}^{k}_{\alpha\beta 0} \end{cases} \tag{2.1.8}$$

In order to obtain the equivalent circuit it should be noticed the following:

$$\boldsymbol{u}^{n}_{\alpha\beta 0}=\boldsymbol{u}_{n}\cdot\left[\boldsymbol{T}_{\alpha\beta 0}\right]=\begin{bmatrix}0\\0\\u_{n}\end{bmatrix},\ \boldsymbol{u}^{n1}_{\alpha\beta 0}=\boldsymbol{u}_{n1}\cdot\left[\boldsymbol{T}_{\alpha\beta 0}\right]=\begin{bmatrix}0\\0\\u_{n1}\end{bmatrix} \tag{2.1.9}$$

Considering the symmetrical transmission line the neutral voltages u_n and u_{n1} can be assumed equal to zero. The equivalent circuit in *α-β-0* domain corresponding to the equations 2.1.8 and 2.1.9 is given in Figure 2.1.2.

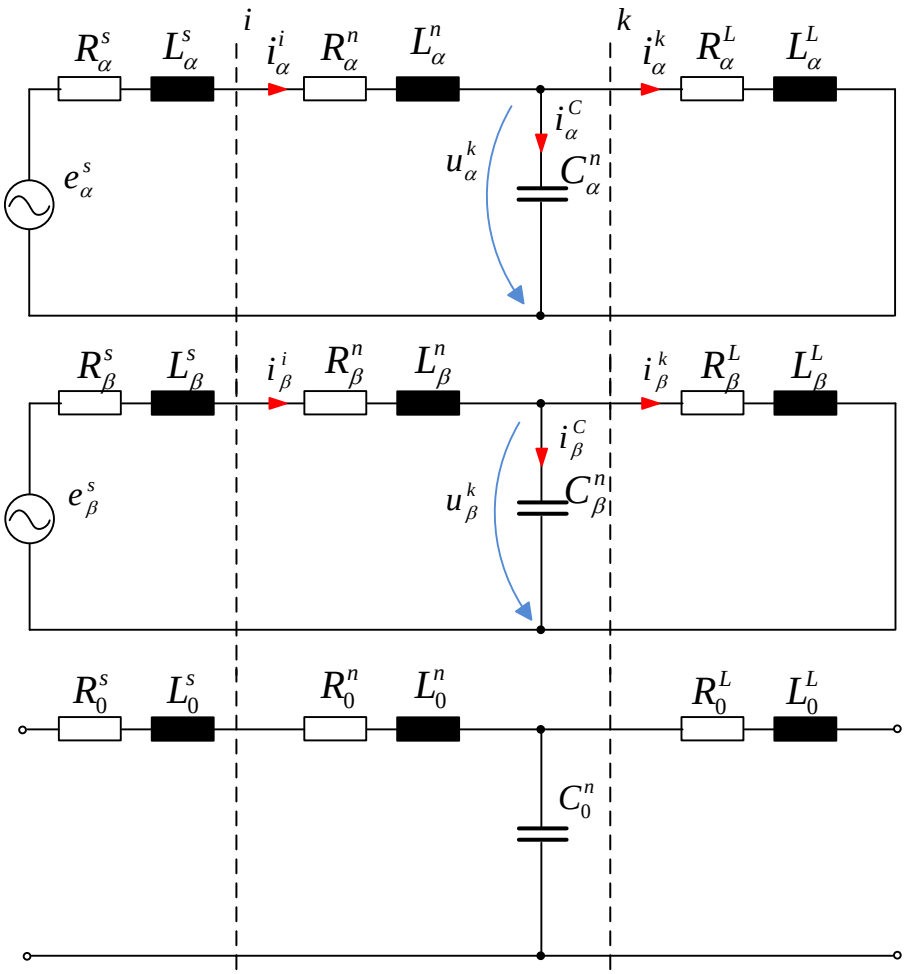

Figure 2.1.2 Equivalent circuit in *α-β-0* domain

One-phase to ground fault case

Considering the one-phase to ground fault as in Figure 1.6, the fault point can be depicted in Figure 2.1.3.

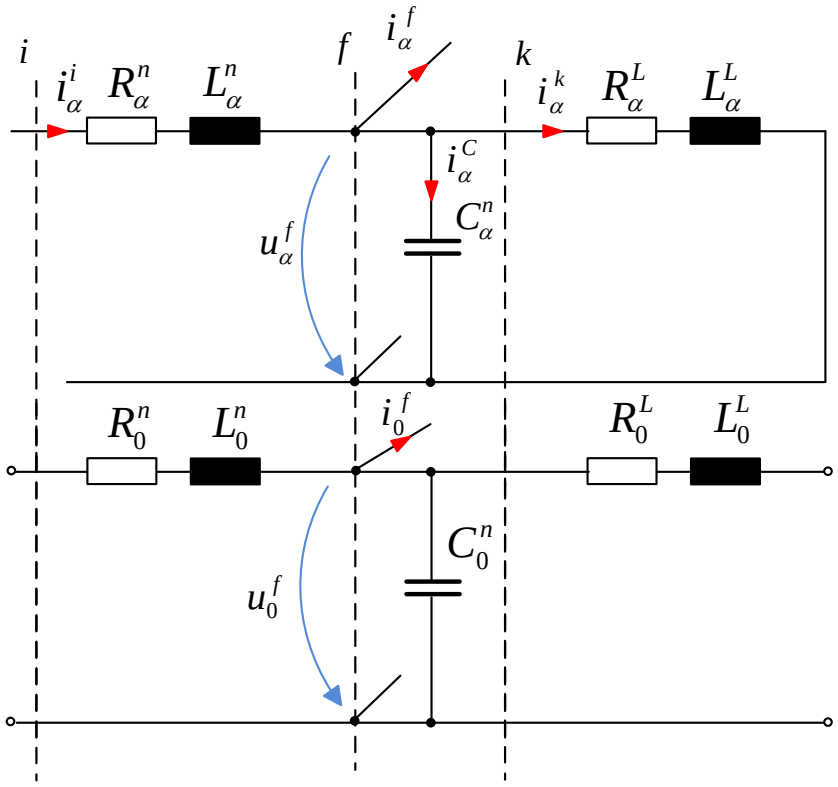

Figure 2.1.3 Equivalent fault conditions circuit in *α-β-0* domain

In order to obtain the equations, the fault conditions at the point *f* (Figure 2.3) should be written. The fault conditions in *abc* domain are (the simplest case of the fault):

$$u_a^f = 0, i_b^f = i_c^f = 0 \tag{2.1.10}$$

Transforming the equations 2.1.10 into *α-β-0* domain the following equations can be obtained:

$$\begin{bmatrix} 0 \\ u_b^f \\ u_c^f \end{bmatrix} = \left[T_{\alpha\beta 0}\right]^{-1} \cdot \begin{bmatrix} u_\alpha^f \\ u_\beta^f \\ u_0^f \end{bmatrix} \Rightarrow u_\alpha^f + u_0^f = 0$$

$$\begin{bmatrix} i_a^f \\ 0 \\ 0 \end{bmatrix} = \left[T_{\alpha\beta 0}\right]^{-1} \cdot \begin{bmatrix} i_\alpha^f \\ i_\beta^f \\ i_0^f \end{bmatrix} \Rightarrow \begin{cases} -\frac{1}{2} i_\alpha^f + \frac{\sqrt{3}}{2} i_\beta^f + i_0^f = 0 \\ -\frac{1}{2} i_\alpha^f - \frac{\sqrt{3}}{2} i_\beta^f + i_0^f = 0 \end{cases} \Rightarrow \begin{cases} i_\alpha^f = 2 i_0^f \\ i_{f\beta} = 0 \end{cases} \tag{2.1.11}$$

The equation 2.1.11 shows the existence of the coupling between *α* and *0* equivalent circuits. The circuit of the *β* component does not affect the GF in this case. The GF equivalent circuit is shown in Figure 2.1.4.

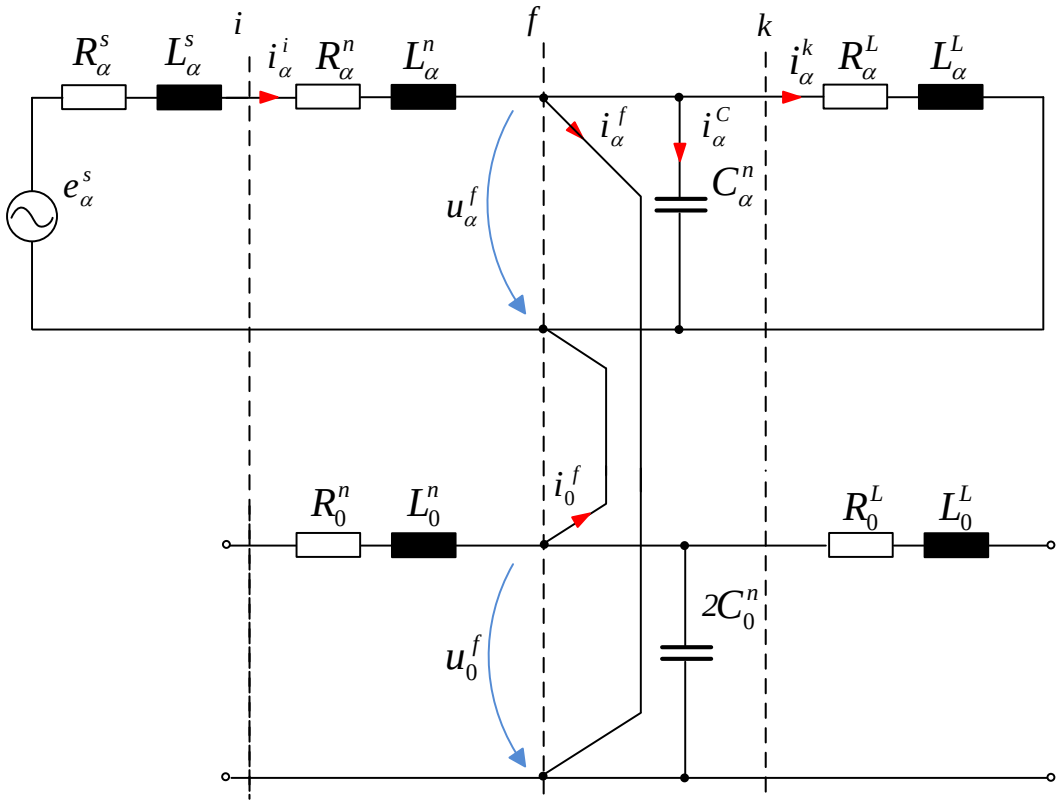

Figure 2.1.4 Equivalent fault circuit in *α-β-0* domain

It should be noticed that in the case of *b* or *c* phase fault, the equivalent circuit would look different and the *β* component would be involved as well. However, in order to study the principles of the coupling and compensation only *a* phase fault can be considered.

In order to obtain the equation for the ground fault current the equivalent circuit should be solved in complex values. As one can see from Figure 2.1.4 the load does not has any effect on the zero current. Thus, the load can be neglected or considered as the current source. The load, for example a thyristor bridge, would influence only on the high frequency components of the ground fault (it will be shown in the chapter 3). All subsequent calculations are made with the condition $X_\alpha^n = X_0^n$. Given the above and equation 2.1.1, the fault current in the steady state can be obtained as follows:

$$\underline{I^f} = \underline{I_a^f} = \underline{I_\alpha^f} + \underline{I_0^f} = 1.5\underline{I_\alpha^f}$$

$$\underline{I_\alpha^i} = \frac{\underline{E_\alpha^s} - j \cdot \frac{X_\alpha^{nC}}{3} \cdot \underline{I_\alpha^k}}{(R_\alpha^s + j \cdot X_\alpha^{sL} + R_\alpha^n + j \cdot X_\alpha^{nL} - j \cdot \frac{X_\alpha^{nC}}{3})}$$

$$\underline{I_\alpha^C} + \underline{I_\alpha^f} = \underline{I_\alpha^i} - \underline{I_\alpha^k} = \frac{\underline{E_\alpha^s} - \underline{I_\alpha^k} \cdot (R_\alpha^s + j \cdot X_\alpha^{sL} + R_\alpha^n + j \cdot X_\alpha^{nL})}{(R_\alpha^s + j \cdot X_\alpha^{sL} + R_\alpha^n + j \cdot X_\alpha^{nL} - j \cdot \frac{X_\alpha^{nC}}{3})}$$

$$\underline{I_\alpha^f} = \left(\underline{I_\alpha^i} - \underline{I_\alpha^k}\right) \cdot \frac{-j \cdot X_\alpha^{nC}}{-j \cdot X_\alpha^{nC} - j \cdot \frac{X_\alpha^{nC}}{2}} =$$

$$= \frac{2}{3} \cdot \frac{\underline{E_\alpha^s} - \underline{I_\alpha^k} \cdot (R_\alpha^s + j \cdot X_\alpha^{sL} + R_\alpha^n + j \cdot X_\alpha^{nL})}{(R_\alpha^s + j \cdot X_\alpha^{sL} + R_\alpha^n + j \cdot X_\alpha^{nL} - j \cdot \frac{X_\alpha^{nC}}{3})} \qquad (2.1.12)$$

It is obvious being the active and inductive resistance very small. Thus in equation 2.1.12 it can be also neglected:

$$\underline{I^f} = 1.5 \cdot \underline{I_\alpha^f} = \frac{\underline{E_\alpha^s}}{-j \cdot \frac{X_\alpha^{nC}}{3}} \qquad (2.1.13)$$

ASC and converter grounded system

The ASC grounded system is shown in Figure 1.9. The transformation into *α-β-0* domain can be carried out in the same way (equations 2.1.3 – 2.1.9). And the equation for the neutral voltage should be considered as well (Figure 1.9 and 2.1.1):

$$u_n = R_{ASC} \cdot (i_a^i + i_b^i + i_c^i) + L_{ASC} \cdot (\dot{i}_a^i + \dot{i}_b^i + \dot{i}_c^i) = 3 \cdot R_{ASC} \cdot i_0 + 3 \cdot L_{ASC} \cdot \dot{i}_0 \qquad (2.1.14)$$

Considering the equation 2.1.8 the equivalent circuit for the ASC compensated system in the case of the ground fault is depicted in Figure 2.1.5.

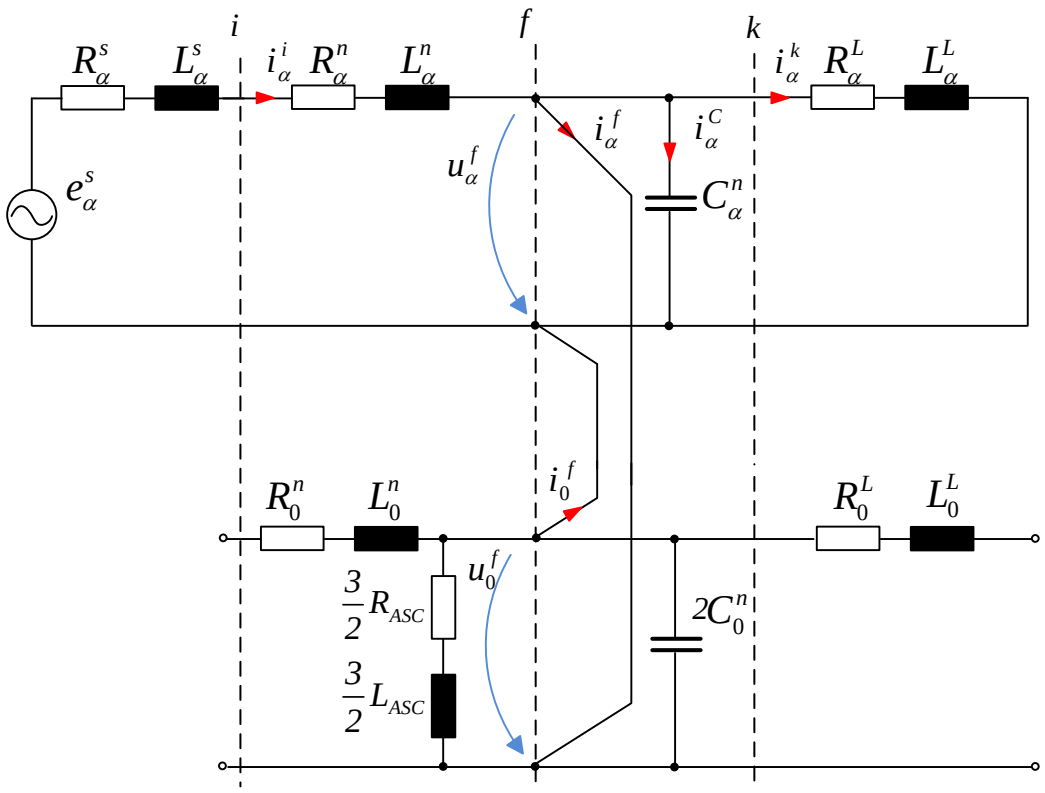

Figure 2.1.5 ASC compensated equivalent fault circuit in *α-β-0* domain

It should be noticed that the ASC resistance and inductance multiplying by 3 and divided by 2 according to the equations 2.1.14 and 2.1.11 respectively. The ground fault current value in this case can be found as follows:

$$\underline{I^f} = \underline{I_a^f} = \underline{I_\alpha^f} + \underline{I_0^f} = 1.5\underline{I_\alpha^f};\quad \underline{Z_{ASC}} = \frac{3}{2}R_{ASC} + \frac{3}{2}X_{LASC}$$

$$\underline{Z} = \frac{-j\cdot\frac{X_\alpha^{nC}}{3}\cdot\underline{Z_{ASC}}}{-j\cdot\frac{X_\alpha^{nC}}{3}+\underline{Z_{ASC}}};\ \underline{Z_0} = \frac{-j\cdot\frac{X_\alpha^{nC}}{2}\cdot\underline{Z_{ASC}}}{-j\cdot\frac{X_\alpha^{nC}}{2}+\underline{Z_{ASC}}} \tag{2.1.15}$$

$$\underline{I_\alpha^i} = \frac{\underline{E_\alpha^s} + \underline{Z}\cdot\underline{I_\alpha^k}}{(R_\alpha^s + j\cdot X_\alpha^{sL} + R_\alpha^n + j\cdot X_\alpha^{nL} + \underline{Z})}$$

$$\underline{I_\alpha^C} + \underline{I_\alpha^f} = \underline{I_\alpha^i} - \underline{I_\alpha^k} = \frac{\underline{E_\alpha^s} - \underline{I_\alpha^k}\cdot(R_\alpha^s + j\cdot X_\alpha^{sL} + R_\alpha^n + j\cdot X_\alpha^{nL})}{(R_\alpha^s + j\cdot X_\alpha^{sL} + R_\alpha^n + j\cdot X_\alpha^{nL} + \underline{Z})} \approx \frac{\underline{E_\alpha^s}}{\underline{Z}}$$

$$\underline{I_\alpha^f} = \left(\underline{I_\alpha^C} + \underline{I_\alpha^f}\right) \cdot \frac{-j \cdot X_\alpha^{nC}}{-j \cdot X_\alpha^{nC} + \underline{Z_0}} = \frac{\underline{E_\alpha^s}}{\underline{Z}} \cdot \frac{-j \cdot X_\alpha^{nC}}{-j \cdot X_\alpha^{nC} + \underline{Z_0}}$$

$$= \underline{E_\alpha^s} \cdot \frac{-j \cdot X_\alpha^{nC} + 2 \cdot Z_{ASC}}{-j \cdot X_\alpha^{nC} \cdot Z_{ASC}} = \frac{\underline{E_\alpha^s}}{\underline{Z_0}} \qquad (2.1.16)$$

$$\underline{I^f} = 1.5 \cdot \underline{I_\alpha^f} = 1.5 \cdot \frac{\underline{E_\alpha^s}}{\underline{Z_0}}$$

It can be seen the ground fault current dependence on the zero sequence impedance. From the equation 2.1.16 the well-known resonance tuning conditions can be obtained.

Now, the equations for the active converter grounded system can be obtained. The converter can be represented as three current sources. The three phase connection is shown in Figure 2.1.6.

Knowing the active power converter features, in *α-β-0* domain the converter can be presented as three independent current sources. It is shown in Figure 2.1.7 (*β* circuit is supposed to be the same as *α*).

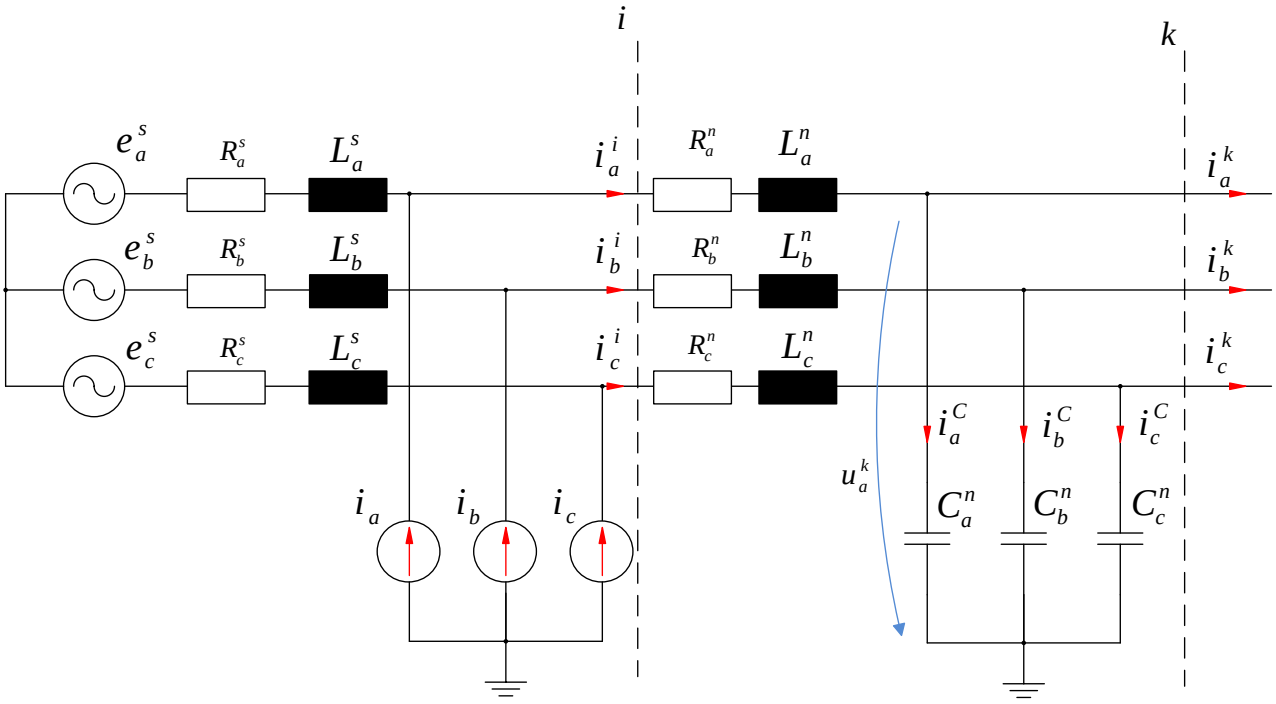

Figure 2.1.6 Active converter grounded circuit

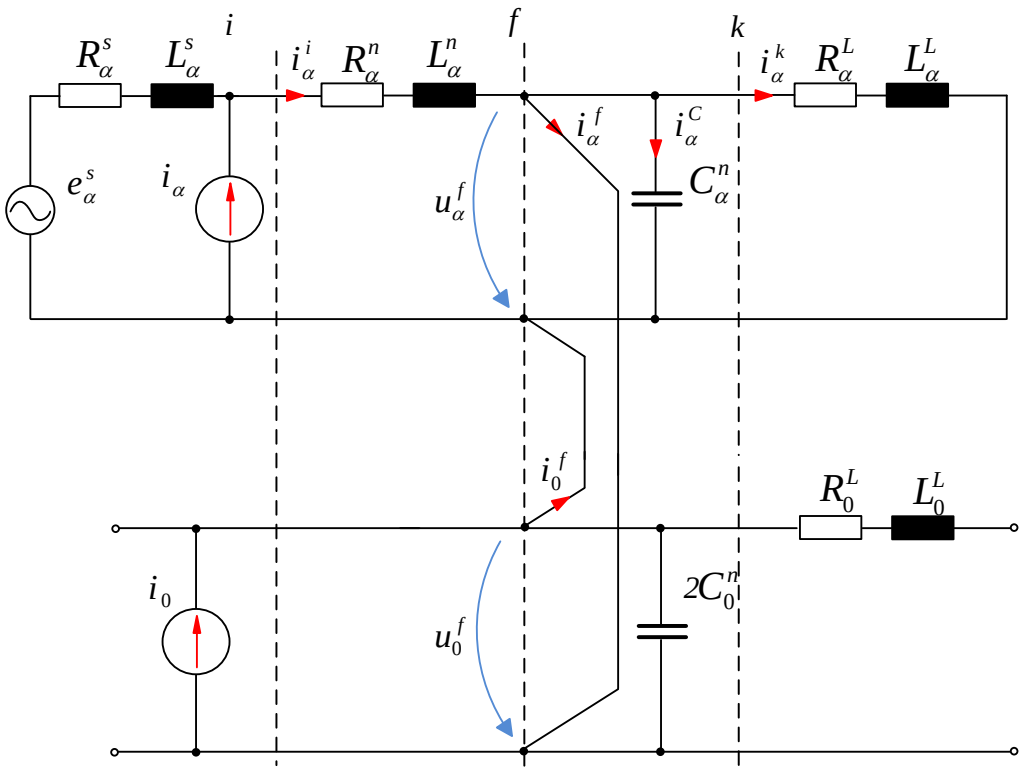

Figure 2.1.7 Active converter compensated equivalent fault circuit in *α-β-0* domain

According to the equivalent circuit in Figure 2.1.7 the ground fault current in steady state can be found as follows($\underline{I}_{(C+C0)}$ is the total current of the *α* and *0* capacitance):

$$\underline{I}_\alpha^i = \frac{\underline{E}_\alpha^s + j\cdot\frac{X_\alpha^{nC}}{3}\left(\underline{I}_0 - \underline{I}_\alpha^k\right)}{\left(R_\alpha^s + j\cdot X_\alpha^{sL} + R_\alpha^n + j\cdot X_\alpha^{nL} - j\cdot\frac{X_\alpha^{nC}}{3}\right)}$$

$$\underline{I}_{(C+C0)} = \underline{I}_\alpha^i - \underline{I}_\alpha^k + \underline{I}_0 = \frac{\underline{E}_\alpha^s + \left(\underline{I}_0 - \underline{I}_\alpha^k\right)\cdot\left(R_\alpha^s + j\cdot X_\alpha^{sL} + R_\alpha^n + j\cdot X_\alpha^{nL}\right)}{\left(R_\alpha^s + j\cdot X_\alpha^{sL} + R_\alpha^n + j\cdot X_\alpha^{nL} - j\cdot\frac{X_\alpha^{nC}}{3}\right)}$$

$$\underline{I}_{C0} = \underline{I}_{(C+C0)}\cdot\frac{2}{3};\ \ \underline{Z}_{RL} = R_\alpha^s + j\cdot X_\alpha^{sL} + R_\alpha^n + j\cdot X_\alpha^{nL} \qquad (2.1.17)$$

$$\underline{I}_\alpha^f = \underline{I}_{C0} - \underline{I}_0 = \frac{2}{3}\cdot\frac{\underline{E}_\alpha^s - \underline{I}_0\cdot\left(\frac{\underline{Z}_{RL} - j\cdot X_\alpha^{nC}}{2}\right) - 2\cdot\underline{I}_\alpha^k\cdot\underline{Z}_{RL}}{\left(\underline{Z}_{RL} - j\cdot\frac{X_\alpha^{nC}}{3}\right)}$$

$$\underline{I^f} = 1.5 \cdot \underline{I_\alpha^f} = \frac{\underline{E_\alpha^s} - \underline{I_0} \cdot \left(\frac{\underline{Z_{RL}} - j \cdot X_\alpha^{nC}}{2} \right) - 2 \cdot \underline{I_\alpha^k} \cdot \underline{Z_{RL}}}{\left(\underline{Z_{RL}} - j \cdot \frac{X_\alpha^{nC}}{3} \right)} \approx$$

$$\approx \frac{\underline{E_\alpha^s} - \underline{I_0} \cdot \left(\frac{-j \cdot X_\alpha^{nC}}{2} \right)}{\left(-j \cdot \frac{X_\alpha^{nC}}{3} \right)} = \frac{\underline{E_\alpha^s}}{\left(-j \cdot \frac{X_\alpha^{nC}}{3} \right)} + \frac{3}{2} \underline{I_0} \quad (2.1.18),$$

Thus, in any case there can be found I_0 value to match and compensate ground fault current. This process could be considered as equivalent to ASC resonance tuning. However, the tuning process is one of the problems to be solved. The ground fault current cannot be measured directly due to the absence of the neutral conductor. It will be discussed in the Chapter 3.2. All the network currents and voltages can be found using the inverse transformation (equation 2.1.4). The obtained expressions can be found in APPENDIX (equations 5.1.1 – 5.1.3).

Figure 2.1.8 shows the ground fault current dependency on the converter current value with the different network capacitance.

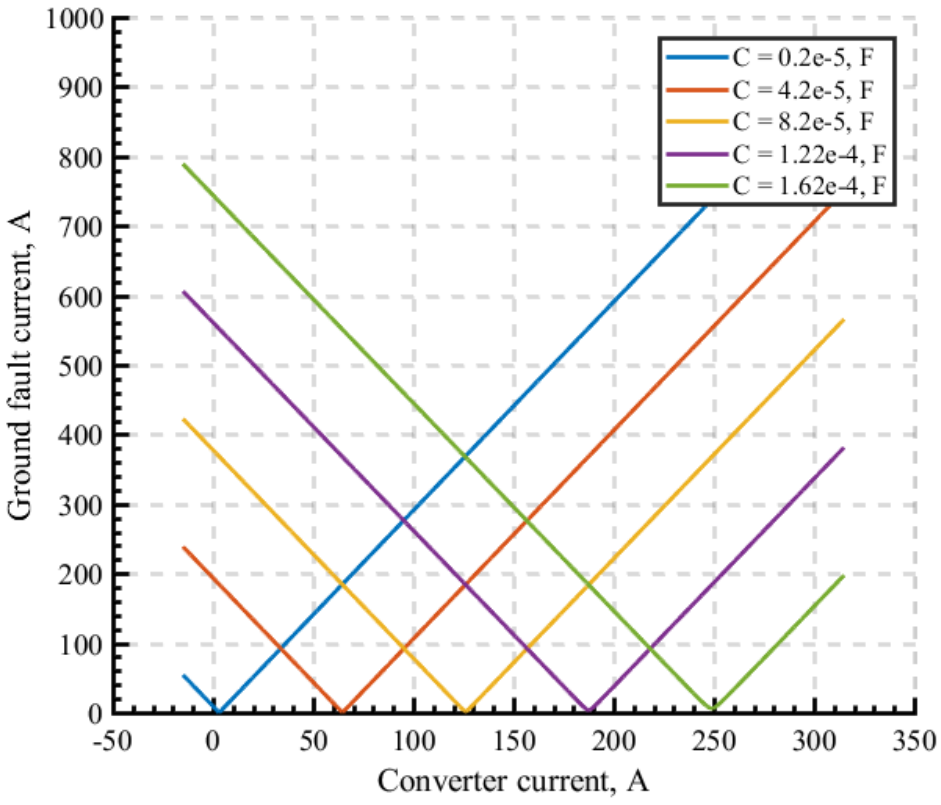

Figure 2.1.8 GF current dependency on the converter current value

For L, C, R the typical 6/10 kV network cable parameters are used (C=0.5 μF/km). It can be seen that there is the converter current value at which the ground fault current is totally compensated. Also the resonant dependency can be seen. One can conclude that there is no necessity to compensate ground fault current with capacity less than 1-2e-5 F due to the lack of the high currents. And economically it is not effectively due to the large ASC inductance value required.

The ASC and the active converter can be operated at the same time as well. In this case the converter is operated to complement the ASC (see Figure 1.11(b)) and would be required to compensate only a remainder of the ground fault current and the high frequency components. The equivalent circuit for this case is shown in Figure 2.1.9.

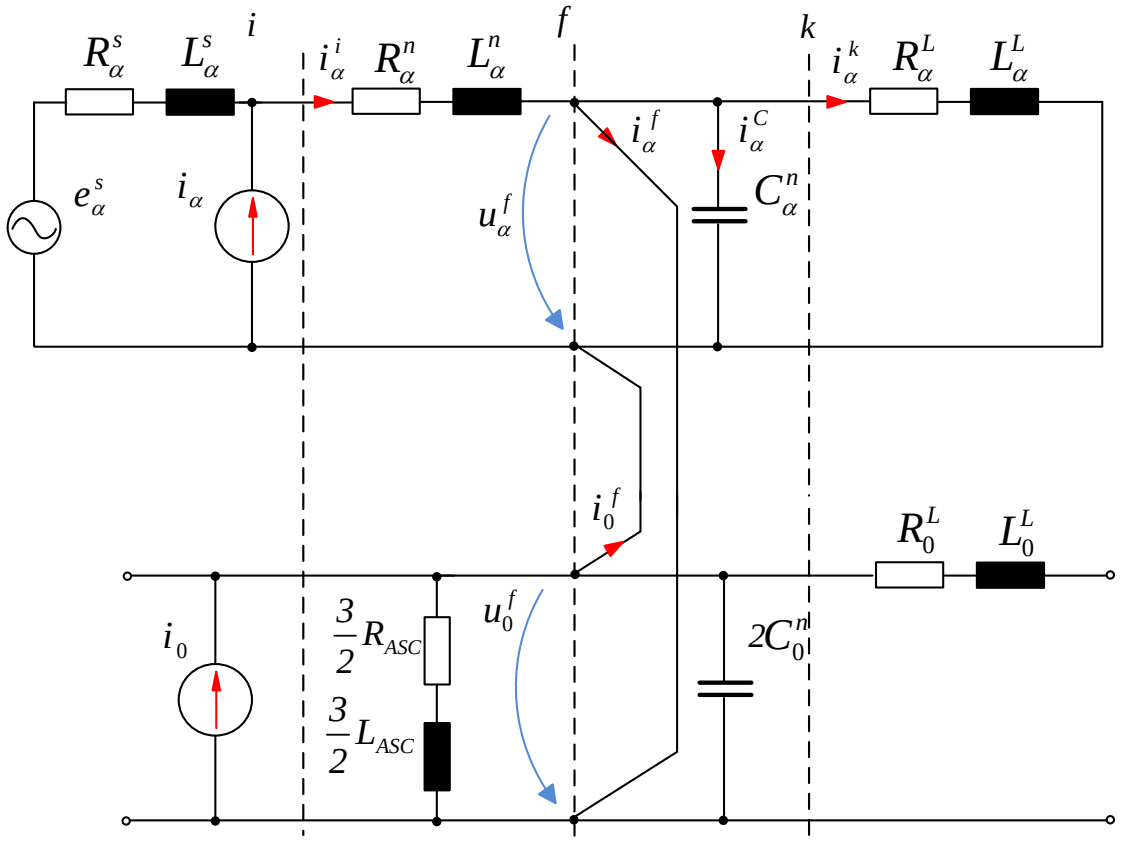

Figure 2.1.9 Hybrid compensated (the converter + ASC) equivalent fault circuit in α-β-0 domain

In this case the GF current in steady state can be found as follows:

$$\underline{I}^f = \frac{3}{2}\frac{\underline{E_\alpha^s}\cdot\left(-j\cdot X_\alpha^{nC}+2\cdot\underline{Z_{ASC}}\right)}{X_\alpha^{nC}\cdot\underline{Z_{ASC}}}-\frac{3}{2}\cdot\underline{I_0} \qquad (2.1.19)$$

Figure 2.1.10 shows the required converter current depending on the ASC inductance value for different network capacitance values.

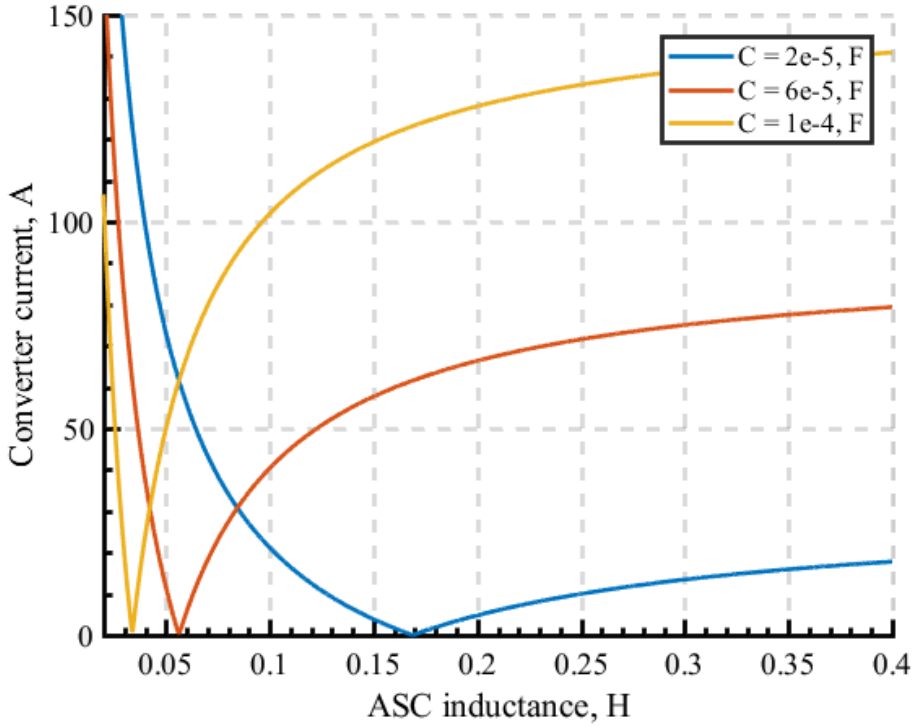

Figure 2.1.10 Converter current dependency on the ASC inductance

It can be seen from Figure 2.1.10 the complexity to match close to the network capacitance. Due to the step inductance change (in most cases) the AEFCC would be operated as the additional device to compensate the capacitive current and its high frequency or active component. At the same time with the ASC already installed the converter total power could be also reduced (in terms of the GF current compensation) depending on the coil's inductance. And as it has been said before, with the capacitance less than 1-2e-5 the economic inefficiency can be seen from Figure 2.1.10 (with the capacitance 2e-5 F the required inductance is already 0.156 H). But in the networks with the small capacitance the functionality of the operated active power filter (if one is installed) can be expanded.

In order to obtain the current waveforms in steady state and in the transient process, the obtained equations should be determined analytically. The obtained equations can be found in the APPENDIX.

Figure 2.1.11 show time diagrams of the Laplace inverse transformation of the equations 5.1.4-5.1.6 in the APPENDIX for the fault mode without converter (the fault have occurs in 0.02 s).

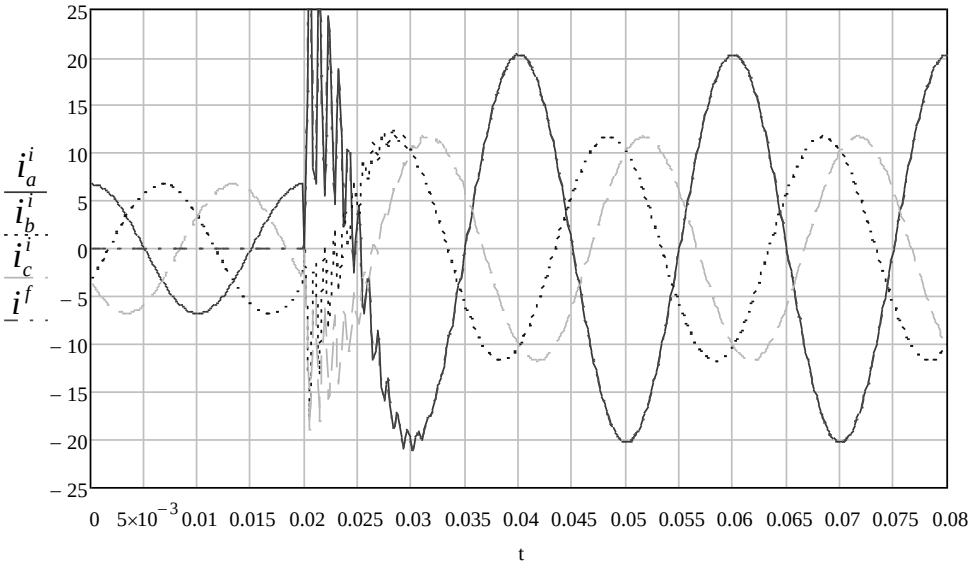

Figure 2.1.11 Networks currents in the fault mode and ground fault current

It can be seen from Figure 2.1.11 appearing the unsymmetrical currents after the ground fault. The mode without any loads was considered and the GF current is equal to the faulted phase current in this case. With the system capacitance growth the system asymmetry would increase. It could create the additional damage for the system equipment as well.

Figures 2.1.12, 2.1.13 show time diagrams of Laplace inverse transformation of the equations 5.1.7-5.1.9 in the APPENDIX for the fault mode with converter (the fault occurs in 0.02 s, the converter starts to operate in 0.055 s).

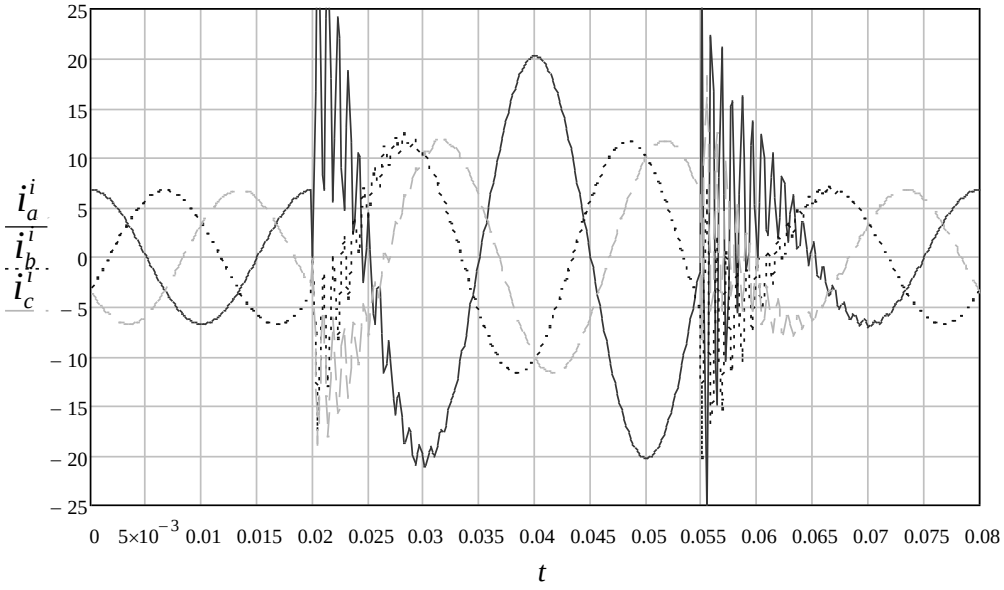

Figure 2.1.12 Converter grounded network currents in the fault mode

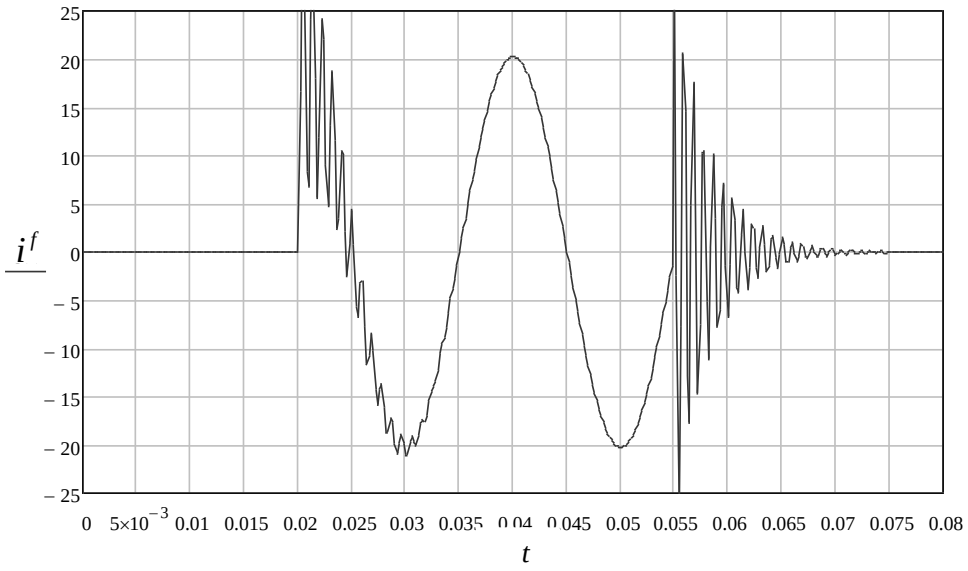

Figure 2.1.13 GF current with converter operating

After the converter has started to operate (in 0.055 s) the network currents become symmetrical as well as the GF current becomes zero.

2.2 Symmetrical component transformation

The best current and voltage control quality can be reached by the separation control system into three independent loops (positive, negative and zero). It allows reacting more sensitively to a load distortion. Controller limiting properties can be also improved. As it will be shown in Chapter 3 the negative and positive sequence controller should be used to compensate high frequency components as well.

To control the AEFCC, initially the symmetrical components are to be decomposed. The different decomposition techniques will be considered in this section.

Classical symmetrical component method

The classical symmetrical component method based on the representation of the any unsymmetrical system in the form of the symmetric components sum: the positive, the negative and the zero sequence [32, 33]. According to the method the voltage sequences can be determined as follows:

$$u_{abc} = \begin{bmatrix} u_a \\ u_b \\ u_c \end{bmatrix} = u^{+}_{abc} + u^{-}_{abc} + u^{0}_{abc}$$

$$\begin{bmatrix} u^{+}_a \\ u^{+}_b \\ u^{+}_c \end{bmatrix} = u^{+}_{abc} = \frac{1}{3}\begin{bmatrix} 1 & \underline{a} & \underline{a^2} \\ \underline{a^2} & 1 & \underline{a} \\ \underline{a} & \underline{a^2} & 1 \end{bmatrix} \cdot \begin{bmatrix} u_a \\ u_b \\ u_c \end{bmatrix} \tag{2.2.1}$$

$$\begin{bmatrix} u^{-}_a \\ u^{-}_b \\ u^{-}_c \end{bmatrix} = u^{-}_{abc} = \frac{1}{3}\begin{bmatrix} 1 & \underline{a^2} & \underline{a} \\ \underline{a} & 1 & \underline{a^2} \\ \underline{a^2} & \underline{a} & 1 \end{bmatrix} \cdot \begin{bmatrix} u_a \\ u_b \\ u_c \end{bmatrix}$$

$$\boldsymbol{u}^{0}_{\boldsymbol{abc}} = \begin{bmatrix} u^0 \\ u^0 \\ u^0 \end{bmatrix} = \frac{1}{3}\left(u_a + u_b + u_c\right) \tag{2.2.2}$$

The operator $\underline{a}$ in the equation 2.2.1 is 120° phase shifting operator. It can be defined as follows:

$$\begin{aligned} \underline{a} &= e^{j\cdot\frac{2\cdot\pi}{3}} \\ \underline{a^2} &= e^{-j\cdot\frac{2\cdot\pi}{3}} \end{aligned} \tag{2.2.3}$$

The operator $\underline{a}$ can be implemented by digital filters. It can be implemented using for example the first-order IIR (infinite impulse response) filter or the delay. The transfer function in z-domain can be written as follows:

$$H(z) = \frac{b_0 + b_1 \cdot z^{-1}}{1 + a_0 \cdot z^{-1}} \tag{2.2.4}$$

In order to obtain the effect of the phase-shifting by 120° and to have the gain close to 1 the following conditions are to be performed:

$$\begin{aligned} \mathrm{R}\left\{H\left[\exp\left(j\frac{2\cdot\pi\cdot f_0}{f_d}\right)\right]\right\} &= -\frac{1}{2} \\ \mathrm{I}\left\{H\left[\exp\left(j\frac{2\cdot\pi\cdot f_0}{f_d}\right)\right]\right\} &= \frac{\sqrt{3}}{2} \end{aligned} \tag{2.2.5}$$

To determine the coefficients b_0, b_1 and a_0 the following replacement in equations 2.2.4 should be performed:

$$z = \exp\left(j\frac{2\cdot\pi\cdot f_0}{f_d} \right) \tag{2.2.6}$$

After the transformation and separating into the real and the imaginary part the following equation system can be obtained:

$$\begin{cases} \dfrac{(a_1\cdot b_0 + b_1)\cdot\cos\left(\dfrac{2\cdot\pi\cdot f_0}{f_d}\right) + a_1\cdot b_1 + b_0}{1+2\cdot a_1\cdot\cos\left(\dfrac{2\cdot\pi\cdot f_0}{f_d}\right) + a^2{}_1} = -\dfrac{1}{2} \\ \dfrac{(a_1\cdot b_0 - b_1)\cdot\sin\left(\dfrac{2\cdot\pi\cdot f_0}{f_d}\right)}{1+2\cdot a_1\cdot\cos\left(\dfrac{2\cdot\pi\cdot f_0}{f_d}\right) + a^2{}_1} = \dfrac{\sqrt{3}}{2} \end{cases} \tag{2.2.7}$$

From equations 2.2.7 b_0, b_1 coefficients can be expressed:

$$b_0 = \frac{\sqrt{3}\cdot\left[a_1 + \cos\left(\dfrac{2\cdot\pi\cdot f_0}{f_d}\right)\right] - \sin\left(\dfrac{2\cdot\pi\cdot f_0}{f_d}\right)}{2\cdot\sin\left(\dfrac{2\cdot\pi\cdot f_0}{f_d}\right)} \tag{2.2.8}$$

$$b_1 = \frac{\sqrt{3}\cdot\left[1 + a_1\cdot\cos\left(\dfrac{2\cdot\pi\cdot f_0}{f_d}\right)\right] + a_1\cdot\sin\left(\dfrac{2\cdot\pi\cdot f_0}{f_d}\right)}{2\cdot\sin\left(\dfrac{2\cdot\pi\cdot f_0}{f_d}\right)} \tag{2.2.9}$$

Now the coefficient a_1 can be calculated. At the random frequency f_E the expression for the transfer function module, taking into account the equation 2.2.5, is:

$$|H(z)| = \sqrt{\frac{b_0^2 + 2\cdot b_0\cdot b_1\cdot\cos\left(\dfrac{2\cdot\pi\cdot f_E}{f_d}\right) + b_1^2}{1 + a_1\cdot 2\cdot\cos\left(\dfrac{2\cdot\pi\cdot f_E}{f_d}\right) + a_1^2}} \tag{2.2.10}$$

Further, the equation 2.2.10 should be squared and equated to 1. With the substitution of equations 2.2.8 and 2.2.9 the following expression for the coefficient a_1 can be obtained:

$$a_1 = \frac{2 \cdot \sqrt{3} \cdot \sin\left(\frac{2 \cdot \pi \cdot f_0}{f_d}\right) - 3}{3 \cdot \cos\left(\frac{2 \cdot \pi \cdot f_0}{f_d}\right) + \sqrt{3} \cdot \sin\left(\frac{2 \cdot \pi \cdot f_0}{f_d}\right)} \tag{2.2.11}$$

Taking into account the equation 2.2.11 equations 2.2.8, and 2.2.9 can be rewritten as follows:

$$b_0 = -\frac{2 \cdot \sqrt{3} \cdot \sin\left(\frac{2 \cdot \pi \cdot f_0}{f_d}\right) - 3}{3 \cdot \cos\left(\frac{2 \cdot \pi \cdot f_0}{f_d}\right) + \sqrt{3} \cdot \sin\left(\frac{2 \cdot \pi \cdot f_0}{f_d}\right)} \tag{2.2.12}$$

$$b_1 = -1 \tag{2.2.13}$$

Figure 2.2.1 shows the structural diagram of obtained algorithm.

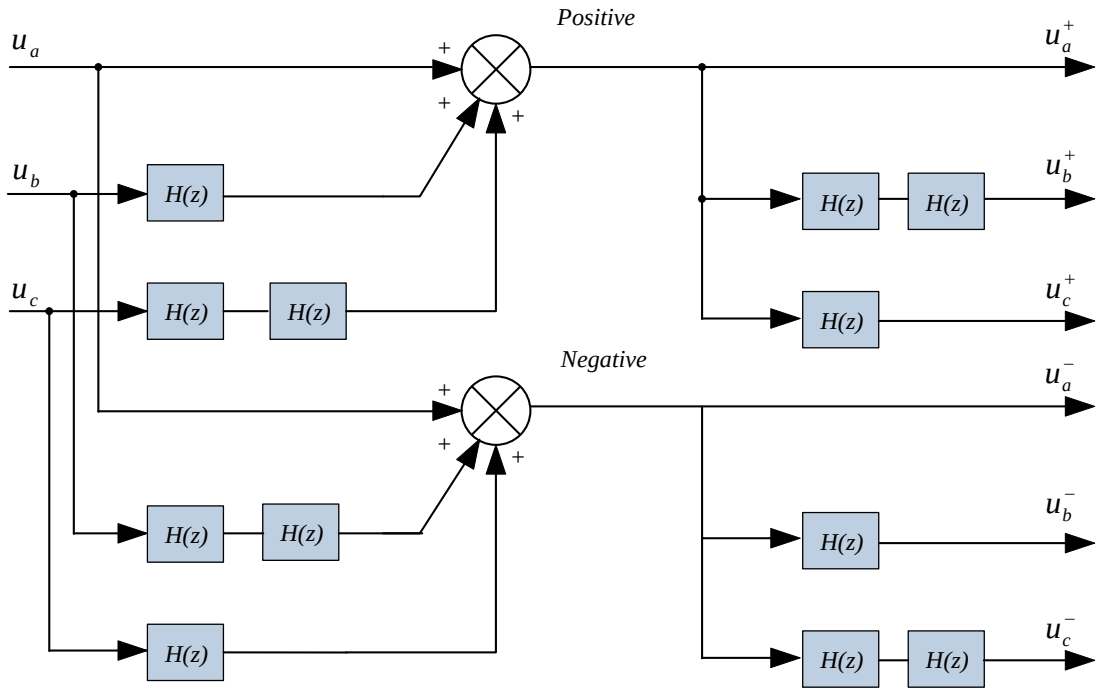

Figure 2.2.1 Structural diagram of the classical symmetrical component method

To confirm the developed algorithm Matlab/Simulink simulations are performed. The following unsymmetrical system was considered (Figure 2.2.2):

$$u_a = 130 \cdot \sin(\omega \cdot t)$$
$$u_b = 100 \cdot \sin\left(\omega \cdot t - \frac{2\pi}{3}\right) + 20 \cdot \sin\left(\omega \cdot t + \frac{2\pi}{3}\right) + 10 \cdot \sin(\omega \cdot t) \quad (2.2.14)$$
$$u_b = 100 \cdot \sin\left(\omega \cdot t + \frac{2\pi}{3}\right) + 20 \cdot \sin\left(\omega \cdot t - \frac{2\pi}{3}\right) + 10 \cdot \sin(\omega \cdot t)$$

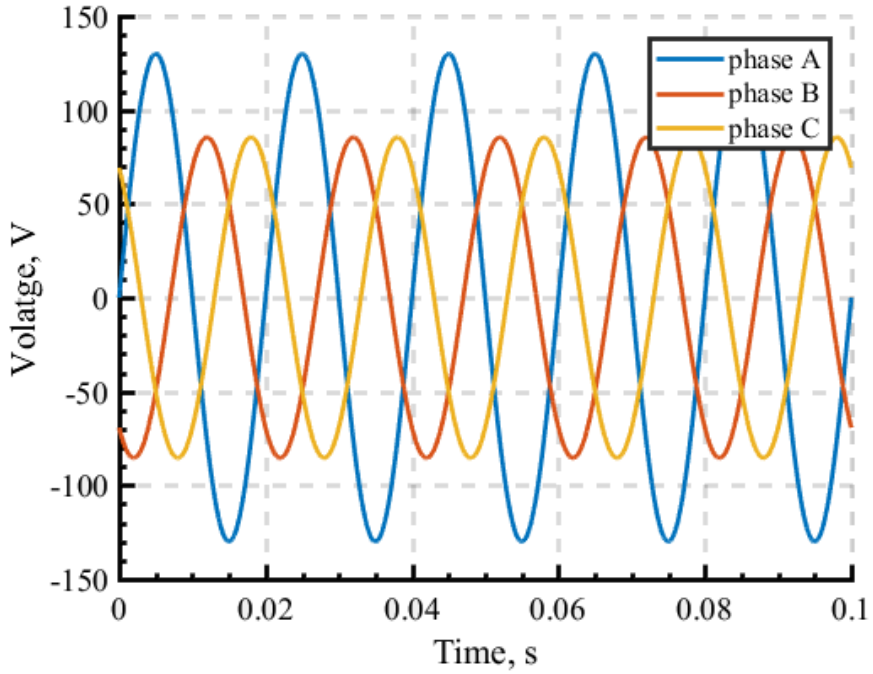

Figure 2.2.2 Initial unsymmetrical voltage system

Using the developed algorithm the following results have been obtained. Figures 2.2.3 – 2.2.5 show the extracted positive and negative sequence components.

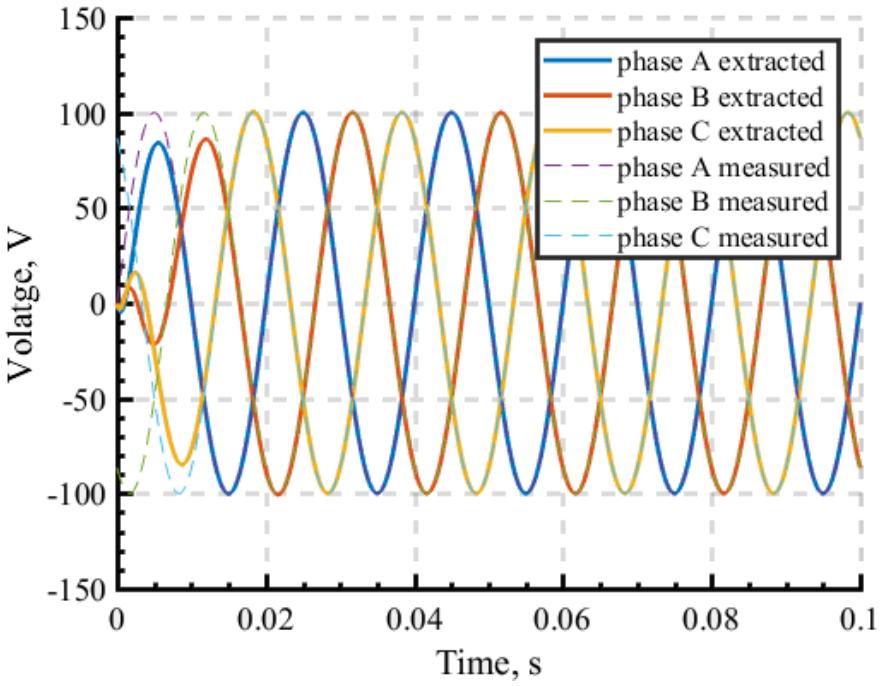

Figure 2.2.3 Positive sequence voltage components

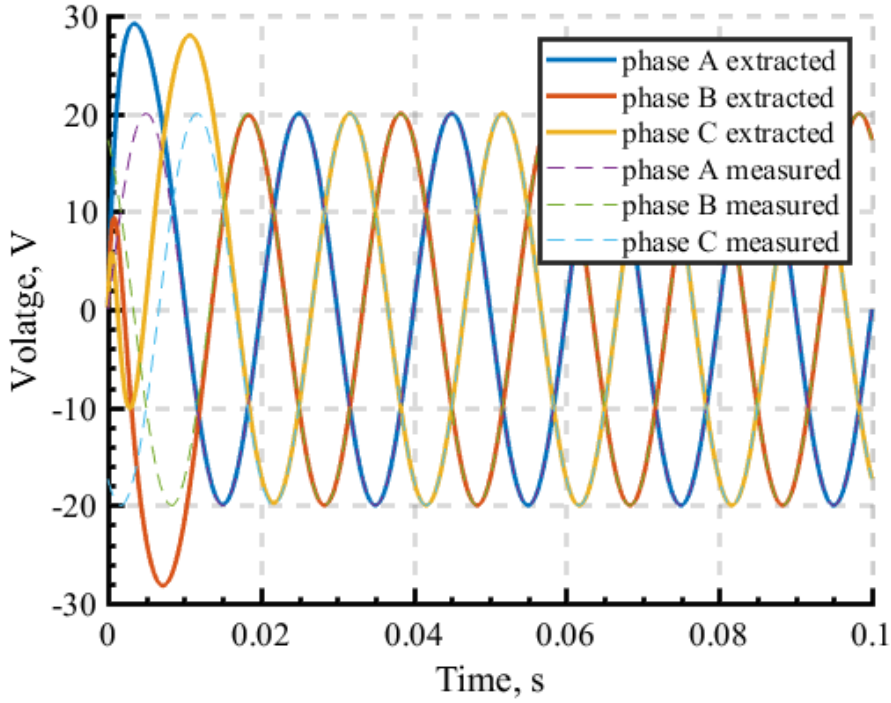

Figure 2.2.4 Negative sequence voltage components

The efficiency of the obtained algorithm can be seen from figures. This method shows relatively fast transient process but can be used only at main frequency. The large number of the filters to be used is the disadvantage as well. Therefore there are some restrictions of the method. It cannot be used to decompose system changing main frequency.

Generalized symmetrical component method

Similarly to the classical method for the three phase system the decomposition method for m-phase nonsinusoidal system can be considered [34, 35].

Let an initial arbitrary asymmetric m-phase electric quantity system be given by the vector $\boldsymbol{u}$ with components depending on v ($v = \omega_0 t$).

The functions belong to $L_2[0, 2\pi]$ space with the norm $\|u_i\| = \sqrt{\frac{1}{2\pi}\int_0^{2\pi} (u_i)^2 dv}$, respond the condition $\int_0^{2\pi} u_i \, dv = 0$ and have the limited frequency spectrum:

$$\boldsymbol{u} = \begin{bmatrix} u_1 & u_2 & \dots & u_{m-1} & u_m \end{bmatrix}^T \tag{2.2.15}$$

Then the generalized symmetrical component method allows representing the vector $\boldsymbol{u}$ as the following sum:

$$\boldsymbol{u} = \boldsymbol{u^0} + \boldsymbol{u}^+ + \boldsymbol{u}^- \tag{2.2.16},$$

where $\boldsymbol{u^0} = \begin{bmatrix} u^0 & u^0 & \dots & u^0 & u^0 \end{bmatrix}^T$ is the vector of quantities, forming the zero sequence system and consisting of m identical functions u^0;

$\boldsymbol{u}^+ = \begin{bmatrix} u_1^+ & u_2^+ & \dots & u_{m-1}^+ & u_m^+ \end{bmatrix}^T$ is the vector of quantities, forming the positive sequence system and consisting of functions u_i^+;

$\boldsymbol{u}^- = \begin{bmatrix} u_1^- & u_2^- & \dots & u_{m-1}^- & u_m^- \end{bmatrix}^T$ is the vector of quantities forming the negative sequence system consisting of functions u_i^-.

The positive and negative sequence vectors satisfy the following conditions:

$$\sum_{i=1}^{m} u_i^+ = 0, \quad u_i^+(v) = u_1^+[v - (i-1)2\pi/m],$$

$$\|u_i^+\| = \hat{U}^+, \quad (u_i^+, u_{i+1}^+) = \cos(2\pi/m);$$

$$\sum_{i=1}^{m} u_i^- = 0, \quad u_i^-(v) = u_1^-[v - (i-1)2\pi/m],$$

$$\|u_i^-\| = \hat{U}^-, \quad (u_i^-, u_{i+1}^-) = \cos(2\pi/m);$$

According to proposed in [36] geometric analogies, for decomposition algorithm development the analytical signal concept was used [37]. Representing from the initial asymmetric m-phase electric quantity system $\boldsymbol{E}$ the analytical signal by adding the Hilbert transform of $\boldsymbol{e}$ as the imaginary part:

$$\underline{\vec{\boldsymbol{u}}} = \boldsymbol{u} + j \cdot \boldsymbol{u}_{\boldsymbol{h}} \qquad (2.2.17),$$

where $\boldsymbol{u}_{\boldsymbol{h}} = \left[u_{1h} \quad u_{2h} \quad \ldots \quad u_{(m-1)h} \quad u_{mh}\right]^T$ is the Hilbert transform of $\boldsymbol{u}$.

The Hilbert transformation of $\boldsymbol{u}$ can be obtained as follows:

$$\begin{aligned} &\boldsymbol{u}_h = \mathrm{H}\{\boldsymbol{u}\} = \mathrm{H}\{\boldsymbol{u}^0 + \boldsymbol{u}^+ + \boldsymbol{u}^-\} = \mathrm{H}\{\boldsymbol{u}^0\} + \mathrm{H}\{\boldsymbol{u}^+\} + \mathrm{H}\{\boldsymbol{u}^-\} = \\ &\boldsymbol{u}_{\boldsymbol{h}}^{\boldsymbol{0}} + \boldsymbol{u}_{\boldsymbol{h}}^{+} + \boldsymbol{u}_{\boldsymbol{h}}^{-} \end{aligned} \qquad (2.2.18)$$

$$\mathrm{H}\{\boldsymbol{u}\} = \begin{bmatrix} \frac{1}{\pi}\int_{-\infty}^{\infty} \frac{\{\boldsymbol{u}\}}{v-\tau} d\tau & \ldots & 0 \\ 0 & \ldots & 0 \\ 0 & \ldots & \frac{1}{\pi}\int_{-\infty}^{\infty} \frac{\{\boldsymbol{u}\}}{v-\tau} d\tau \end{bmatrix} \qquad (2.2.19),$$

The analytical signal has the following properties:

$$\begin{cases} \|\boldsymbol{u}_{\boldsymbol{h}}\| = \|\boldsymbol{u}\|, \\ (\boldsymbol{u}_{\boldsymbol{h}}, \boldsymbol{u}) = 0, \\ \left\|\underline{\vec{\boldsymbol{u}}}\right\| = \sqrt{2}\|\boldsymbol{u}\|, \\ \boldsymbol{u} = \mathrm{R}\left(\underline{\vec{\boldsymbol{u}}}\right). \end{cases} \qquad (2.2.20)$$

The elements of the zero sequence vector and its Hilbert transform are expressed by:

$$\begin{aligned} &\underline{\vec{\boldsymbol{u}}}^{0} = \left[\boldsymbol{T}^0\right] \cdot \underline{\vec{\boldsymbol{u}}} \\ &\left[\boldsymbol{T}^0\right] = \left[1 \quad 1 \quad \ldots 1 \quad 1\right]/m \end{aligned} \qquad (2.2.21)$$

Or in the scalar form:

$$\underline{\vec{\boldsymbol{u}}}^{0} = \left[\underline{\vec{u}}^{0} \ldots \underline{\vec{u}}^{0}\right], \quad \underline{\vec{u}}^{0} = u^{0} + ju_{h}^{0}$$
$$u^{0} = \frac{1}{m}\sum_{1}^{m} u_{i}, \quad u_{h}^{0} = \frac{1}{m}\sum_{1}^{m} u_{ih} \tag{2.2.22}$$

The analytical signal concept can be considered as the symbolic method generalization. With the symbolic method sinusoidal signals can be represented by complex numbers. Thus, for the non-sinusoidal signals the classical symmetrical component method for the decomposition can be applied as follows:

$$\underline{\vec{\boldsymbol{u}}}^{+} = \left[\boldsymbol{T}^{+}\right] \cdot \underline{\vec{\boldsymbol{u}}}, \quad \underline{\vec{\boldsymbol{u}}}^{-} = \left[\boldsymbol{T}^{-}\right] \cdot \underline{\vec{\boldsymbol{u}}} \tag{2.2.23}$$

$$\left[\boldsymbol{T}^{+}\right] = \frac{1}{m} \cdot \begin{bmatrix} 1 & \underline{a} & \ldots & \underline{a}^{m-2} & \underline{a}^{m-1} \\ \underline{a}^{m-1} & 1 & \ldots & \underline{a}^{m-2} & \underline{a}^{m-2} \\ \ldots & \ldots & \ldots & \ldots & \ldots \\ \underline{a}^{2} & \underline{a}^{1} & \ldots & 1 & \underline{a} \\ \underline{a} & \underline{a}^{2} & \ldots & \underline{a}^{m-1} & 1 \end{bmatrix} \tag{2.2.24}$$

$$\left[\boldsymbol{T}^{-}\right] = \frac{1}{m} \cdot \begin{bmatrix} 1 & \underline{a}^{m-1} & \ldots & \underline{a}^{2} & \underline{a} \\ \underline{a} & 1 & \ldots & \underline{a}^{3} & \underline{a}^{2} \\ \ldots & \ldots & \ldots & \ldots & \ldots \\ \underline{a}^{m-2} & \underline{a}^{m-1} & \ldots & 1 & \underline{a} \\ \underline{a}^{m-1} & \underline{a}^{m-2} & \ldots & \underline{a} & 1 \end{bmatrix} \tag{2.2.25},$$

In the scalar form equations 2.2.23 can be rewritten as follows:

$$\underline{\vec{\boldsymbol{u}}}^{+} = \left[\underline{\vec{u}}_{1}^{+} \ldots \underline{\vec{u}}_{m}^{+}\right], \quad \underline{\vec{u}}_{i}^{+} = u_{i}^{+} + ju_{ih}^{+}$$
$$\underline{\vec{\boldsymbol{u}}}^{-} = \left[\underline{\vec{u}}_{1}^{-} \ldots \underline{\vec{u}}_{m}^{-}\right], \quad \underline{\vec{u}}_{i}^{-} = u_{i}^{-} + ju_{ih}^{-} \tag{2.2.26}$$

$$u_{i}^{+} = \frac{1}{m}\sum_{k=1}^{m} \underline{a}^{(k-i)} u_{k}, \quad u_{ih}^{+} = \frac{1}{m}\sum_{k=1}^{m} \underline{a}^{(k-i)} u_{kh},$$
$$u_{i}^{-} = \frac{1}{m}\sum_{k=1}^{m} \underline{a}^{-(k-i)} u_{k}, \quad u_{ih}^{-} = \frac{1}{m}\sum_{k=1}^{m} \underline{a}^{-(k-i)} u_{kh}. \tag{2.2.27}$$

The real parts of the symmetrical components (i.e. vectors $\boldsymbol{u^0}$, $\boldsymbol{u^+}$, $\boldsymbol{u^-}$) according to the equation 2.2.20 are defined as follows:

$$\boldsymbol{u^0} = \mathrm{R}\left(\underline{\vec{\boldsymbol{u^0}}}\right), \quad \boldsymbol{u^+} = \mathrm{R}\left(\underline{\vec{\boldsymbol{u^+}}}\right), \quad \boldsymbol{u^-} = \mathrm{R}\left(\underline{\vec{\boldsymbol{u^-}}}\right) \tag{2.2.26}$$

Considering the arbitrary 3-phase system (zero components are defined according to the equation 2.2.22) the following equations can be obtained:

$$\boldsymbol{u^{+-}} = \boldsymbol{u} - \boldsymbol{u^0} \tag{2.2.27}$$

$$\boldsymbol{u^{+-}} = \left[u_1^{+-} \quad u_2^{+-} \quad u_3^{+-}\right]^{\boldsymbol{T}} \tag{2.2.28}$$

$$u_{\boldsymbol{i}}^{+-} = u_{\boldsymbol{i}} - u^0 \tag{2.2.29}$$

$$\boldsymbol{u_h^{+-}} = \left[u_{1h}^{+-} \quad u_{2h}^{+-} \quad u_{3h}^{+-}\right]^{\boldsymbol{T}} \tag{2.2.30}$$

The voltage multiplied by the operator *a* can be expressed as follows:

$$\begin{aligned} u\left(v+\frac{2\pi}{3}\right) &= u(v)\cdot \underline{a} = u\cdot e^{j\cdot\frac{2\cdot\pi}{3}} = u\cdot e^{j\cdot\left(\frac{\pi}{6}+\frac{\pi}{2}\right)} = \\ &= u\cdot e^{j\cdot\frac{\pi}{2}}\left(\cos\frac{\pi}{6} + j\sin\frac{\pi}{6}\right) = \frac{\sqrt{3}}{2}\cdot u\cdot e^{j\cdot\frac{\pi}{2}} - \frac{1}{2}\cdot u = -\frac{1}{2}\cdot u + \frac{\sqrt{3}}{2}\cdot u_h \end{aligned} \tag{2.2.31}$$

Finally, taking into account equations 2.2.23-2.2.25 the positive and negative components of the a-b-c system can be expressed:

$$\begin{aligned} \begin{bmatrix} u_a^+ \\ u_b^+ \\ u_c^+ \end{bmatrix} &= \frac{1}{3}\begin{bmatrix} 1 & -\frac{1}{2} & -\frac{1}{2} \\ -\frac{1}{2} & 1 & -\frac{1}{2} \\ -\frac{1}{2} & -\frac{1}{2} & 1 \end{bmatrix}\cdot\begin{bmatrix} u_a^{+-} \\ u_b^{+-} \\ u_c^{+-} \end{bmatrix} - \frac{1}{2\sqrt{3}}\begin{bmatrix} 0 & 1 & -1 \\ -1 & 0 & 1 \\ 1 & -1 & 0 \end{bmatrix}\cdot\begin{bmatrix} u_{ah}^{+-} \\ u_{bh}^{+-} \\ u_{ch}^{+-} \end{bmatrix} \\ \begin{bmatrix} u_a^- \\ u_b^- \\ u_c^- \end{bmatrix} &= \frac{1}{3}\begin{bmatrix} 1 & -\frac{1}{2} & -\frac{1}{2} \\ -\frac{1}{2} & 1 & -\frac{1}{2} \\ -\frac{1}{2} & -\frac{1}{2} & 1 \end{bmatrix}\cdot\begin{bmatrix} u_a^{+-} \\ u_b^{+-} \\ u_c^{+-} \end{bmatrix} + \frac{1}{2\sqrt{3}}\begin{bmatrix} 0 & 1 & -1 \\ -1 & 0 & 1 \\ 1 & -1 & 0 \end{bmatrix}\cdot\begin{bmatrix} u_{ah}^{+-} \\ u_{bh}^{+-} \\ u_{ch}^{+-} \end{bmatrix} \end{aligned} \tag{2.3.32}$$

Applying the Clarke transformation to the positive sequence vector (2.3.32) and recalling that $u_{ah}^{+-} = \boldsymbol{j} \cdot u_a^{+-}$ one can obtain:

$$\underline{\vec{\boldsymbol{u}}_{\alpha\beta}^{+}} = \boldsymbol{u}_{abc}^{+} \cdot \left[\boldsymbol{T}_{\alpha\beta}\right] = \begin{bmatrix} \frac{1}{3} & -\frac{1}{6} & -\frac{1}{6} \\ -\frac{1}{6} & \frac{1}{3} & -\frac{1}{6} \\ -\frac{1}{6} & -\frac{1}{6} & \frac{1}{3} \end{bmatrix} \cdot \begin{bmatrix} u_a^{+-} \\ u_b^{+-} \\ u_c^{+-} \end{bmatrix} \cdot \begin{bmatrix} \frac{2}{3} & -\frac{1}{3} & -\frac{1}{3} \\ 0 & \frac{\sqrt{3}}{3} & -\frac{\sqrt{3}}{3} \end{bmatrix} -$$

$$-\frac{j}{2\sqrt{3}} \begin{bmatrix} 0 & 1 & -1 \\ -1 & 0 & 1 \\ 1 & -1 & 0 \end{bmatrix} \cdot \begin{bmatrix} u_a^{+-} \\ u_b^{+-} \\ u_c^{+-} \end{bmatrix} \cdot \begin{bmatrix} \frac{2}{3} & -\frac{1}{3} & -\frac{1}{3} \\ 0 & \frac{\sqrt{3}}{3} & -\frac{\sqrt{3}}{3} \end{bmatrix} = \tag{2.3.33}$$

$$= \begin{bmatrix} \left(\frac{u_a^{+-}}{3} - \frac{u_b^{+-}}{6} - \frac{u_c^{+-}}{6}\right) - j \cdot \left(\frac{\sqrt{3}}{6} u_b^{+-} - \frac{\sqrt{3}}{6} u_c^{+-}\right) \\ j \cdot \left(\frac{u_a^{+-}}{3} - \frac{u_b^{+-}}{6} - \frac{u_c^{+-}}{6}\right) + \left(\frac{\sqrt{3}}{6} u_b^{+-} - \frac{\sqrt{3}}{6} u_c^{+-}\right) \end{bmatrix}$$

One can see that the expressions in brackets can be considered as α-β components for the initial quantities $\boldsymbol{u}_{\boldsymbol{abc}}^{+-}$ without the zero sequence. Considering this the following equations can be obtained:

$$\underline{\vec{\boldsymbol{u}}_{\alpha\beta}^{+}} = \frac{1}{2} \begin{bmatrix} u_\alpha^{+-} - j \cdot u_\beta^{+-} \\ j \cdot u_\alpha^{+-} + u_\beta^{+-} \end{bmatrix} = \frac{1}{2} \begin{bmatrix} u_\alpha^{+-} - u_{\beta h}^{+-} \\ u_{\alpha h}^{+-} + u_\beta^{+-} \end{bmatrix} \tag{2.3.34}$$

Transforming the negative sequence vector:

$$\underline{\vec{\boldsymbol{u}}_{\alpha\beta}^{-}} = \boldsymbol{u}_{abc}^{-} \cdot \left[\boldsymbol{T}_{\alpha\beta}\right] = \begin{bmatrix} \frac{1}{3} & -\frac{1}{6} & -\frac{1}{6} \\ -\frac{1}{6} & \frac{1}{3} & -\frac{1}{6} \\ -\frac{1}{6} & -\frac{1}{6} & \frac{1}{3} \end{bmatrix} \cdot \begin{bmatrix} u_a^{+-} \\ u_b^{+-} \\ u_c^{+-} \end{bmatrix} \cdot \begin{bmatrix} \frac{2}{3} & -\frac{1}{3} & -\frac{1}{3} \\ 0 & \frac{\sqrt{3}}{3} & -\frac{\sqrt{3}}{3} \end{bmatrix} +$$

$$+\frac{j}{2\sqrt{3}} \begin{bmatrix} 0 & 1 & -1 \\ -1 & 0 & 1 \\ 1 & -1 & 0 \end{bmatrix} \cdot \begin{bmatrix} u_a^{+-} \\ u_b^{+-} \\ u_c^{+-} \end{bmatrix} \cdot \begin{bmatrix} \frac{2}{3} & -\frac{1}{3} & -\frac{1}{3} \\ 0 & \frac{\sqrt{3}}{3} & -\frac{\sqrt{3}}{3} \end{bmatrix} = \tag{2.3.35}$$

$$= \frac{1}{2} \begin{bmatrix} u_\alpha^{+-} + j \cdot u_\beta^{+-} \\ - j \cdot u_\alpha^{+-} + u_\beta^{+-} \end{bmatrix}$$

$$\underline{\vec{\boldsymbol{u}}^{+}_{\alpha\beta}} = \frac{1}{2}\begin{bmatrix} u^{+-}_{\alpha} - u^{+-}_{\beta h} \\ u^{+-}_{\alpha h} + u^{+-}_{\beta} \end{bmatrix}$$
$$\underline{\vec{\boldsymbol{u}}^{-}_{\alpha\beta}} = \frac{1}{2}\begin{bmatrix} u^{+-}_{\alpha} + u^{+-}_{\beta h} \\ u^{+-}_{\beta} - u^{+-}_{\alpha h} \end{bmatrix} \qquad (2.3.36)$$

Equations 2.3.34 and 2.3.36 can simplify the transformation into the positive and negative sequences. Only two Hilbert filters are required to obtain the $u^{+-}_{\alpha h}$ and $u^{+-}_{\beta h}$ signals compared to the previous method. The positive sequence component could be used as PLL as well. It will be considered in the next section.

The method described could be applied in a specific frequency range of interest where the Hilbert transform is performed. The range is defined by the Hilbert filter bandwidth had been selected beforehand.

Hilbert filter synthesis

There are some situations, where the real and imaginary parts of Fourier transform related to each other by the Hilbert transform [38]. The Hilbert transform is important in the signal processing as well, where it derives the analytic representation of a real-valued signal. Let the signal $s(t)$ with existing a nonzero orthogonal complement $s_h(t)$ related by:

$$\int_{-\infty}^{\infty} s(t) \cdot s_h(t) \cdot dt = 0 \qquad (2.2.37)$$

The Hilbert transform allows to determine the orthogonal complement by:

$$s_h(t) = \int_{-\infty}^{\infty} \frac{s(\tau)}{\pi \cdot (t-\tau)} d\tau \qquad (2.2.38)$$

It can be seen the Hilbert transform being the convolution of the signal $s(t)$ with the function $h(t) = 1/(\pi t)$. The function $h(t)$ is the impulse response of the linear filter creating the orthogonal component of the input signal. The frequency response of the Hilbert filter can be obtained applying the Fourier transform on the function $h(t)$:

$$H(j\omega) = \int_{-\infty}^{\infty} \frac{1}{\pi \cdot t} \cdot e^{-j \cdot \omega \cdot t} dt = -j \cdot sign(\omega) \qquad (2.3.39)$$

Thus, the frequency response defined by:

$$H(j\omega)=\begin{cases} j, & for\,\omega<0 \\ -j, & for\,\omega>0 \end{cases} \tag{2.2.40}$$

It follows from the equation 2.2.40, having the Hilbert filter the effect of shifting the phase of the negative frequency components by +90° and the phase of the positive frequency components by −90°.

The impulse response of the Hilbert filter in accordance with the equation 2.2.40 is expressed by:

$$h(n)=\frac{1}{2\pi}\int_{-\pi}^{0} j\cdot e^{j\omega n}d\omega-\frac{1}{2\pi}\int_{0}^{\pi} j\cdot e^{j\omega n}d\omega= \\ =\begin{cases} \frac{2}{\pi}\cdot\frac{\sin^2(\pi\cdot n/2)}{n}, n>0 \\ 0, \quad n<0 \end{cases} \tag{2.2.41}$$

However, these ideal systems cannot be realized since the impulse response is non-causal. Nevertheless, the approximation of the Hilbert filter can be obtained. In this section some approximation techniques for using in converter control systems will be considered. First some requirements and assumptions are to be imposed. Currently various PWM techniques are used to produce the sinusoidal output voltage and current. At the output of the converter the filter is used to obtain the first current and voltage harmonic. However, the output current and voltages still contain high harmonics which are processed in the control system including the Hilbert filter. Thus, the Hilbert filter should have the phase and magnitude stability at the main frequency. It means having constant phase shift and gain close to 1. Having gain close to 1 at the high frequencies is required as well.

Hilbert transformers can be designed either as Finite Impulse Response (FIR) or as Infinite Impulse Response (IIR) digital filters. FIR Hilbert transformers perform the magnitude approximation and can have the exact linear phase with the stability guaranteed. The simples Hilbert filter design method is truncating the impulse response to finite length. The Hilbert filter transfer function in this case is expressed as follows:

$$H(z)=\sum_{n=0}^{N-1} h(n)\cdot z^{-n} \tag{2.2.42},$$

where N is the filter order.

However while truncating the frequency response ripples appeared known as Gibbs phenomena. Using the windowing method it can be avoided. This method uses the truncating by applying a window. By retaining the central section of the impulse response in this truncation, the linear phase FIR filter can be obtained. The impulse response can be expressed by the product of the Hilbert filter impulse response (equation 2.2.41) and the window:

$$H(n) = h(n) \cdot w(n) \tag{2.2.43}$$

There are following most commonly used windows:

$$w(n) = \begin{cases} 1, \ for \quad -(\frac{N-1}{2}) \le n \le \frac{N-1}{2} \\ 0, \ for \ another \ n \end{cases} \tag{2.2.44}$$

$$w(n) = \begin{cases} \alpha + (1-\alpha) \cdot \cos(\frac{2\pi n}{N}), \ for \quad -(\frac{N-1}{2}) \le n \le \frac{N-1}{2} \\ 0, \ for \ another \ n \end{cases} \tag{2.2.45}$$

$$w(n) = \begin{cases} 0.42 - 0.5 \cdot \cos(\frac{2\pi n}{N}) + 0.08 \cdot \cos(\frac{4\pi n}{N}), \ for \quad -(\frac{N-1}{2}) \le n \le \frac{N-1}{2} \\ 0, \ for \ another \ n \end{cases} \tag{2.2.46}$$

The equation 2.2.44 is the rectangular window, 2.2.45 is the Hann window when α=0.5 and the Hamming window when α=0.54, 2.2.46 is the Blackman window. Figure 2.2.5 shows the frequency responses of the 31-oreder Hilbert filter using different window types (equations 2.2.44-2.2.46).

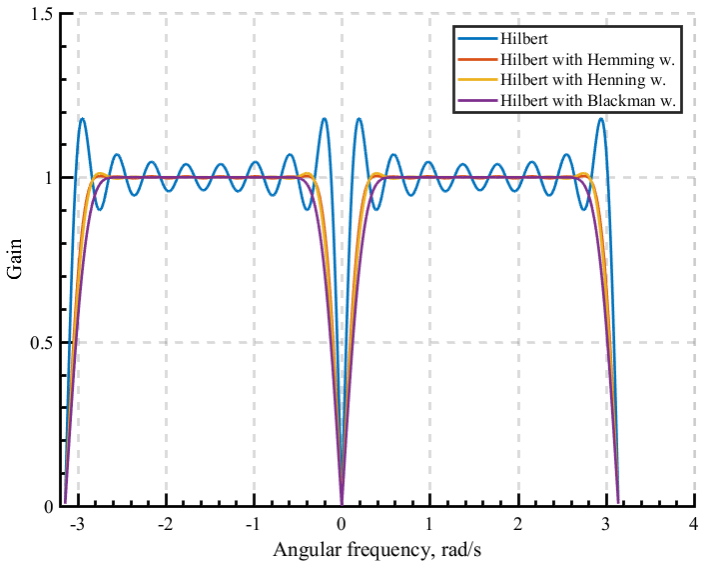

Figure 2.2.5 Frequency responses of 31-oreder Hilbert filter using different window types

It can be seen, that the optimal frequency response has the Hamming window in terms of the gain. However in terms of Chebyshev criteria the windowing method is not optimal due to the fact that the maximal approximation error is not minimized. Thus there is the optimal filter design method with the minimax error. The optimal filter synthesis is implemented by using Remez algorithm [33]. Matlab/Fdatool can be used for the synthesis due to the method complexity. Figure 2.2.6 shows the filter frequency responses with the different order have been designed using Remez algorithm. The all filters are designed for the 50 Hz main frequency component with the band-pass up to 19 harmonic (950 Hz).

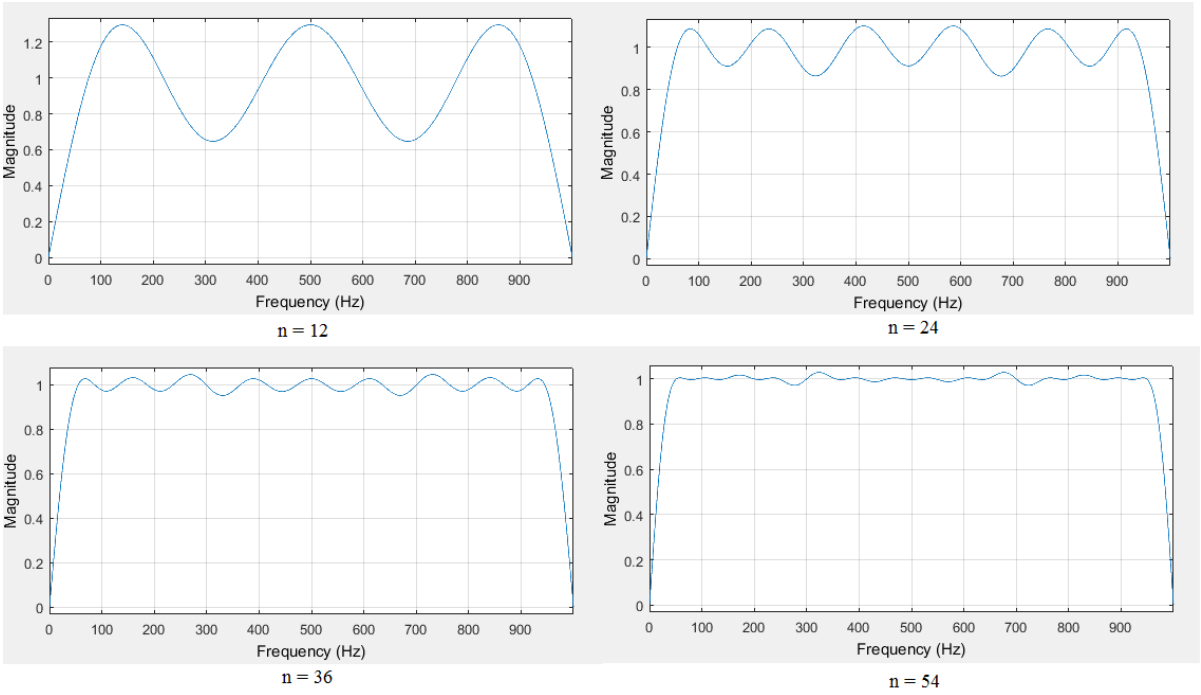

Figure 2.2.6 Hilbert filters frequency responses with the different order

It can be seen that for n>24 the acceptable quality can be achieved. However, in each case the individual approach is required. The harmonic spectrum, the available tools for the design and implementation are to be analyzed. In some cases first the Butterworth filter is to be used to reduce the Hilbert filter order.

The IIR filter (equation 2.2.4) can be applied in systems with the stable main frequency. The IIR Hilbert transformer performs the phase approximation. It means that the phase response of the system is approximated to the desired values in the given range of frequencies. The magnitude response allows passing all the frequencies, with the magnitude obtained around the desired value within the given tolerance [34].

The 2-order Hilbert filter (equation 2.2.4) is used as the example. According to the method described above, to obtain the effect of shifting the phase-angle by 90 degree and having gain close to 1 at the frequency f_0 the following conditions are to be performed:

$$\begin{aligned} \mathrm{R}\left\{H\left[\exp\left(j\frac{2\cdot\pi\cdot f_0}{f_d}\right)\right]\right\}&=0\\ \mathrm{I}\left\{H\left[\exp\left(j\frac{2\cdot\pi\cdot f_0}{f_d}\right)\right]\right\}&=1 \end{aligned} \tag{2.2.47}$$

After the transformation and separating into the real and the imaginary parts the following equation system can be obtained:

$$\begin{cases} \dfrac{(a_1\cdot b_0+b_1)\cdot\cos\left(\dfrac{2\cdot\pi\cdot f_0}{fd}\right)+a_1\cdot b_1+b_0}{1+a_1\cdot 2\cdot\cos\left(\dfrac{2\cdot\pi\cdot f_0}{fd}\right)+a_1^2}=0\\ \dfrac{(a_1\cdot b_0-b_1)\cdot\sin\left(\dfrac{2\cdot\pi\cdot f_0}{fd}\right)}{1+a_1\cdot 2\cdot\cos\left(\dfrac{2\cdot\pi\cdot f_0}{fd}\right)+a_1^2}=1 \end{cases} \tag{2.2.48}$$

From the equation 2.2.48 b_0, b_1 coefficients can be expressed as:

$$\begin{cases} b_0=-\cot\left(\dfrac{2\cdot\pi\cdot f_0}{fd}\right)-a_1\cdot\sin^{-1}\left(\dfrac{2\cdot\pi\cdot f_0}{fd}\right)\\ b_1=a_1\cdot\cot\left(\dfrac{2\cdot\pi\cdot f_0}{fd}\right)+\sin^{-1}\left(\dfrac{2\cdot\pi\cdot f_0}{fd}\right) \end{cases} \tag{2.2.49}$$

For the random frequency f_E after writing the expression for the transfer function module and equating it to 1, with taking into account the equation 2.2.49, for the a_1 coefficient the following expression can be obtained:

$$a_1=\frac{\sin\left(\dfrac{2\cdot\pi\cdot f_0}{f_d}\right)-1}{\cos\left(\dfrac{2\cdot\pi\cdot f_0}{f_d}\right)} \tag{2.2.50}$$

And after substituting the equation 2.2.50 into 2.2.49:

$$\begin{aligned} b_0&=a_1\\ b_1&=1 \end{aligned} \tag{2.2.51}$$

To verify the filter efficiency the signal with high frequency harmonics was used. Figure 2.2.7 shows signals at the filter input and output.

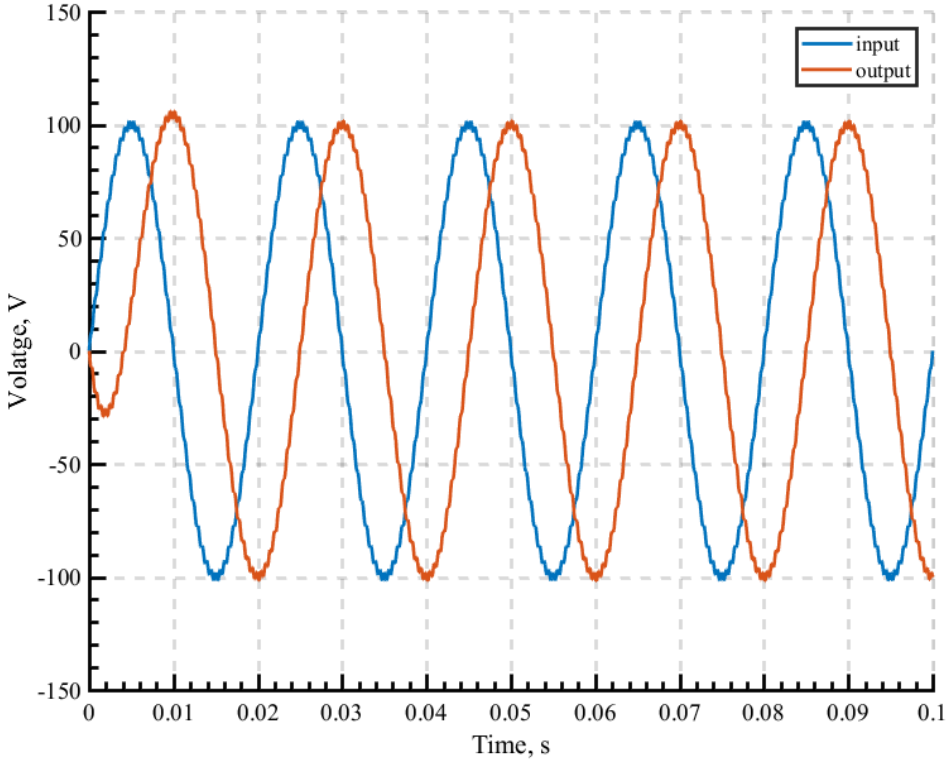

Figure 2.2.7 Input and output of the Hilbert filter

It can be seen from Figure 2.2.7 that the phase shift between the input and the output is -90°. Thus, the filter designed can be used for the symmetrical component decomposition in the systems with the stable main frequency.

It should be noticed that the power distribution system can be considered as the system with the stable frequency (49 – 51 Hz). Then, the obtained filter characteristics should be examined. The amplitude response and the frequency response can be obtained as follows:

$$\begin{aligned} |\mathrm{H}(\omega)| &= \left|\mathrm{H}\left(e^{j\omega}\right)\right| = \sqrt{\left(\mathrm{I}\left(\mathrm{H}\left(e^{j\omega}\right)\right)\right)^2 + \left(\mathrm{R}\left(\mathrm{H}\left(e^{j\omega}\right)\right)\right)^2} \\ \Phi(\omega) &= \arg\left(\mathrm{H}\left(e^{j\omega}\right)\right) = arctg\left(\frac{\mathrm{I}\left(\mathrm{H}\left(e^{j\omega}\right)\right)}{\mathrm{R}\left(\mathrm{H}\left(e^{j\omega}\right)\right)}\right) \end{aligned} \qquad (2.2.51)$$

According to the equation 2.2.51 the amplitude and the frequency response can be obtained. Figure 2.2.8 show the responses.

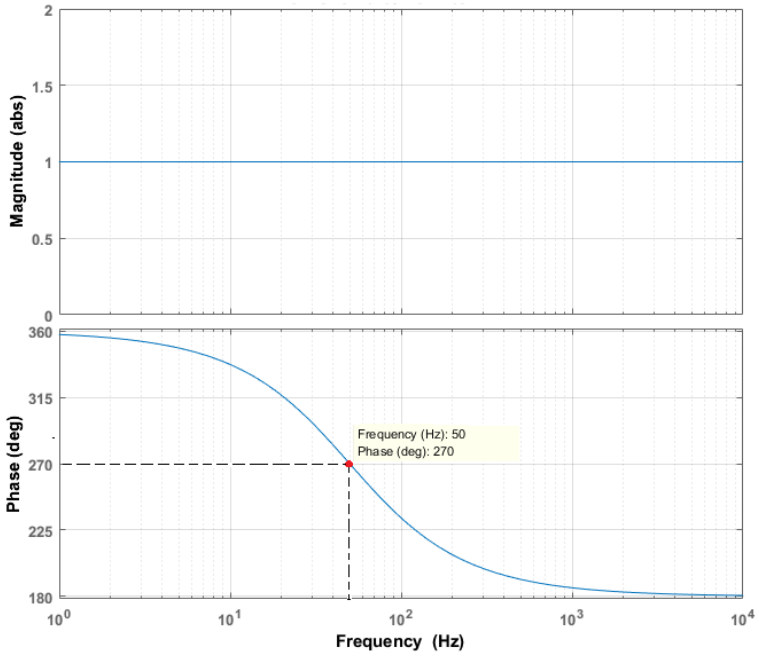

Figure 2.2.8 Amplitude and frequency responses of the Hilbert filter

It can be seen from Figure 2.2.8 being the gain equal to 1 and the phase response is acceptable. While the frequency is being changed within 49-51 Hz the filter phase shift is changed within 268 -272 degrees. The stability of the whole control system will be examined later.

The whole transformation algorithm is depicted in Figure 2.2.9.

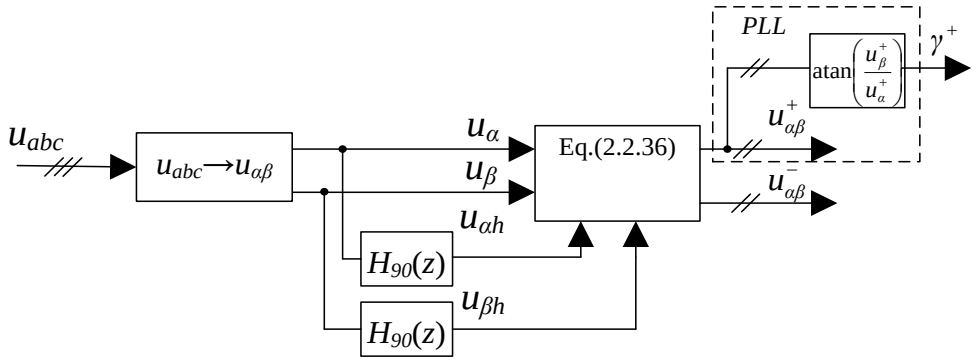

Figure 2.2.9 Transformation algorithm into the positive and negative sequence

To verify the generalized symmetrical component method the same unsymmetrical voltage system as for the classical method was used (equation 2.2.14).

Figures 2.2.10 and 2.2.11 show the estimated positive and negative sequence components respectively.

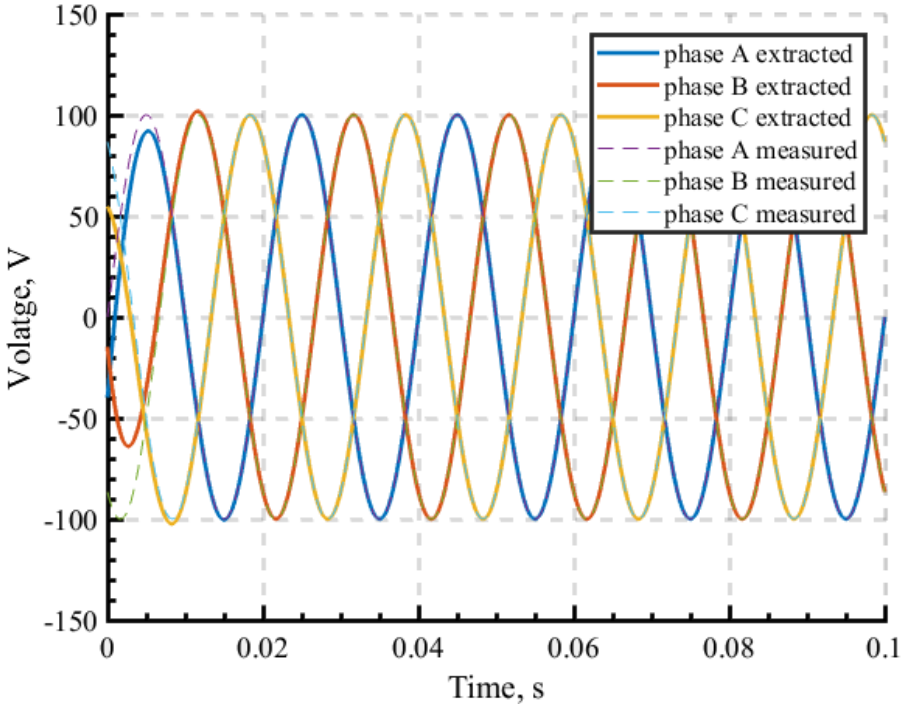

Figure 2.2.10 Positive sequence voltage components

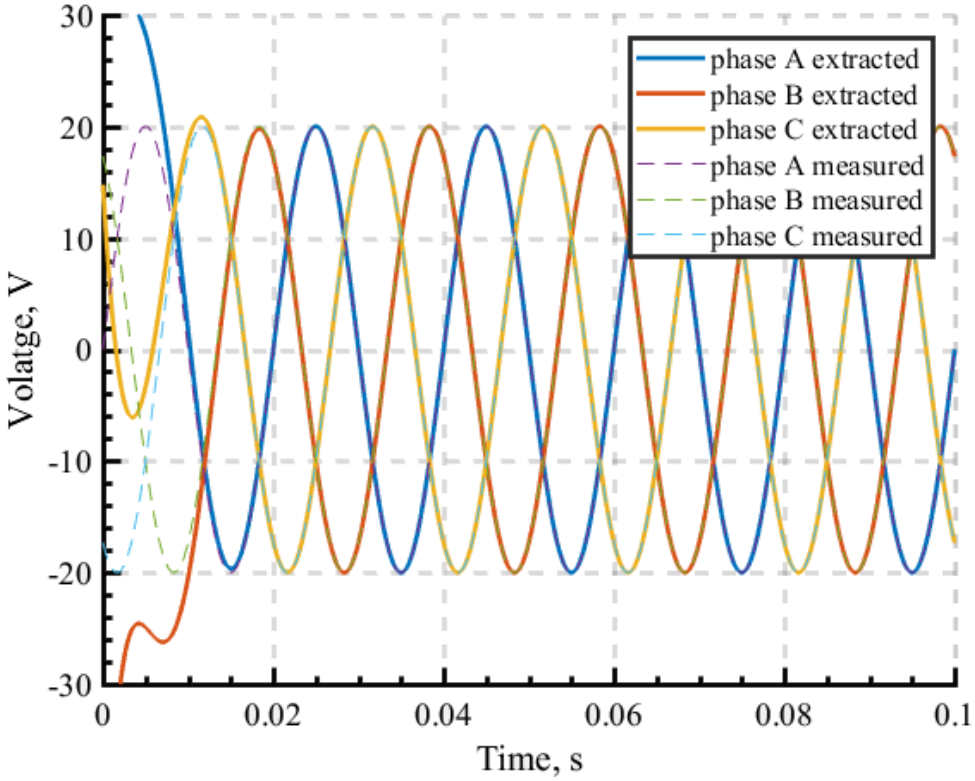

Figure 2.2.11 Negative sequence voltage components

It can be seen from figures that generalized symmetrical component method can be used for decomposition.

Section conclusions and recommendations

1) The analytical expressions for the mathematical network model in α-β-0 domain in the different operating modes are obtained.

2) With the high capacitance values the network currents could be unbalanced and affect the supply and load transformers.

3) The ground fault current could not be compensated accurately due to the ASC control discreteness and its resonance dependency on the coil inductance.

4) The ground fault current cannot be measured directly due to the absence of the connection between the system ground and the neutral point. The zero sequence current cannot be calculated by measuring the network currents as well.

5) The total converter power could be decreased by the joint use of the AEFCC and ASC already installed. At the same time the ground fault compensation quality could be improved due to the converter features.

6) The AEFCC has to be able to control the zero current. The positive and negative currents control can allow the converter use as the active power filter or STATCOM and to improve the control quality.

7) The classical symmetrical component method is computationally more complex. And it has the one disadvantage being able to operate only with the main harmonic. This disadvantage imposes some restrictions on the use in the systems with the floating frequency and limited microprocessor capacity.

8) The generalized symmetrical component method is multipurpose in terms of the input harmonic composition. It is simpler compared to the classical method besides the Hilbert filter realization. While using the generalized components method a specific frequency range of interest to be decomposed can be selected.

9) Before the Hilbert filter synthesizing, first the filter structure (IIR or FIR) has to be selected. It depends on the system operated with and the microprocessor capacity. Then the order and the band-pass restrictions are to be imposed.

10) It is recommended to use the IIR filter in power generation systems with the stable frequency and the FIR filter in systems with floating frequency.

11) The power distribution system can be considered as the system with the stable frequency. Thus the obtained IIR filter can be used for the control algorithm.

CHAPTER 3. POWER CONVERTER CONTROL

Modern converter control systems are built in constant values. To convert three-phase sinusoidal values Park and Clark transformations are used. It allows to obtain the reduced number of controllers with the astatic regulation and the zero error in steady state.

The equivalent circuit transformation of the converter into *d-q-0* domain will be considered in this chapter to synthesize the converter control algorithms. Further the high frequency harmonic equivalent circuit of the network will be considered and its influence on the GF current. The algorithm to determine the ground fault current value will be developed as well. The modes controller is introduced, which allows switching between different network modes, including the fault.

The chapter closes with the conclusions and recommendations.

3.1. Current loops design

Zero sequence dq-transform

To define the AC zero component the equation 2.2.2 can be used for the three-phase system. However, to transform the zero signal into *α-β-0* domain at least two signals are required. It can be performed using the analytical signal notion and the Hilbert transform. The zero sequence component u^0 can be represented as a *α-β-0* pseudo space vector as follows:

$$\underline{\vec{u}^0_{\alpha\beta}} = u^0 + j \cdot u^0_h \tag{3.1.1}$$

Further the input signal can be considered as the *α*-component and its Hilbert transform as the *β*-component. Thus, the equation 3.1.1 can be transformed into the *d-q-0* reference frame as follows:

$$\begin{aligned} \underline{\vec{u}^0_{dq}} &= \underline{\vec{u}^0_{\alpha\beta}} \cdot e^{-j\cdot\gamma^0} \\ \gamma^0 &= \operatorname{atan}\left(\frac{u^0_\beta}{u^0_\alpha}\right) \end{aligned} \tag{3.1.2}$$

Obtaining the zero *dq* signals the controller can be designed.

Positive and negative sequence

In order to synthesize the control algorithm, the equivalent converter circuit shown in Figure 3.1.1 is used (it is based on Figure 2.1.6). The converter can be considered as three ideal voltage sources without high harmonic components with the LR filter. It is supposed that during one switching period the converter voltages are constant.

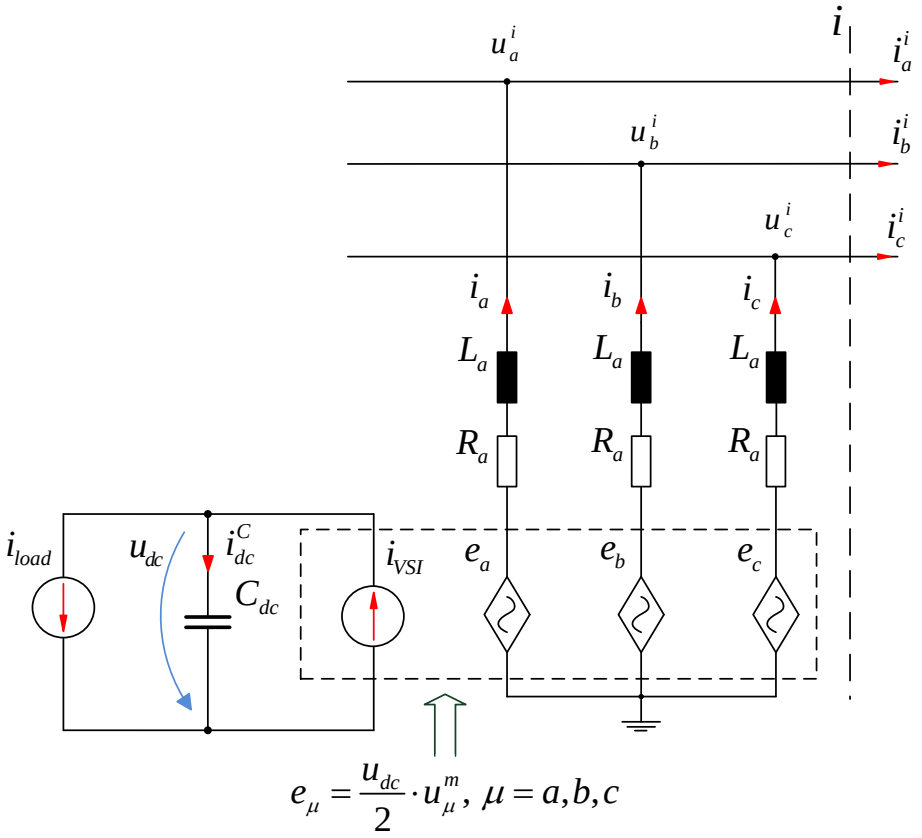

Figure 3.1.1 Equivalent converter circuit

The following equation system can be written for this circuit:

$$\begin{cases} e_a = i_a \cdot R + L \cdot \dot{i}_a + u_a^i \\ e_b = i_b \cdot R + L \cdot \dot{i}_b + u_b^i \\ e_c = i_c \cdot R + L \cdot \dot{i}_c + u_c^i \end{cases} \tag{3.1.3}$$

The equation 2.3.3) can be written in the matrix form:

$$\boldsymbol{e} - \boldsymbol{i} \cdot [\boldsymbol{R}] - \dot{\boldsymbol{i}} \cdot [\boldsymbol{L}] = \boldsymbol{u}^{\boldsymbol{i}} \tag{3.1.4}$$

On the basis of the equation 2.3.4 the following equations can be written for the positive, negative and zero sequence:

$$\begin{cases} \boldsymbol{e}^{+} - \boldsymbol{i}^{+} \cdot \left[\boldsymbol{R}^{+} \right] - \dot{\boldsymbol{i}}^{+} \cdot \left[\boldsymbol{L}^{+} \right] = \boldsymbol{u}^{\boldsymbol{i}+} \\ \boldsymbol{e}^{-} - \boldsymbol{i}^{-} \cdot \left[\boldsymbol{R}^{-} \right] - \dot{\boldsymbol{i}}^{-} \cdot \left[\boldsymbol{L}^{-} \right] = \boldsymbol{u}^{\boldsymbol{i}-} \\ \boldsymbol{e}^{0} - \boldsymbol{i}^{0} \cdot \left[\boldsymbol{R}^{0} \right] - \dot{\boldsymbol{i}}^{0} \cdot \left[\boldsymbol{L}^{0} \right] = \boldsymbol{u}^{\boldsymbol{i}0} \end{cases} \tag{3.1.5}$$

First, the positive sequence equation *dq*-transform is considered. Initially αβ-transform is to be performed. The first equation 3.1.5 should be multiplied by the transformation matrix $\left[\boldsymbol{T}_{\alpha\beta}\right]$ (without considering zero sequence) as in equations 2.1.5 and 2.1.6:

$$\boldsymbol{e}^{+} \cdot \left[\boldsymbol{T}_{\alpha\beta} \right] - \boldsymbol{i}^{+} \cdot \left[\boldsymbol{T}_{\alpha\beta} \right] \cdot \left[R^{+} \right] \cdot \left[\boldsymbol{T}_{\alpha\beta} \right] \cdot \left[\boldsymbol{T}_{\alpha\beta} \right]^{-1} - \dot{\boldsymbol{i}}^{+} \cdot \left[\boldsymbol{T}_{\alpha\beta} \right] \cdot \left[\boldsymbol{L}^{+} \right] \cdot \left[\boldsymbol{T}_{\alpha\beta} \right] \cdot \left[\boldsymbol{T}_{\alpha\beta} \right]^{-1} = \boldsymbol{u}^{i+} \cdot \left[\boldsymbol{T}_{\alpha\beta} \right]$$

$$\left[\boldsymbol{T}_{\alpha\beta} \right] = \begin{bmatrix} \frac{2}{3} & -\frac{1}{3} & -\frac{1}{3} \\ 0 & \frac{\sqrt{3}}{3} & -\frac{\sqrt{3}}{3} \end{bmatrix} \tag{3.1.6}$$

After transformation of the equation 3.1.6 the following can be obtained:

$$\boldsymbol{e}^{+}_{\alpha\beta} - \boldsymbol{i}^{+}_{\alpha\beta} \cdot \left[\boldsymbol{R}^{+}_{\alpha\beta} \right] - \dot{\boldsymbol{i}}^{+}_{\alpha\beta} \cdot \left[\boldsymbol{L}^{+}_{\alpha\beta} \right] = \boldsymbol{u}^{i+}_{\alpha\beta} \tag{3.1.7}$$

Further, the *dq*-transformation is used. The equation 3.1.7 has to be multiplied by the following transformation matrix:

$$\left[\boldsymbol{T}^{+}_{dq} \right] = \begin{bmatrix} \cos\left(\gamma^{+}(t)\right) & \sin\left(\gamma^{+}(t)\right) \\ -\sin\left(\gamma^{+}(t)\right) & \cos\left(\gamma^{+}(t)\right) \end{bmatrix} \tag{3.1.8},$$

$$\gamma^{+}(t) = \frac{u^{i+}_{\beta}}{u^{i+}_{\alpha}}$$

where $\gamma^{+}(t)$ is the positive sequence instantaneous angle of the network ($\boldsymbol{u}_{\alpha\beta}^{i+}$).

The transformation can be derived as follows:

$$\boldsymbol{e}_{\alpha\beta}^{+}\cdot\left[\boldsymbol{T}_{dq}^{+}\right]-\boldsymbol{i}_{\alpha\beta}^{+}\cdot\left[\boldsymbol{T}_{dq}^{+}\right]\cdot\left[\boldsymbol{R}_{\alpha\beta}^{+}\right]\cdot\left[\boldsymbol{T}_{dq}^{+}\right]\cdot\left[\boldsymbol{T}_{dq}^{+}\right]^{-1}-$$
$$-\dot{\boldsymbol{i}}_{\alpha\beta}^{+}\cdot\left[\boldsymbol{T}_{dq}^{+}\right]\cdot\left[\boldsymbol{L}_{\alpha\beta}^{+}\right]\cdot\left[\boldsymbol{T}_{dq}^{+}\right]\cdot\left[\boldsymbol{T}_{dq}^{+}\right]^{-1}=\boldsymbol{u}_{\alpha\beta}^{i+}\cdot\left[\boldsymbol{T}_{dq}^{+}\right]$$

$$\dot{\boldsymbol{i}}_{\alpha\beta}^{+}\cdot\left[\boldsymbol{T}_{dq}^{+}\right]\cdot\left[\boldsymbol{L}_{\alpha\beta}^{+}\right]\cdot\left[\boldsymbol{T}_{dq}^{+}\right]\cdot\left[\boldsymbol{T}_{dq}^{+}\right]^{-1}=\left[\boldsymbol{L}_{dq}^{+}\right]\cdot\left[\boldsymbol{T}_{dq}^{+}\right]\cdot\dot{\boldsymbol{i}}_{\alpha\beta}^{+}=$$
$$=\left[\boldsymbol{L}_{dq}^{+}\right]\cdot\left[\boldsymbol{T}_{dq}^{+}\right]\cdot\frac{d}{dt}\left(\left[\boldsymbol{T}_{dq}^{+}\right]\cdot\left[\boldsymbol{T}_{dq}^{+}\right]^{-1}\cdot\boldsymbol{i}_{\alpha\beta}^{+}\right)=$$
$$=\left[\boldsymbol{L}_{dq}^{+}\right]\cdot\left[\boldsymbol{T}_{dq}^{+}\right]\cdot\frac{d}{dt}\left(\left[\boldsymbol{T}_{dq}^{+}\right]^{-1}\cdot\boldsymbol{i}_{dq}^{+}\right)=$$
$$=\left[\boldsymbol{L}_{dq}^{+}\right]\cdot\left[\boldsymbol{T}_{dq}^{+}\right]\cdot\left(\boldsymbol{i}_{dq}^{+}\cdot\frac{d}{dt}\left[\boldsymbol{T}_{dq}^{+}\right]^{-1}+\left[\boldsymbol{T}_{dq}^{+}\right]^{-1}\cdot\frac{d}{dt}\boldsymbol{i}_{dq}^{+}\right)=$$
$$=\left[\boldsymbol{L}_{dq}^{+}\right]\cdot\left(\boldsymbol{i}_{dq}^{+}\cdot\left[\boldsymbol{T}_{dq}^{+}\right]\cdot\frac{d}{dt}\left[\boldsymbol{T}_{dq}^{+}\right]^{-1}+\frac{d}{dt}\boldsymbol{i}_{dq}^{+}\right)=$$
$$\left[\boldsymbol{L}_{dq}^{+}\right]\cdot\omega\cdot\left[\boldsymbol{W}^{+}\right]\cdot\boldsymbol{i}_{dq}^{+}+\left[\boldsymbol{L}_{dq}^{+}\right]\cdot\dot{\boldsymbol{i}}_{dq}^{+};$$

$$\left[\boldsymbol{T}_{dq}^{+}\right]\cdot\frac{d}{dt}\left[\boldsymbol{T}_{dq}^{+}\right]^{-1}=\begin{bmatrix}\cos\left(\gamma^{+}(t)\right) & \sin\left(\gamma^{+}(t)\right)\\ -\sin\left(\gamma^{+}(t)\right) & \cos\left(\gamma^{+}(t)\right)\end{bmatrix}\cdot\begin{bmatrix}-\sin\left(\gamma^{+}(t)\right) & -\cos\left(\gamma^{+}(t)\right)\\ \cos\left(\gamma^{+}(t)\right) & -\sin\left(\gamma^{+}(t)\right)\end{bmatrix}\cdot\omega=$$
$$\begin{bmatrix}0 & -1\\ 1 & 0\end{bmatrix}\cdot\omega=\left[\boldsymbol{W}^{+}\right]\cdot\omega$$

Finally the following equation for the positive sequence can be obtained:

$$\boldsymbol{e}_{dq}^{+}-\boldsymbol{i}_{dq}^{+}\cdot\left[\boldsymbol{R}_{dq}^{+}\right]-\left[\boldsymbol{L}_{dq}^{+}\right]\cdot[\boldsymbol{W}]\cdot\boldsymbol{i}_{dq}^{+}\cdot-\dot{\boldsymbol{i}}_{dq}^{+}\cdot\left[\boldsymbol{L}_{dq}^{+}\right]=\boldsymbol{u}_{dq}^{i+}\qquad(3.1.9)$$

In the scalar form the following equation system can be written:

$$\begin{cases}e_{d}^{+}=i_{d}^{+}\cdot R+L\cdot\dot{i}_{d}^{+}-\omega\cdot L\cdot i_{q}^{+}+u_{d}^{i+}\\ e_{q}^{+}=i_{q}^{+}\cdot R+L\cdot\dot{i}_{q}^{+}+\omega\cdot L\cdot i_{d}^{+}+u_{q}^{i+}\end{cases}\qquad(3.1.10)$$

Similarly, the transformation for the negative sequence can be performed. The second equation 3.1.5 has to be multiplied by the transformation matrix $\left[\boldsymbol{T}_{\alpha\beta}\right]$ first. The following equation can be obtained for the negative sequence:

$$\boldsymbol{e}_{\alpha\beta}^{-} - \boldsymbol{i}_{\alpha\beta}^{-} \cdot \left[\boldsymbol{R}_{\alpha\beta}^{-}\right] - \dot{\boldsymbol{i}}_{\alpha\beta}^{-} \cdot \left[\boldsymbol{L}_{\alpha\beta}^{-}\right] = \boldsymbol{u}_{\alpha\beta}^{i-} \tag{3.1.11}$$

In order to use the *dq*-transformation the equation 3.1.11 has to be multiplied by the following transformation matrix:

$$\begin{aligned} \left[\boldsymbol{T}_{dq}^{-}\right] &= \begin{bmatrix} \cos\left(\gamma^{-}(t)\right) & -\sin\left(\gamma^{-}(t)\right) \\ \sin\left(\gamma^{-}(t)\right) & \cos\left(\gamma^{-}(t)\right) \end{bmatrix} \\ \gamma^{-}(t) &= \frac{u_{\beta}^{i-}}{u_{\alpha}^{i-}} = -\gamma^{+}(t) \end{aligned} \tag{3.1.12}$$

After multiplying the following equation can be obtained:

$$\begin{aligned} &\boldsymbol{e}_{dq}^{-} - \boldsymbol{i}_{dq}^{-} \cdot \left[\boldsymbol{R}_{dq}^{-}\right] - \left[\boldsymbol{L}_{dq}^{-}\right] \cdot \left[\boldsymbol{W}^{-}\right] \cdot \boldsymbol{i}_{dq}^{-} \cdot - \dot{\boldsymbol{i}}_{dq}^{-} \cdot \left[\boldsymbol{L}_{dq}^{-}\right] = \boldsymbol{u}_{dq}^{i-} \\ &\left[\boldsymbol{W}^{-}\right] = \begin{bmatrix} 0 & 1 \\ -1 & 0 \end{bmatrix} \end{aligned} \tag{3.1.13}$$

In the scalar form the equation 2.3.17 can be written as follows:

$$\begin{cases} e_{d}^{-} = i_{d}^{-} \cdot R + L \cdot \dot{i}_{d}^{-} + \omega \cdot L \cdot i_{q}^{-} + u_{d}^{i-} \\ e_{q}^{-} = i_{q}^{-} \cdot R + L \cdot \dot{i}_{q}^{-} - \omega \cdot L \cdot i_{d}^{-} + u_{q}^{i-} \end{cases} \tag{3.1.14}$$

The zero sequence dq-transformation is performed using equations 3.1.1 and 3.1.2. The zero sequence system equation in the scalar form can be written as follows:

$$\begin{cases} e_{d}^{0} = i_{d}^{0} \cdot R + L \cdot \dot{i}_{d}^{0} - \omega \cdot L \cdot i_{q}^{0} + u_{d}^{i0} \\ e_{q}^{0} = i_{q}^{0} \cdot R + L \cdot \dot{i}_{q}^{0} + \omega \cdot L \cdot i_{d}^{0} + u_{q}^{i0} \end{cases} \tag{2.3.19}$$

The obtained equations 2.3.12, 2.3.18, 2.3.19 can be represented by the equivalent circuits showed in Figures 3.1.2 – 1.1.4.

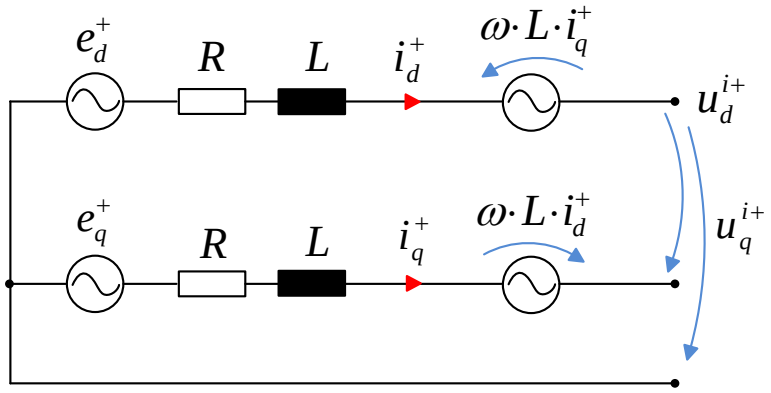

Figure 3.1.2 *dq* positive sequence equivalent circuit

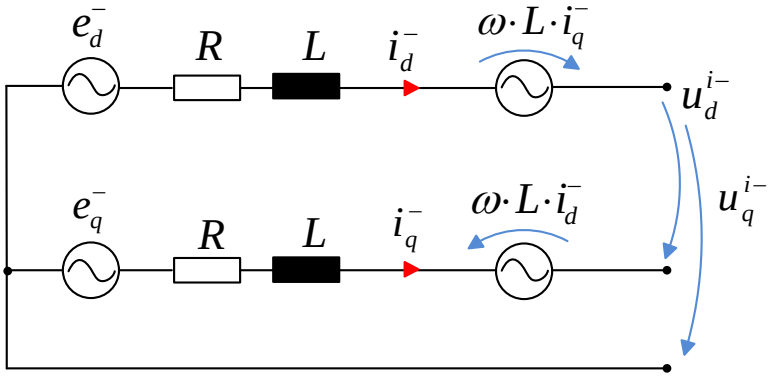

Figure 3.1.3 *dq* negative sequence equivalent circuit

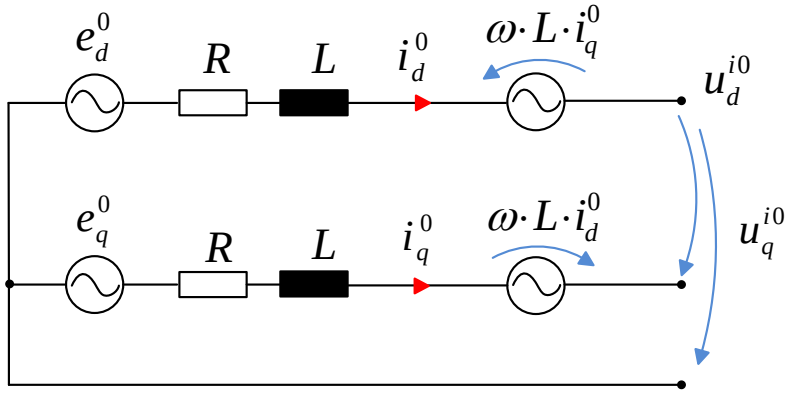

Figure 3.1.4 *dq* zero sequence equivalent circuit

The equation 3.1.10 can be written as follows:

$$\begin{cases} k_v \cdot u_d^{m+} = i_d^+ \cdot R + L \cdot \overset{\bullet}{i_d^+} - \omega \cdot L \cdot i_q^+ + u_d^{i+} \\ k_v \cdot u_q^{m+} = i_q^+ \cdot R + L \cdot \overset{\bullet}{i_q^+} + \omega \cdot L \cdot i_d^+ + u_q^{i+} \end{cases} \tag{3.1.11}$$

To synthesize the control system the direct method for DC-DC convertors is used [35]. After using the Laplace transform of the equation 2.3.20 the following system for the positive sequence can be written:

$$\begin{cases} k_v \cdot u_d^{m+}(s) = i_d^+(s) \cdot R \cdot \left(1 + \frac{L}{R} \cdot s\right) - \omega \cdot L \cdot i_q^+(s) + u_d^{i+}(s) \\ k_v \cdot u_q^{m+}(s) = i_d^-(s) \cdot R \cdot \left(1 + \frac{L}{R} \cdot s\right) + \omega \cdot L \cdot i_d^+(s) + u_q^{i+}(s) \end{cases} \tag{3.1.12}$$

The positive sequence controller has the task to drive the signals as follows (k_v is converter gain):

$$\begin{bmatrix} i_d^+ \\ i_q^+ \end{bmatrix} = k_v \begin{bmatrix} i_d^{+*} \\ i_q^{+*} \end{bmatrix} \tag{3.1.13}$$

As it can be seen from the equation 3.1.12 the output current independence from voltages $u_d^{i+}(s)$, $u_d^{i-}(s)$ has to be provided as well as the cross coupling influence has to be eliminated. It can be performed by adjusting the signals as follows:

$$\begin{bmatrix} u_d^{m+}(s) \\ u_q^{m+}(s) \end{bmatrix} = \begin{bmatrix} u_d^{+*}(s) + \frac{1}{k_v} \cdot \left(-\omega \cdot L \cdot i_q^+(s) + u_d^{i+}(s)\right) \\ u_q^{+*}(s) + \frac{1}{k_v} \cdot \left(\omega \cdot L \cdot i_d^+(s) + u_q^{i+}(s)\right) \end{bmatrix} \tag{3.1.14}$$

Substituting the equation 3.1.14 into 3.1.12:

$$\begin{cases} k_v \cdot u_d^{+*}(s) = i_d^+(s) \cdot R \cdot \left(1 + \frac{L}{r} \cdot s\right) \\ k_v \cdot u_q^{+*}(s) = i_d^-(s) \cdot R \cdot \left(1 + \frac{L}{r} \cdot s\right) \end{cases} \tag{3.1.15}$$

Further, L and R parameters influence on the output current should be eliminated. Thus, the voltage reference signals have to be driven as follows:

$$\begin{bmatrix} u_d^{+*}(s) \\ u_q^{+*}(s) \end{bmatrix} = \begin{bmatrix} i_d^{+*}(s) \cdot R \cdot \left(1 + \frac{L}{r} \cdot s\right) \\ i_q^{+*}(s) \cdot R \cdot \left(1 + \frac{L}{r} \cdot s\right) \end{bmatrix} \tag{3.1.16}$$

However, from the equation 3.1.16 one can see the presence of the differentiating element $\left(1 + \frac{L}{R} \cdot s\right)$ having Bode magnitude plot illustrated in Figure 3.1.5 ($\omega_2 = \frac{R}{L}$).

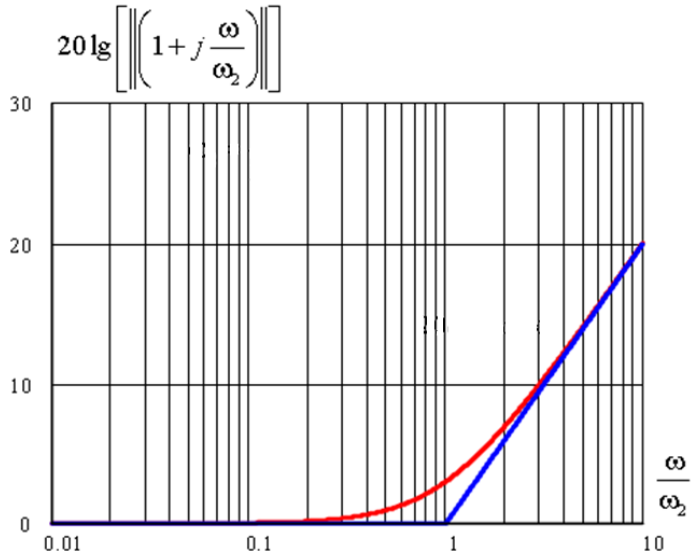

Figure 3.1.5 Bode magnitude plot of the differentiating element

It can be seen from Figure 3.1.5 the amplification of the signal at frequencies from above the main frequency. It would cause the high frequency harmonics increasing in the control loops and the stability loss. To avoid this impact, the current feedback and the integrating element $R \cdot k_i / s \cdot \frac{L}{R}$ should be used (k_i is the PI gain). Then, the voltage reference signals should be driven as follows:

$$\begin{bmatrix} u_d^{+*}(s) \\ u_q^{+*}(s) \end{bmatrix} = \begin{bmatrix} \left(i_d^{+*}(s) - \frac{1}{k_v} \cdot i_d^{+}(s) \right) \cdot R \cdot k_i \cdot \left(1 + \frac{1}{s \cdot \frac{L}{R}} \right) \\ \left(i_q^{+*}(s) - \frac{1}{k_v} \cdot i_q^{+}(s) \right) \cdot R \cdot k_i \cdot \left(1 + \frac{1}{s \cdot \frac{L}{R}} \right) \end{bmatrix} \tag{3.1.17}$$

Substituting the equation 3.1.17 into 3.1.15 the following system can be obtained:

$$\begin{cases} i_d^{+}(s) = i_d^{+*}(s) \cdot \dfrac{k_v}{1 + \dfrac{s \cdot \frac{L}{R}}{k_i}} \\ i_q^{+}(s) = i_q^{+*}(s) \cdot \dfrac{k_v}{1 + \dfrac{s \cdot \frac{L}{R}}{k_i}} \end{cases} \tag{3.1.18}$$

The *dq* signals are DC, therefore the expression $\dfrac{s \cdot \frac{L}{R}}{k_i}$ is obviously aspired to zero. Structurally the positive sequence loop is illustrated in Figure 3.1.6.

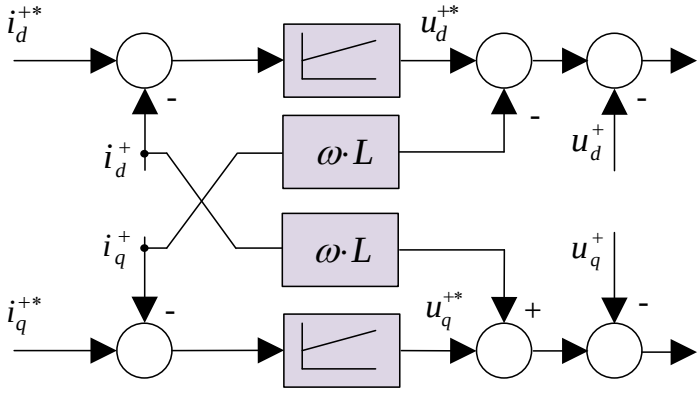

Figure 3.1.6 Block diagram of the positive sequence loop

As one can see, the well-known current control loop is obtained. The method can be used for the systems with 2 and more state-space variables as well.

Analyzing the equations 2.3.12, 2.3.18 and 2.3.19 it can be concluded being the zero sequence loop similarly to the positive sequence loop. The negative sequence loop differs only in the cross coupling sign. Thus, the block diagrams for the negative and zero sequence loops can be depicted as in Figures 3.1.7 and 3.1.8.

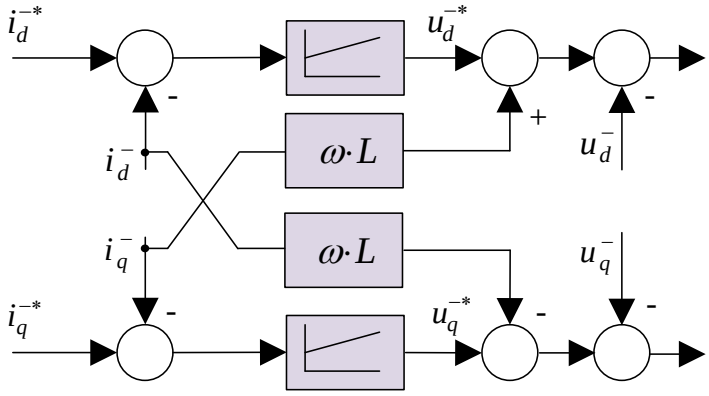

Figure 3.1.7 Block diagram of the negative sequence loop

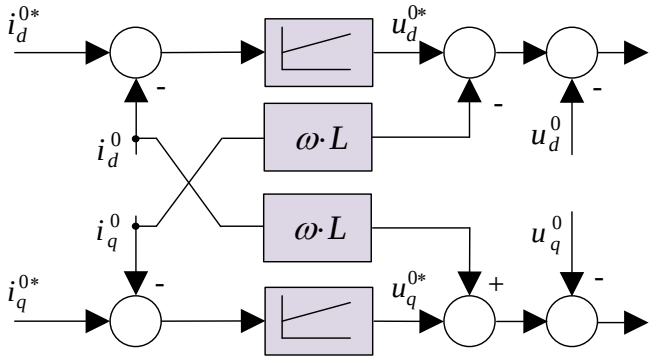

Figure 3.1.8 Block diagram of zero sequence loop

Current controller parameters determination

Using the direct synthesis method the controller structure can be obtained but it does not consider the presence of some transfer functions such as filters. Thus, to take into account the all filters, for the controller parameters determinations the Symmetrical (SO) and Modulus (MO) Optimum criteria are used. First the equivalent circuit has to be composed taking into consideration the all transfer functions and time constants. Since the all loops are identical, the

circuit only for d-component of the positive sequence is considered. Figure 3.1.9 shows the simplified equivalent loop circuit for the *d*-component.

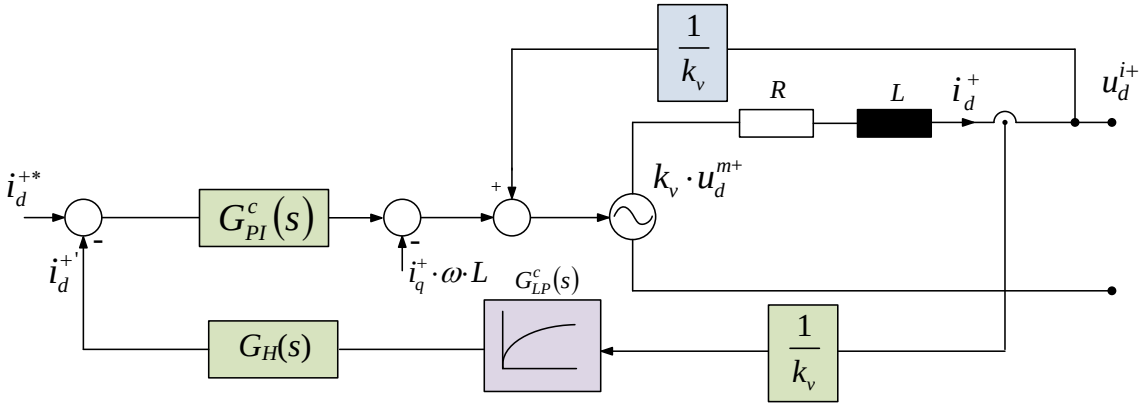

Figure 3.1.9 Simplified equivalent loop circuit for the *d*-component

$G_{PI}^c(s)$– is the transfer function of the current PI regulator, $G_H(s)$ – is the transfer function of the Hilbert filter, $G_{LP}^c(s)$– is the transfer function of the low-pass filter using to avoid the noisy in the control loop.

To apply the SO criteria the circuit showed in Figure 3.1.9 should to be transformed into the open loop circuit. The power circuit is transformed in terms of the transfer function as well. The modified open loop circuit showed in Figure 3.1.10. The cross coupling and the voltage feedback can be neglected.

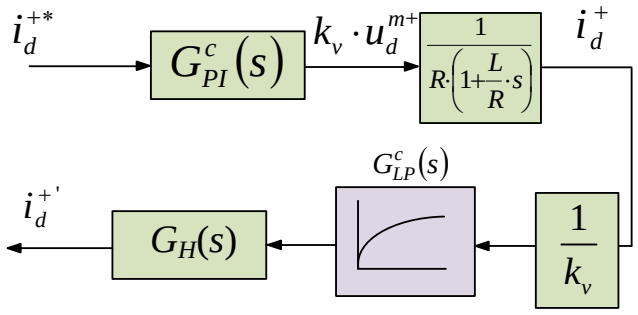

Figure 3.1.10 Open loop equivalent circuit for the d-component

The Hilbert filter can be represented as the transfer function as well. As it mentioned above the Hilbert filter function in z-domain expressed by:

$$H(z) = \frac{b_0 + b_1 \cdot z^{-1}}{a_0 + a_1 \cdot z^{-1}}$$

Using the inverse z-transform the following equation can be obtained by the substitution $z^{-1} = \frac{2 - s \cdot T_d}{2 + s \cdot T_d}$:

$$G_H(s) = \frac{b_0 + \frac{2 - s \cdot T_d}{2 + s \cdot T_d}}{1 + a_1 \cdot \frac{2 - s \cdot T_d}{2 + s \cdot T_d}} = \frac{2 \cdot b_0 + 2 + s \cdot (b_0 \cdot T_d - T_d)}{2 \cdot a_1 + 2 + s \cdot (T_d - a_1 \cdot T_d)} = \\ = \frac{1 + s \cdot \frac{b_0 \cdot T_d - T_d}{2 \cdot b_0 + 2}}{1 + s \cdot \frac{T_d - a_1 \cdot T_d}{2 \cdot a_1 + 2}} \tag{3.1.19}$$

However, the transfer function obtained does not always represent the first-order filter. Thus to approximate the obtained filter transfer function the time constant is to be determined. It can be easily done by using Matlab/Simulink. Or the analytical equation of the step response can be obtained. Applying to the equation 3.1.19 the inverse Laplace transform and taking into account $\frac{T_d - a_1 \cdot T_d}{2 \cdot a_1 + 2} = -\frac{b_0 \cdot T_d - T_d}{2 \cdot b_0 + 2}$:

$$h_H^{IIR}(t) = \mathrm{L}^{-1}[G_H(s)] = \mathrm{L}^{-1}\left[\frac{1 + s \cdot \frac{b_0 \cdot T_d - T_d}{2 \cdot b_0 + 2}}{1 + s \cdot \frac{T_d - a_1 \cdot T_d}{2 \cdot a_1 + 2}}\right] = \\ = -2 \cdot e^{-\frac{b_0 \cdot T_d - T_d}{2 \cdot b_0 + 2} \cdot t} + 1 \tag{3.1.20}$$

Finally, the following expression can be obtained to determine a time constant:

$$T_H^{\mu} = 1{,}7 \cdot \frac{b_0 \cdot T_d - T_d}{2 \cdot b_0 + 2} \tag{3.1.30}$$

In the case of using the FIR filter the approximation procedure is more complicated and requires the computer programs (Matlab, Mathcad etc.) due to the high filter order (see Section 2.2). In general it can be expressed by:

$$h_H^{FIR}(t) = \mathcal{L}^{-1}[G_H(s)] = \mathcal{L}^{-1}\left[\sum_{n=0}^{m}\left[h_n \cdot \left(\frac{b_0 \cdot T_d - T_d}{2 \cdot b_0 + 2}\right)^n\right]\right] \tag{3.1.31}$$

The time constant can be approximately obtained from the filter features as well. It is known that any physically realizable digital filter delays the input signal by the number of the samples equal to the filter order $n \cdot T$.

After selecting the suitable method and the filter constant determination, the Hilbert filter can be approximated by the first-order transfer function:

$$G_H(s) = \frac{1}{T_\mu^H \cdot s + 1} \tag{3.1.32}$$

After finding the all transfer functions the MO criteria can be applied. According to this method the open loop transfer function should be equal to:

$$G_{open}^c(s) = \frac{1}{2 \cdot T_{\mu\Sigma}^c \cdot s \cdot (T_{\mu\Sigma}^c \cdot s + 1)} \tag{3.1.33}$$

The transfer function of the system (Figure 3.1.10) can be expressed by:

$$\begin{aligned} & G_H(s) \cdot G_{LP}(s) \cdot \frac{1}{R \cdot (1 + T_\mu^{RL} \cdot s)} \cdot G_{PI}^c(s) = \\ & = \frac{1}{T_\mu^H \cdot s + 1} \cdot \frac{1}{T_\mu^{LPc} \cdot s + 1} \cdot \frac{1}{R \cdot (1 + T_\mu^{RL} \cdot s)} = \\ & = \frac{1}{(T_\mu^H + T_\mu^{LPc}) \cdot s + 1} \cdot \frac{1}{R \cdot (1 + T_\mu^{RL} \cdot s)} \cdot G_{PI}^c(s) \end{aligned} \tag{3.1.34}$$

The small time constant can be represented as the sum $T_{\mu\Sigma}^c = T_\mu^H + T_\mu^{LPc}$. Eequating equations 3.1.33 and 3.1.34 the following PI transfer function can be obtained:

$$G_{PI}^c(s) = \frac{(1 + T_\mu^{RL} \cdot s)}{2 \cdot T_{\mu\Sigma}^c \cdot s / R} = \frac{T_\mu^{RL}}{2 \cdot T_{\mu\Sigma}^c / R} \cdot \left[\frac{1 + s \cdot T_\mu^{RL}}{s \cdot T_\mu^{RL}}\right] \tag{3.1.35}$$

The closed-loop transfer function is expressed by:

$$G_{close}^{c}(s)=\frac{1}{2\cdot T_{\mu\Sigma}^{c}\cdot s\cdot(T_{\mu\Sigma}^{c}\cdot s+1)+1}\approx\frac{1}{2\cdot T_{\mu\Sigma}^{c}\cdot s+1}=\frac{1}{T_{\mu}^{c}\cdot s+1}$$
$$T_{\mu}^{c}=2\cdot\left(T_{\mu}^{H}+T_{\mu}^{LPc}\right) \qquad (3.1.36)$$

The negative and zero sequence current controller parameters can be determined in the same way.

Voltage controller parameters determination

To compensate the reactive power of the ground fault the DC link voltage (see Figure 3.1.1) should be maintained consuming the active power from the network. This principle is used in the active power filters without an additional voltage source. Thus, the additional voltage loop should be used in the positive sequence controller as it is depicted in Figure 3.1.11.

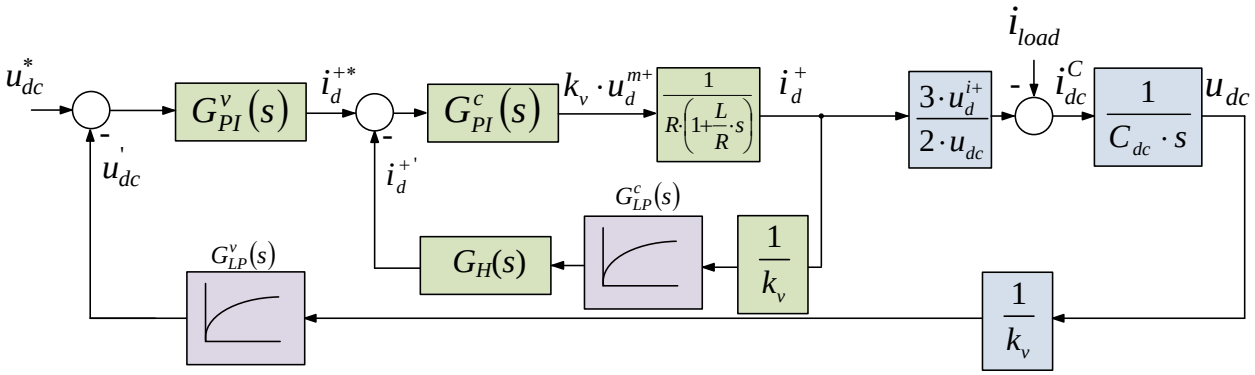

Figure 3.1.11 Equivalent loop circuit for d-component

Usually for voltage outer loop the SO criteria is used. Thus, according to this method the desired voltage open loop transfer function is expressed by:

$$G_{open}^{v}(s)=\frac{4\cdot T_{\mu\Sigma}^{v}\cdot s+1}{8\cdot\left(T_{\mu\Sigma}^{v}\right)^{2}\cdot s^{2}+8\cdot\left(T_{\mu\Sigma}^{v}\right)^{3}\cdot s^{3}} \qquad (3.1.37)$$

The transfer function of the whole system is:

$$G_{PI}^{v}(s)\cdot G_{close}^{c}(s)\cdot\frac{3\cdot\hat{U}_d^{+}}{2\cdot\hat{U}_{dc}}\cdot\frac{1}{C_{dc}\cdot s}\cdot\frac{1}{T_{\mu}^{LPv}\cdot s+1}=$$

$$=G_{PI}^{v}(s)\cdot\frac{1}{T_{\mu}^{c}\cdot s+1}\cdot\frac{3\cdot\hat{U}_d^{+}}{2\cdot\hat{U}_{dc}}\cdot\frac{1}{C_{dc}\cdot s}\cdot\frac{1}{T_{\mu}^{LPv}\cdot s+1}= \tag{3.1.38}$$

$$=G_{PI}^{v}(s)\cdot\frac{3\cdot\hat{U}_d^{+}}{2\cdot\hat{U}_{dc}\cdot C_{dc}}\cdot\frac{1}{s\cdot\left(T_{\mu\Sigma}^{v}\cdot s+1\right)}$$

$$T_{\mu\Sigma}^{v}=T_{\mu}^{c}+T_{\mu}^{LPv}$$

Eequating equations 3.1.37 and 3.1.38 the following PI transfer function can be obtained:

$$G_{PI}^{v}(s)=\frac{4\cdot T_{\mu\Sigma}^{v}\cdot s+1}{8\cdot\left(T_{\mu\Sigma}^{v}\right)^{2}\cdot s^{2}+8\cdot\left(T_{\mu\Sigma}^{v}\right)^{3}\cdot s^{3}}\cdot\frac{s\cdot\left(T_{\mu\Sigma}^{v}\cdot s+1\right)}{1}\cdot\frac{2\cdot\hat{U}_{dc}\cdot C_{dc}}{3\cdot\hat{U}_d^{+}}= \tag{3.1.39}$$

$$=\frac{\hat{U}_{dc}\cdot C_{dc}}{3\cdot\hat{U}_d^{+}}\cdot\frac{4\cdot T_{\mu\Sigma}^{v}\cdot s+1}{4\cdot T_{\mu\Sigma}^{v}\cdot s}$$

3.2. Converter operation modes

Since, the ground fault is the temporary operation mode of the network and respectively the converter, the operation mode controller is required as well. The controller has to be consisted of the following functions:

- Network capacitance measurement to be able to calculate the potential GF current value;
- GF presence criteria definition;
- GF absence criteria definition;

During the operation the controller should be switched between every mode automatically.

Ground fault current value determination

As stated there is no method to measure the GF current directly due to the absence of the connection between the neutral and the ground of the system. Nevertheless, there are several techniques used with the ASC or resistor:

- Periodically use of an additional high value capacitance between the phase and the ground. The current flowed through the capacitance is measured and the network capacitive impedance is determined. Knowing the network capacitance, the ground fault value can be determined. The disadvantage of this method is the use of the additional equipment;

- Analysis of the residual zero current and the free oscillations of the neutral voltage. The system neutral voltage cannot be zero during the operation as well as there is always the residual zero current. It happens due to the variability of the loads and respectively the network capacitance. However this method is mathematically complex and requires an additional equipment;

- Generation of the zero sequence periodically current with the frequency different from the network. This method uses an additional source connected to the signal winding of the ASC. The zero sequence current causes the neutral voltage. Knowing the current and the voltage the system capacitance can be determined.

Analyzing the existing methods one can conclude that the third method suits to the converter and can be used but without the additional equipment and sources. The equivalent circuit in *α-β-0* domain with the converter is shown in Figure 3.2.1.

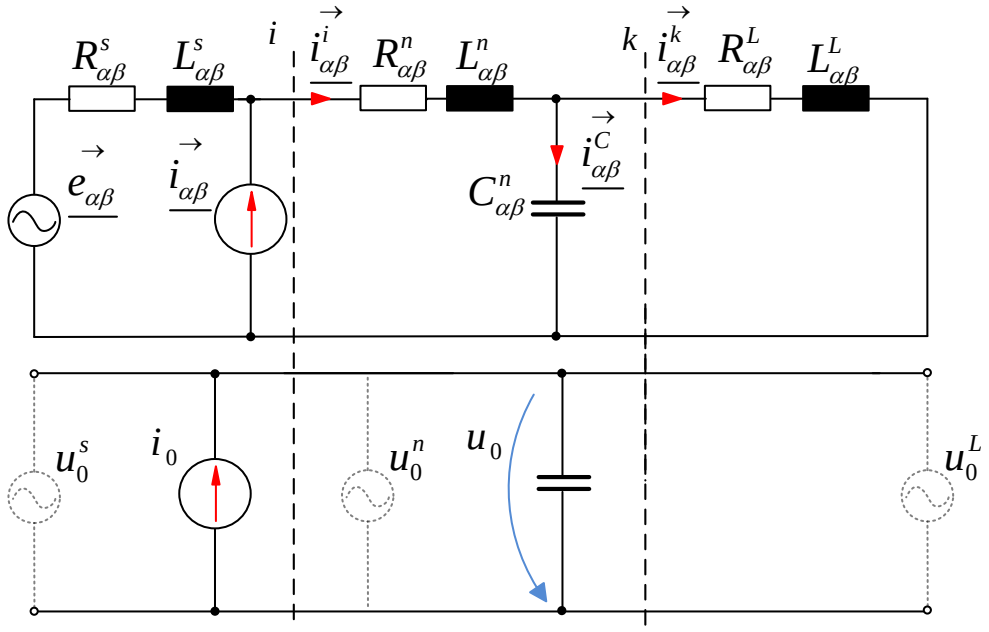

Figure 3.2.1 Equivalent circuit of the system with the converter

The *α-β-0* circuit is represented in vector values. The converter can generate the zero current with any frequency. The zero current with the network frequency could lead to the wrong result due to the existence of the zero voltage (u_0^s, u_0^n or u_0^L). However, the current generation with the lower frequency (25 Hz for example) can be used for the determination. The zero current is defined as follows:

$$i_{0(t)} = \hat{I}_{0(t)} \cdot \sin(2 \cdot \pi \cdot f_{(t)} \cdot t) \tag{3.2.1}$$

It can be seen from Figure 3.2.1 appearing the zero voltage. It can be expressed by:

$$\underline{U_{0(t)}} = -j \cdot X_{C0}^n \cdot \underline{I_{0(t)}} = -j \frac{\underline{I_{0(t)}}}{2 \cdot \pi \cdot f_{(t)} \cdot C_0^n} \tag{3.2.2}$$

From this equation a current network capacitance can be expressed by:

$$C_0^n = \frac{\hat{I}_{0(t)}}{50 \cdot \pi \cdot \hat{U}_{0(t)}} = \frac{i_{d(t)}^0}{50 \cdot \pi \cdot \sqrt{\left(u_{d(t)}^0\right)^2 + \left(u_{q(t)}^0\right)^2}} \tag{3.2.3}$$

The measured neutral voltage u_0 can contain not the only test frequency component. Therefore, the additional low pass filter or the Fourier transform can be applied to extract the test frequency harmonic before using the equation 3.2.3.

At the same time, the GF current can be expressed by:

$$\hat{I}^f = \hat{U}_{ph}^i \cdot 2 \cdot \pi \cdot f \cdot 3 \cdot C_0^n \tag{3.2.4}$$

Finally, the following expression can be obtained to determine the ground fault current amplitude ($\hat{U}_0^i \approx \hat{U}_0^f$):

$$\begin{aligned} &\hat{I}^f = i_d^{0*} = 2 \cdot \pi \cdot f \cdot 3 \cdot C_0^n \cdot \sqrt{\left(u_d^0\right)^2 + \left(u_q^0\right)^2} \approx \\ &\approx 2 \cdot \pi \cdot f \cdot 3 \cdot C_0^n \cdot u_d^0 \end{aligned} \tag{3.2.5}$$

It should be noted the need of the additional current loop to control the test current. The loop parameters can be determined similarly to the previous section.

Ground fault presence and elimination criteria

The ground fault presence can be defined by the neutral voltage value more than 10-15% of the phase voltage. However, there is the problem with the fault elimination criteria definition. Indeed, without the converter the zero (neutral) voltage after the fault elimination (or self-elimination) would be equal to zero. However, due to the converter, even though there is no GF, the converter continues to generate the zero current and "maintains" the GF. The network with the fault place can be considered as in Figure 3.2.2. The closed switch *S* represents the fault and the open switch the normal operation mode.

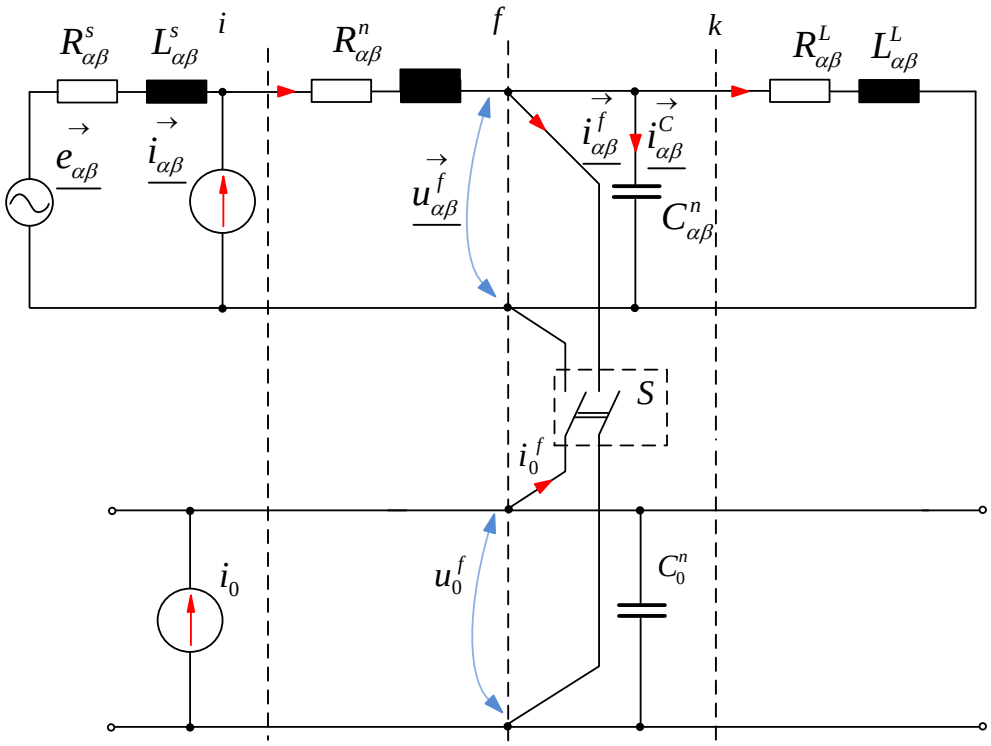

Figure 3.2.2 Equivalent *α-β-0* circuit with the "switch"

Let us consider the fault process. At some point in time the switch is closed creating the fault and the fault conditions. Measuring the zero voltage $u_0 = u_0^f$ the converter starts to operate and generate the zero current i_0 required to compensate the fault current i_0^f until it becomes zero. In the case of the fault elimination (the switch would be opened) nothing would change, as can be seen from Figure 3.2.2. The converter would still generate the current i_0 creating the zero voltage u_0 according to the equation 3.2.2. And measuring the zero voltage u_0 the converter would be operated as if the fault was still existed.

In the first case there is the solid connection between the $\alpha\beta$ circuit and the zero circuit. And the zero voltage equal to the $\alpha\beta$ voltage and cannot be controlled. In the second case the converter makes the fault conditions. Nevertheless, it can be seen from Figure 3.2.2 to be in this case the zero voltage the function of the converter zero current. And the zero voltage dependence on the converter current can be shown.

The zero voltage u_0 expression is:

$$\underline{U_0} = -j \cdot X_0^{nC} \cdot \underline{I_0} \tag{3.2.6}$$

Fig. 3.2.3 shows the zero voltage dependence on the converter current. The dependence can be used to identify the fault elimination. The compensation current should be decreased for a while to check if there any zero voltage changes.

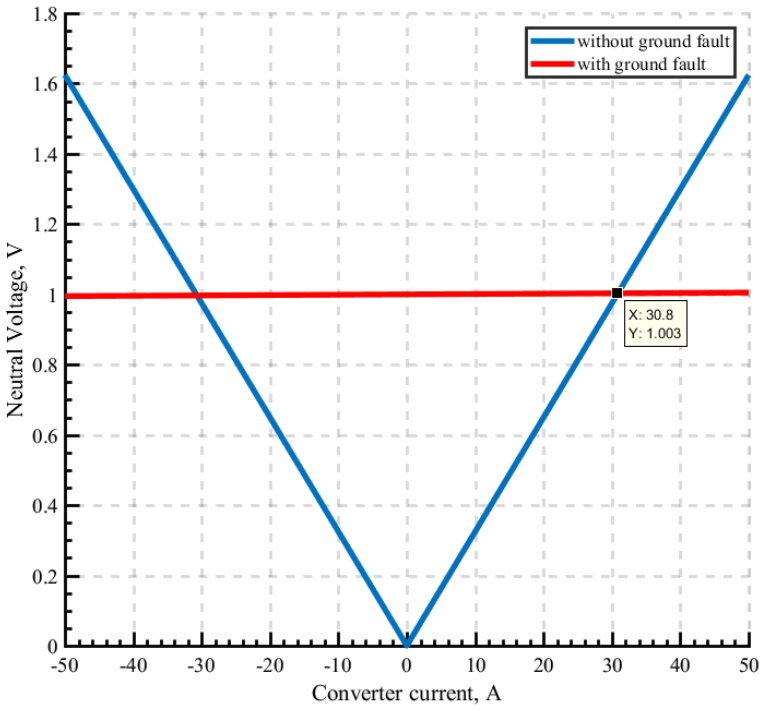

Figure 3.2.3 Zero voltage dependency on the converter current

High frequency components compensation

As it mentioned above the obtained controller structure can be used for the high-frequency components as well. Moreover, in the fault mode the high frequency harmonics compensation is required in some cases (Figure 1.8). The equivalent harmonic circuit is shown in Figure 3.2.4.

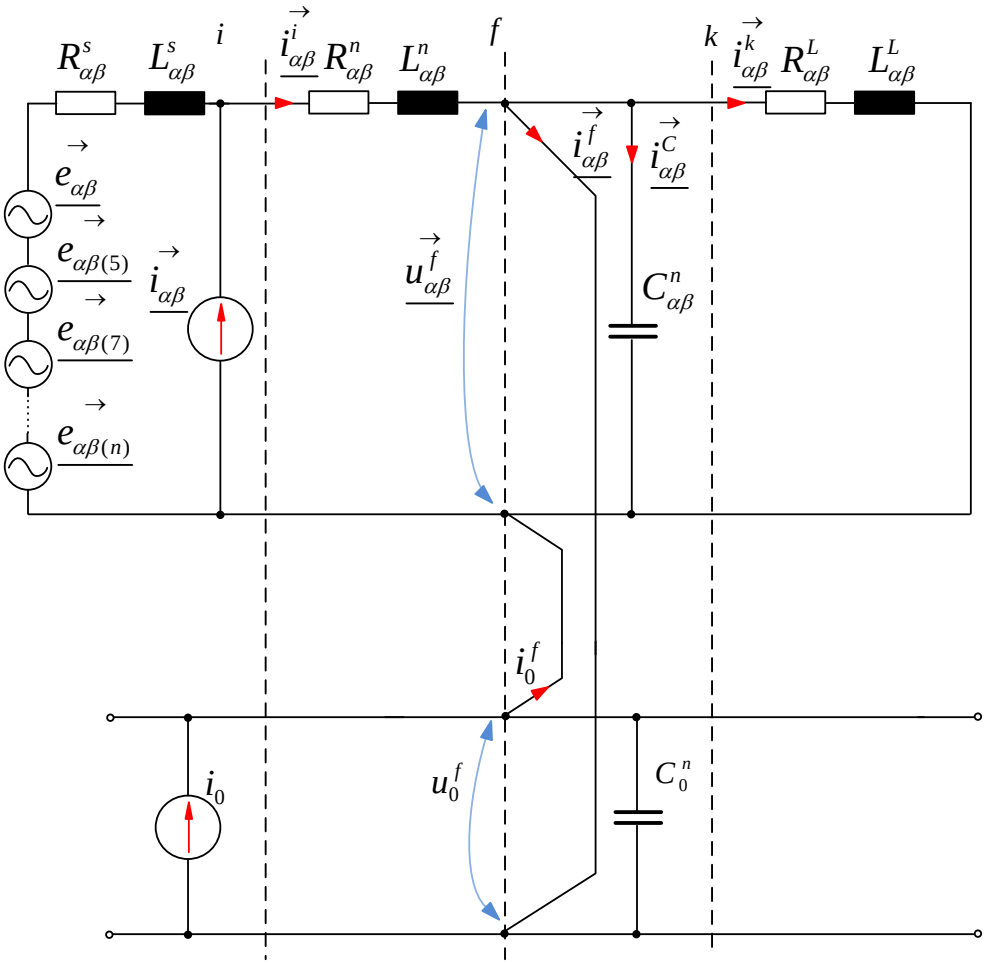

Figure 3.2.4 Equivalent harmonic circuit

Considering the equation 2.1.13, the GF current in this case would consist of the components sum:

$$\underline{I}^{f}_{(1)} \approx \frac{\underline{\vec{E}_{\alpha\beta}}}{-j\cdot\frac{X^{n}_{C\alpha\beta}}{3}},\ \underline{I}^{f}_{(5)} \approx \frac{\underline{\vec{E}_{\alpha\beta(5)}}}{-j\cdot\frac{X^{n}_{C\alpha\beta(5)}}{3}},\ \underline{I}^{f}_{(7)} \approx \frac{\underline{\vec{E}_{\alpha\beta(7)}}}{-j\cdot\frac{X^{n}_{C\alpha\beta(7)}}{3}},...$$

$$...\underline{I}^{f}_{(n)} \approx \frac{\underline{\vec{E}_{\alpha\beta(n)}}}{-j\cdot\frac{X^{n}_{C\alpha\beta(n)}}{3}} \qquad (3.2.7)$$

$$i^{f} = \hat{I}^{f}_{(1)}\cdot\sin(\omega\cdot t+\varphi) + \hat{I}^{f}_{(5)}\cdot\sin(5\cdot\omega\cdot t+\varphi_{(5)}) + \hat{I}^{f}_{(7)}\cdot\sin(7\cdot\omega\cdot t+\varphi_{(7)}) + ...$$

$$+ ...\hat{I}^{f}_{(n)}\cdot\sin(n\cdot\omega\cdot t+\varphi_{(n)})$$

It should be noticed that the coupling between the $\alpha\beta$ – circuit and the zero circuit depend on the faulted phase (*a, b* or *c*). As it noted the sum of the high-frequency harmonics can be larger than the main frequency component. In this case the main frequency component compensation would not lead to the result and the converter installation would not improve anything. However, the converter can generate the frequency components as well. The converter current should be generated as follows:

$$i_{0} = \hat{I}_{(1)}\cdot\sin(\omega\cdot t+\varphi-\pi) + \hat{I}_{(5)}\cdot\sin(5\cdot\omega\cdot t+\varphi_{(5)}-\pi) +$$
$$+\hat{I}_{(7)}\cdot\sin(7\cdot\omega\cdot t+\varphi_{(7)}-\pi) + ... + ...\hat{I}_{(n)}\cdot\sin(n\cdot\omega\cdot t+\varphi_{(n)}-\pi) \qquad (3.2.8)$$

However, as stated in the previous chapter the fault current cannot be measured. Therefore, the high-frequency (HF) current should be determined as well. And one of the key issues is the determination of the HF components. They can be found measuring the system voltage. And building the additional zero current loops the HF current can be completely compensated. The control system is shown in Figure 3.2.5.

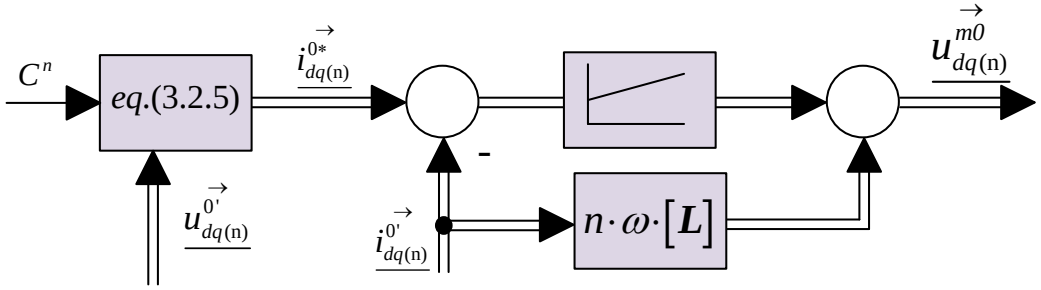

Figure 3.2.5 Zero HF component control structure

The zero sequence reference signals are determined for each harmonic in advance measuring the system voltage. It should be emphasize the requirement of the Hilbert filter for every HF component to obtain the $\alpha\beta$ – transformation (according to equations 3.1.1 and 3.1.2) or the wide-band Hilbert filter. With limited controller capabilities the one-fourth-period delay can be used for HF components. The fault transient process (Figures 2.1.12, 2.1.13) can create some resonances and additional HF overvoltages. To avoid it is possible by compensating the HF components before the fault. It can be done by eliminating the HF voltage sources $\underline{\vec{e}_{\alpha\beta(5)}}$, $\underline{\vec{e}_{\alpha\beta(7)}}$ … $\underline{\vec{e}_{\alpha\beta(n)}}$. Driving the current source $\underline{\vec{i}_{\alpha\beta}}$ the capacitance voltage $\underline{\vec{u}^{i}_{\alpha\beta}}$ can be controlled as well and the source voltages respectively. The additional capacitive filter at the converter output is required.

From Figure 3.2.4 the following equation can be written:

$$\begin{cases} \underline{\vec{e}_{\alpha\beta(5)}} = \underline{\vec{i}^{s}_{\alpha\beta(5)}} \cdot R^{s}_{\alpha\beta(5)} + jX^{s}_{L\alpha\beta(5)} \cdot \underline{\vec{i}^{s}_{\alpha\beta(5)}} + \underline{\vec{i}^{i}_{\alpha\beta(5)}} \cdot Rr^{n}_{\alpha\beta(5)} + jX^{n}_{L\alpha\beta(5)} \cdot \underline{\vec{i}^{s}_{\alpha\beta(5)}} + \underline{\vec{u}^{k}_{\alpha\beta(5)}} \\ \underline{\vec{i}^{s}_{\alpha\beta(5)}} + \underline{\vec{i}_{\alpha\beta(5)}} = \underline{\vec{i}^{i}_{\alpha\beta(5)}} \\ .... \\ \underline{\vec{e}_{\alpha\beta(n)}} = \underline{\vec{i}^{s}_{\alpha\beta(n)}} \cdot R^{s}_{\alpha\beta(n)} + jX^{s}_{L\alpha\beta(n)} \cdot \underline{\vec{i}^{s}_{\alpha\beta(n)}} + \underline{\vec{i}^{i}_{\alpha\beta(n)}} \cdot R^{n}_{\alpha\beta(n)} + jX^{n}_{L\alpha\beta(n)} \cdot \underline{\vec{i}^{s}_{\alpha\beta(n)}} + \underline{\vec{u}^{k}_{\alpha\beta(n)}} \\ \underline{\vec{i}^{s}_{\alpha\beta(n)}} + \underline{\vec{i}_{\alpha\beta(n)}} = \underline{\vec{i}^{i}_{\alpha\beta(n)}} \end{cases} \quad (3.2.9)$$

The source voltages could be compensated by the voltage drop across the source and line impedances. However, the voltage drop across the resistances $R^{s}_{\alpha\beta}$, $R^{n}_{\alpha\beta}$ and the impedances $X^{s}_{L\alpha\beta}, X^{n}_{L\alpha\beta}$ depend on the converter current $\underline{\vec{i}_{\alpha\beta}}$. Thus, the feasibility of the source voltages compensation depends on the impedance value and the required converter current value to create the sufficient voltage drop. Recalling the HF component existence in both positive and negative sequence the control system for the n-component (n=3, 5, …) can be depicted as in Figure 3.2.6.

With the insufficient ratio between the impedance and the current the zero sequence compensation should be applied. The series compensation is the possible option as well [42].

However, its consideration would require the additional research and it is out of the scope of this work.

The ground fault current without and with the HF compensation is shown in Figure 3.2.7.

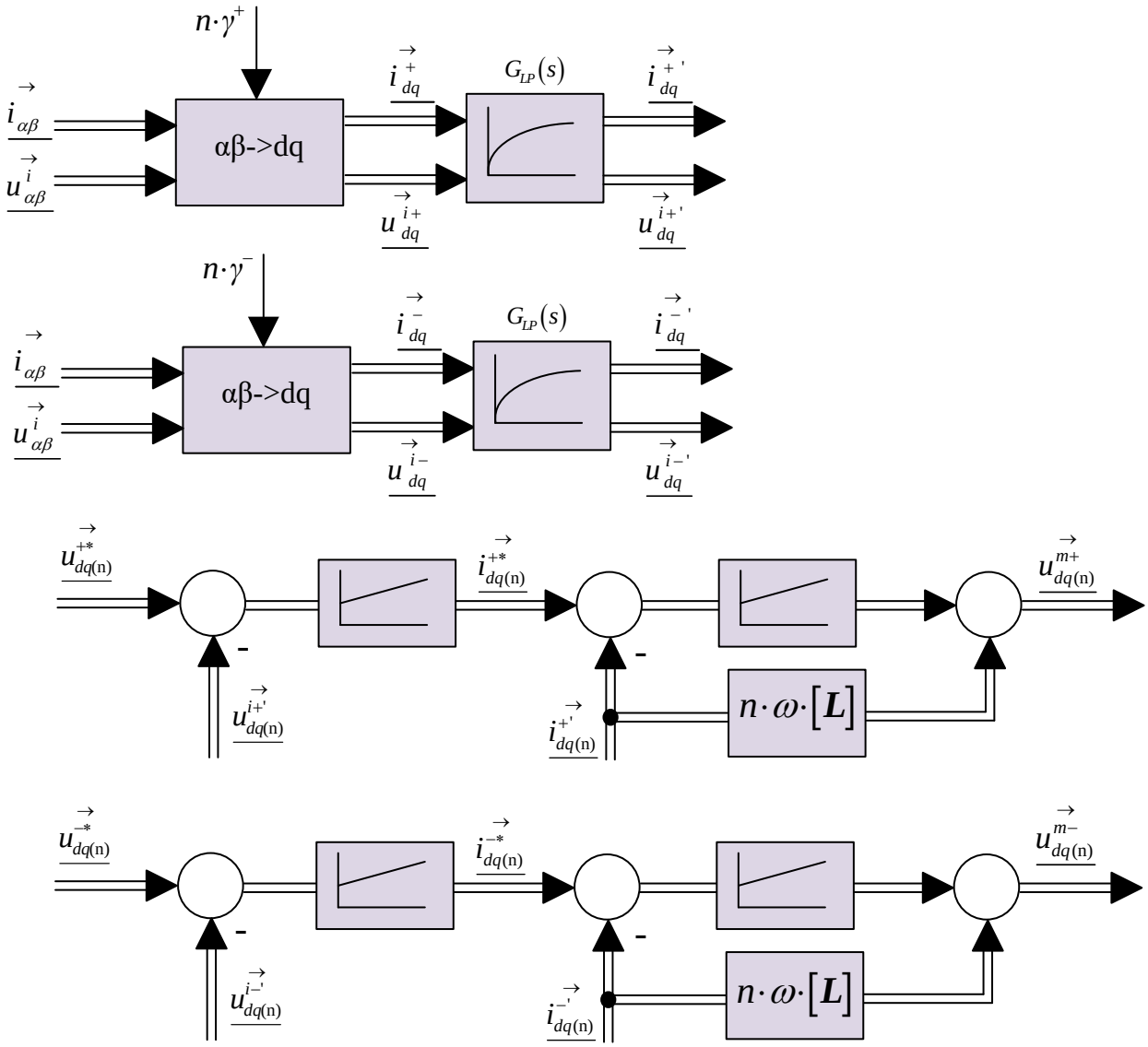

Figure 3.2.6 HF components control structure

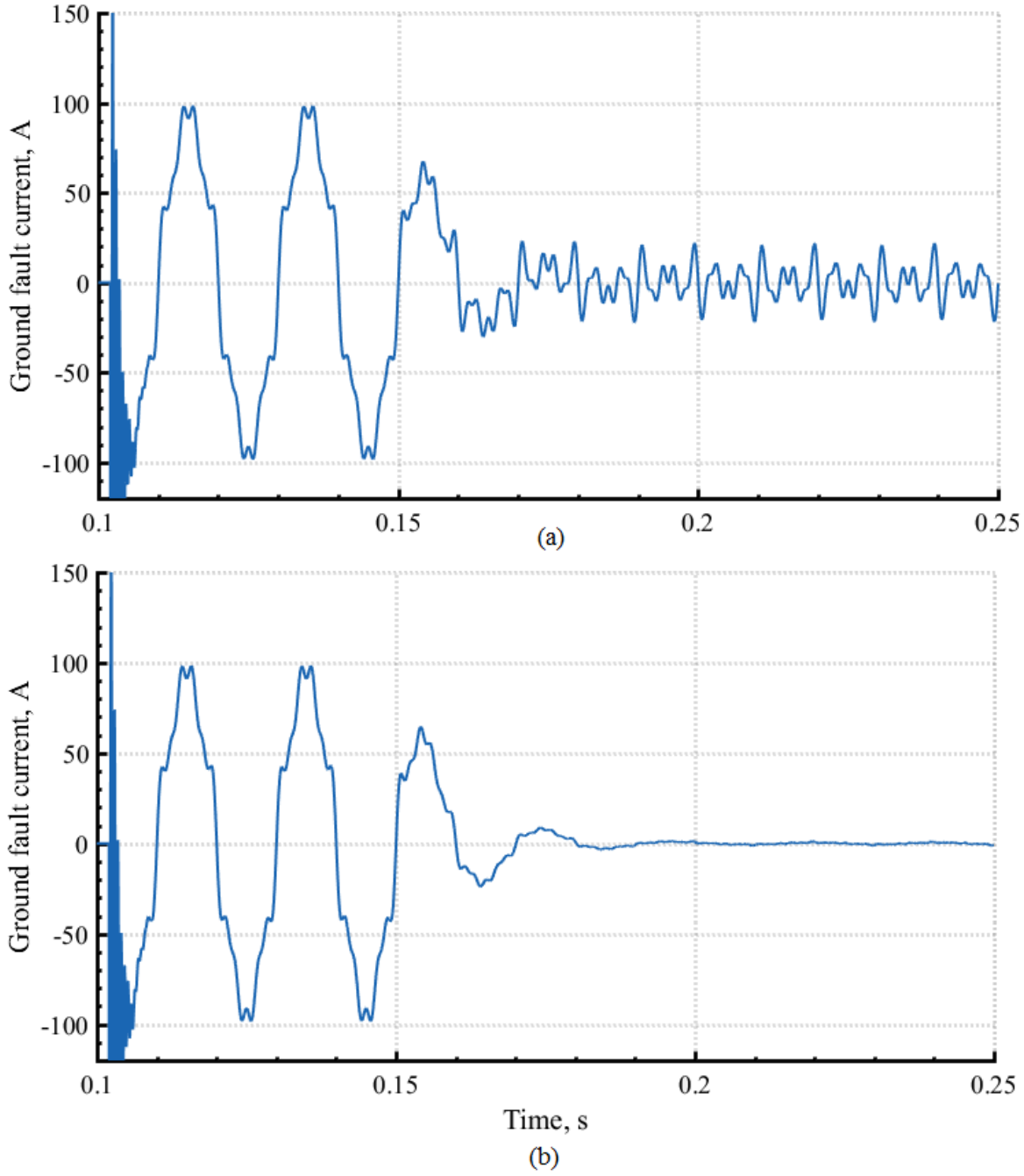

Figure 3.2.7 GF current without (a) and with (b) the HF compensation

It is obvious the ground fault current does not contain the HF components when they had been compensated before the fault. For simulation (Figure 3.2.7) the voltage compensation technique was used.

Operation modes controller

Figure 3.2.8 shows the flowchart of the operation modes controller.

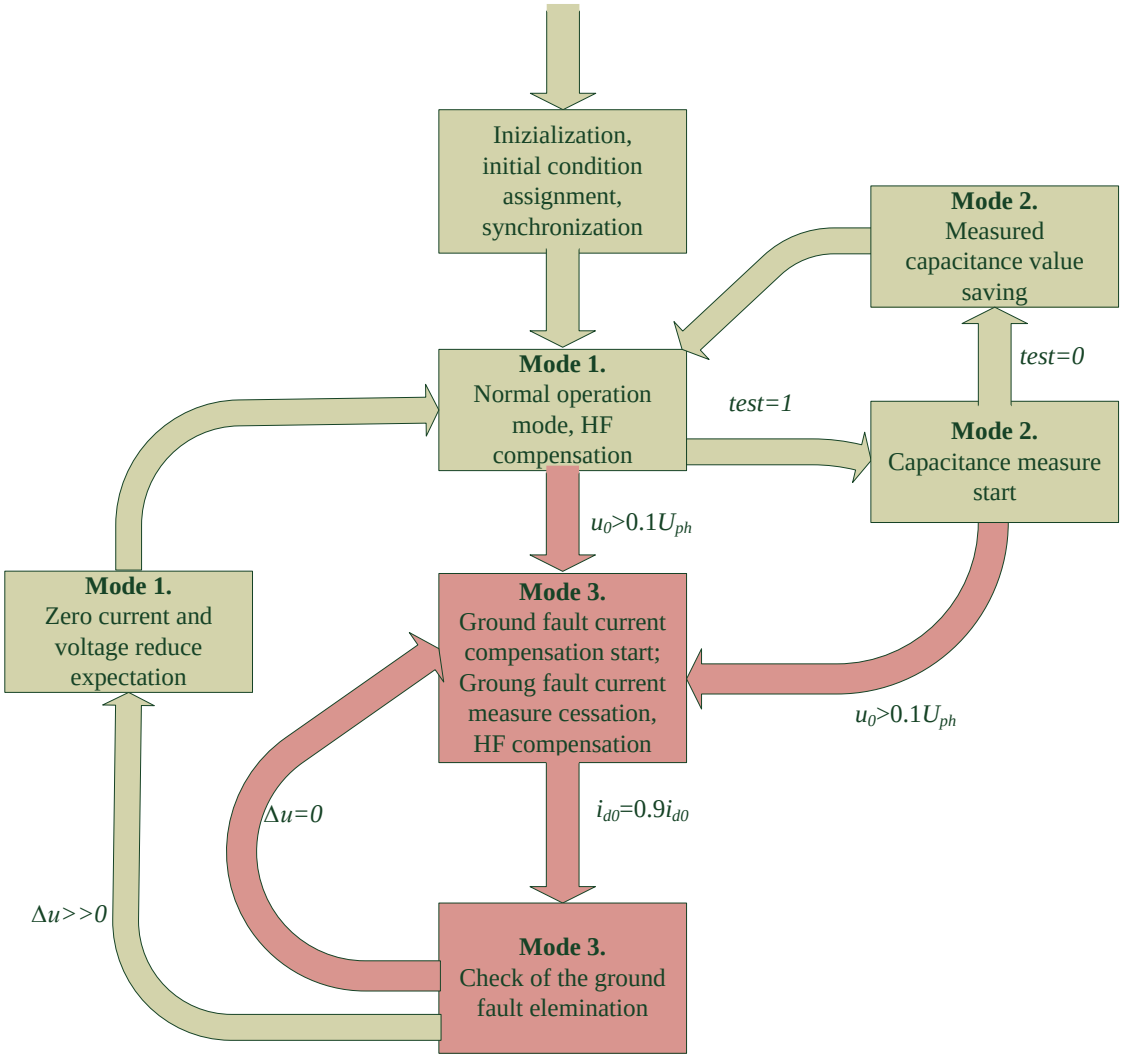

Figure 3.2.8 Operation modes controller

Mode 1: After synchronization with the network and the initial conditions assignment, the converter is ready to operate. In the first mode the u_{dc} voltage is maintained by the *d*-component of the positive sequence current i_d^+ . The HF components of the source voltage are being compensated by the tuning of the corresponding loops. At the same time the ground fault presence is checked continuously and the converter is periodically switched to the mode 2. Current directions of the mode 1 are showed in Figure 3.2.9.

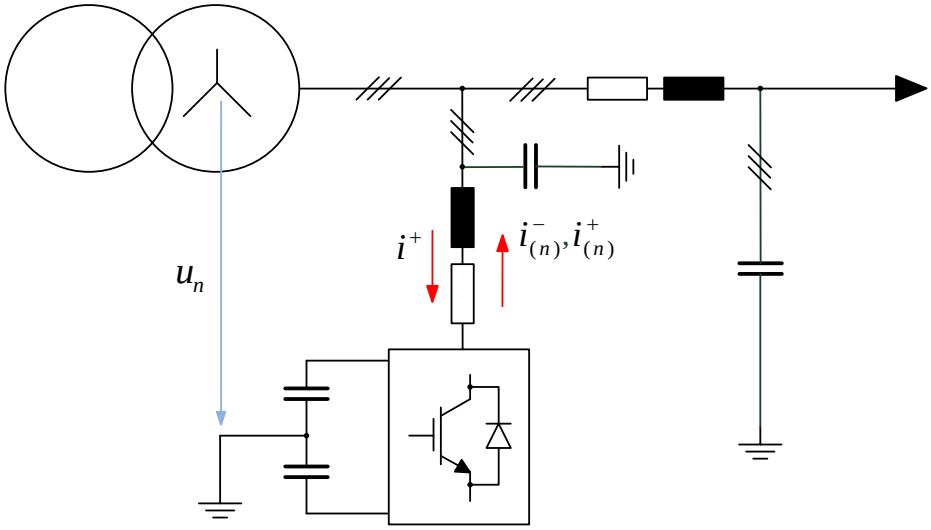

Figure 3.2.9 Operation mode 1

Mode 2: In this mode after receiving the signal test=1, the converter stars to generate the zero testing current of the non-fundamental frequency to measure the network capacitance. The ground fault presence is still checked continuously and the converter at any time can be switched to the fault mode 3. After some time (the period is selected by the designer) the measured value is to be saved and the converter is switched back to the mode 1. The u_{dc} voltage is also maintained by the d component of the positive sequence current i_d^+. The current directions of the mode 2 are shown in Figure 3.2.10.

Mode 3: For the ground fault presence the u_0 voltage change is used. When it is more than 70% of the phase voltage means the fault presence and the converter operates to compensate the ground fault current i^f. But the ground fault can be eliminated by the operational staff or can self-eliminate itself. Thus, during the operation mode 3 the periodic check is required and the obtained dependency (Figure 3.2.3) in the previous section can be used. The compensation current is slightly decreased for a while (the duration is chosen by the designer) to check whether the neutral voltage changes. And then the difference between the voltage measures (before decreasing and after) is compared. When there is still the fault, the voltage would not be changed and the difference would be equal to zero. Otherwise the difference would be greater than zero and the converter can switch to the standby mode to wait for the zero current and voltage become zero. Finally the converter is returned to the normal mode 1.

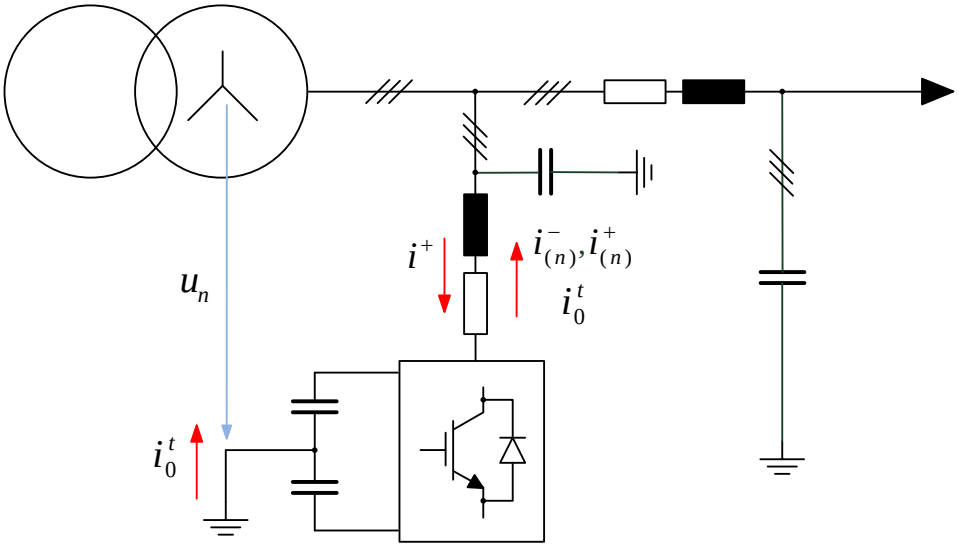

Figure 3.2.10 Operation mode 2

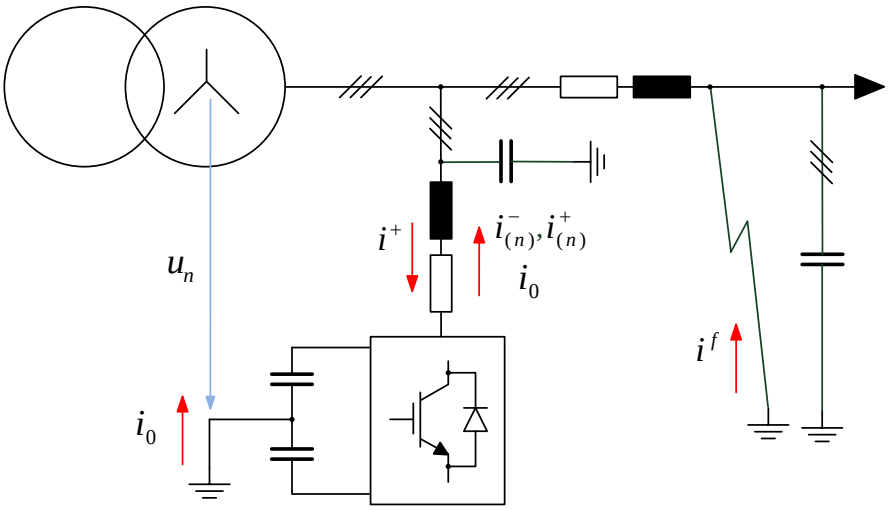

Figure 3.2.11 Operation mode 3

3.3. Complex distribution networks and future research

The distribution network represents the complicated system with plenty of the state variables. In most cases it can be simplified and a lot of parameters can be neglected as it had done in previous chapters. However, in some cases it cannot be performed due to some reasons. In this section some complex network cases are considered.

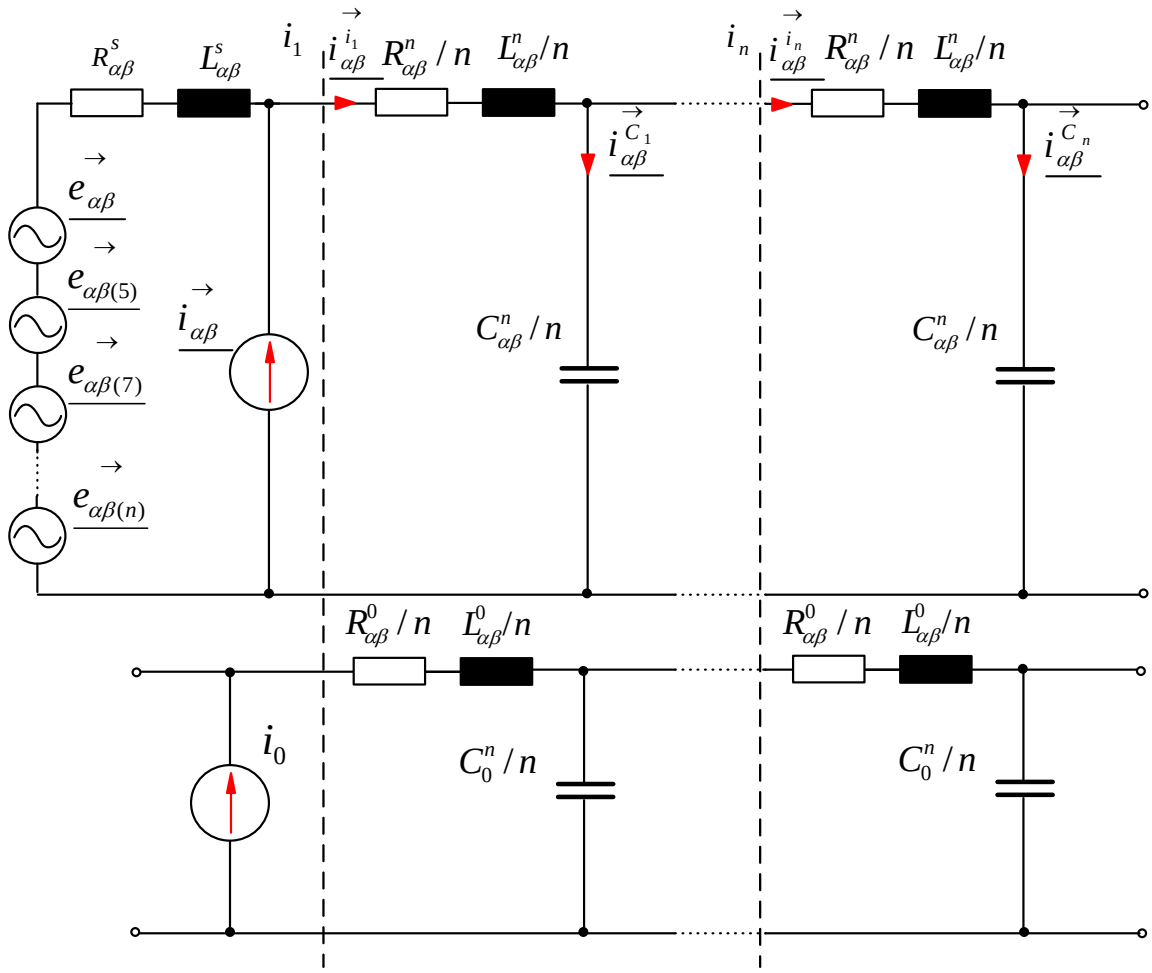

Figure 3.2.12 Long line circuit

Long distribution network

If the circuit in question operates with low AC frequency, the time delay between when the AC source generate a voltage and when the source perceives this voltage back does not matter. It is the round-trip time for the incident wave to reach the end of the line and reflect back to the source. The signal magnitude and phase along the line are not equal due to the signal propagation at some speed (this speed is usually accepted equal to the speed of light). Nevertheless, the input line signal and the output line signal can be assumed equal and in phase with each other. The equation to calculate the wavelength is as follows:

$$\lambda = \frac{c}{n \cdot f} \tag{3.3.1}$$

For 50 Hz overhead lines, the wavelength λ is 6000 km. For line lengths < $\lambda/2$, longitudinal resistances are inductive and lateral resistances are capacitive. If the line length l is sufficiently small (l <250 km for overhead lines and l <30 km for cables), the equivalent circuit diagram can be further simplified, the longitudinal resistance can be considered as combination of R and L, the lateral resistance can be considered as C [43]. The propagation effects are quicker than the period of the signal and all the line impedances can be assumed to be lumped. Thereby, almost all the 50 Hz lines can be considered short.

However, as noted in previous section the voltage source can contain the HF harmonic components. According to the equation 3.3.1 the length of the line will decrease proportionally to the harmonic number. And in some line length cases the system would contain disturbed "Γ" impedance section as it is depicted in Fig. 3.2.12.

The equations 3.2.5 and 3.2.7 cannot be used to determine the ground fault current value. The line can contain different resonances as well. To obtain the equation to determine the ground fault in this case requires an additional research.

Nonlinear loads

The HF harmonics can come not only from the voltage sources but from nonlinear loads. In the case of the radial network as it had been considered in previous section the HF current compensation principle (Figure 3.2.5) with the zero voltage measure would be applied. However, operating the long loop line with different loads along, this principle would face some problems. The example is depicted in Figure 3.2.13.

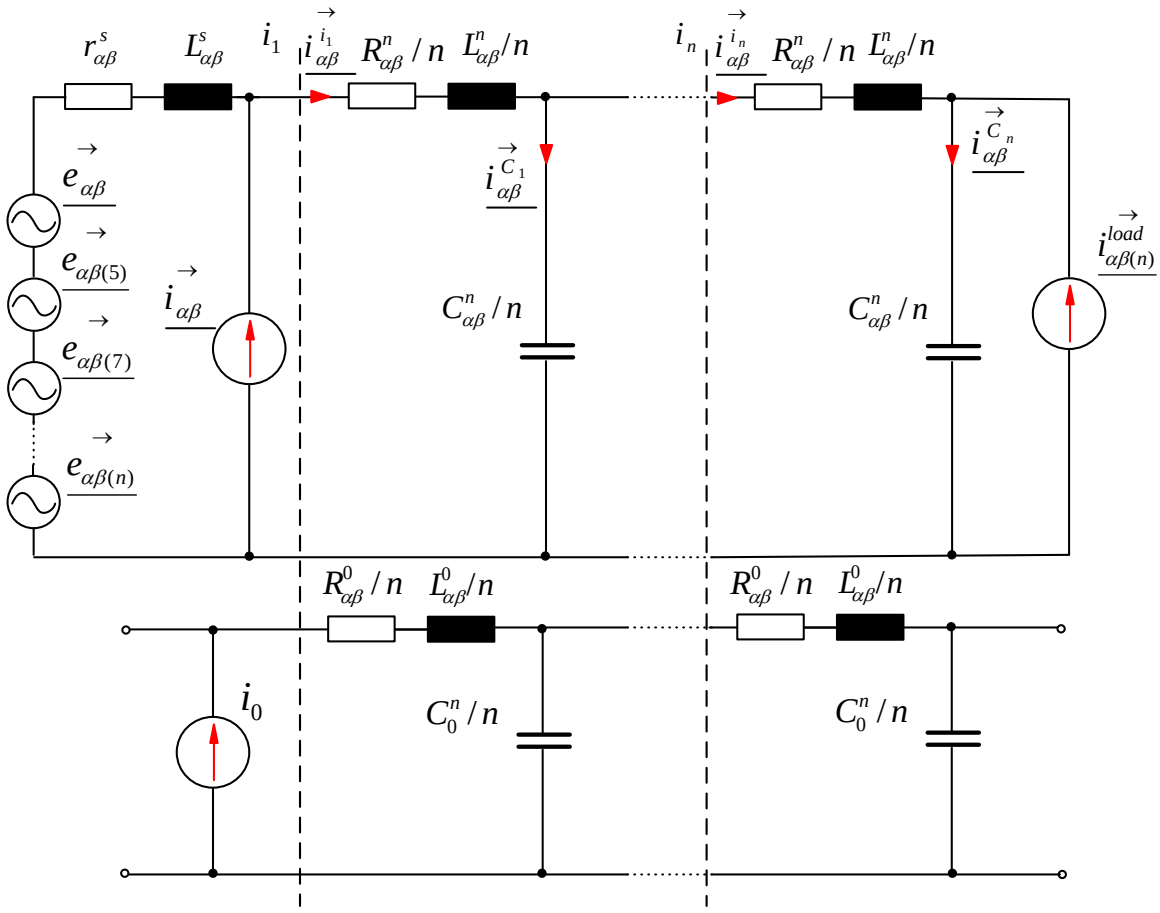

Figure 3.2.13 Nonlinear load long line circuit

When the fault would occurred, all the HF current would affect the ground fault current. In the short radial network knowing the capacitive impedance from the equation 3.2.3 and measuring the zero voltage after the fault, the HF current components to be compensated can be found as follows:

$$\underline{I^f_{(n)}} \approx \frac{\underline{U_{0(n)}}}{-j \cdot \frac{X^n_{C\alpha\beta(n)}}{3}} \qquad (3.3.2)$$

However, in the complex network the disturbed impedance can be represented as the lumped capacitance. Thus, the ground fault current cannot be compensated with the high accuracy using the presented techniques. The zero sequence circuit (model) extension is required as well.

Section conclusions and recommendations

1) The GF current value calculation method is designed allowing algorithmically determine the current network capacitance. The value of the test current and the test frequency are selected by the designer for the network in question. The current value is not allowed to change the neutral voltage more than 5% and to cause the network fluctuation.

2) The GF elimination criteria definition method is designed allowing identify the fault absence during compensation. The manual reset can also be used for this after the fault eliminating by the operational stuff.

3) Two HF zero current compensation techniques are proposed. The first one allows to compensate HF components before the fault but demands the sufficient ratio between the required compensation current and the line impedance. The second one should be used as the replacement, but demands more Hilbert filters to perform the $\alpha\beta$ –transform for every HF component to be compensated.

4) The case not allowing the line representation as the short line was considered. The consideration in detail requires an additional research.

5) The nonlinear load case was considered as well. The HF compensation technique can be applied for the short lines. For the long lines with the disturbed parameters the equivalent circuit and the method to determine the ground fault current were not studied.

6) The complex lines are proposed for the future research in this area.

CHAPTER 4. SIMULATION TESTING

4.1. Simulation circuit

To confirm the obtained algorithms and the compensation principle Matlab Simulink simulations were performed. The simulation block diagram with the whole control structure is shown in Figure 4.1.1.

For the simulation the following network and converter parameters have been used:

Table 4.1.1

Network line-to-line voltage, V	6000
Source (transformer) resistance, Ω	1
Source (transformer) inductive impedance, Ω	0,1
Line resistance, Ω	1,47
Line inductive impedance, Ω	11,9
Line capacitance-to-ground, F	0,2e-4
Commutation frequency, Hz	3000
Test frequency, Hz	25
Test signal period, s	0.5
DC link capacitance, F	10e-3

To study the obtained algorithms, a three-phase three-level neutral-point clamped multilevel converter is used. The modern power electronic devices are able to operate with such network voltage. In real network the converter probably would have to have more levels or the connection transformer. However to examine the algorithms it can be neglected.

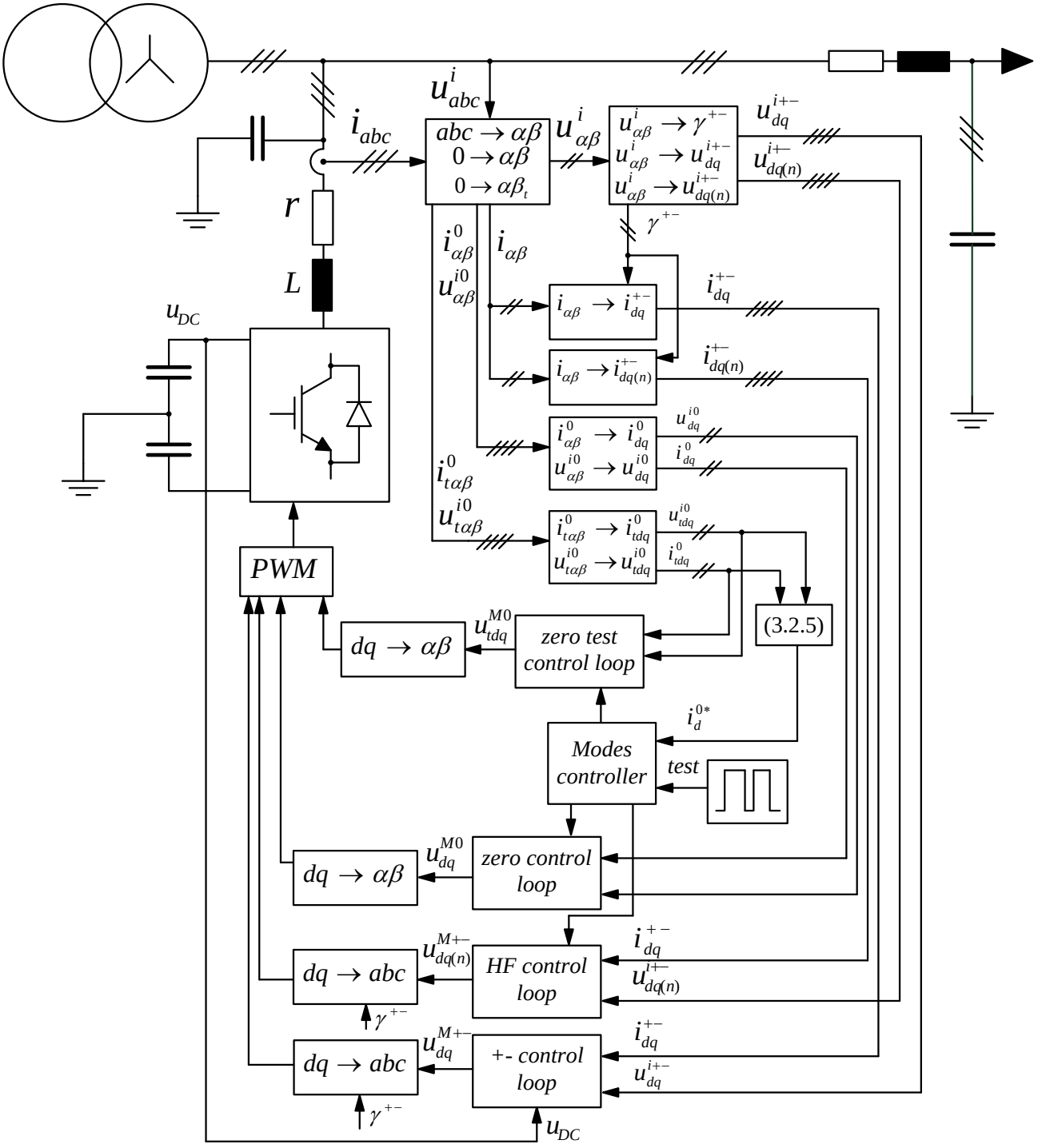

Figure 4.1.1 Simulation circuit with the control structure

To estimate inductance value the following expression can be used:

$$L = \frac{\sqrt{2} \cdot \hat{U}^{i}_{ph}}{\sqrt{3} \cdot 4 \cdot f_k} \approx 0.2\,\mathrm{H} \qquad (4.1.1)$$

Usually, the ground fault current value is within 20-150 A depending on the network capacitance. Thus to be able to compensate 150 A current the converter power should have the following power:

$$S = 3 \cdot \frac{\hat{U}_{ph}^{i}}{\sqrt{3}} \cdot \hat{I}_{ph} = 3 \cdot 4890 \cdot 50 = 733{,}5 \text{ kVA} \tag{4.1.2}$$

Since the converter should be able to operate under the line-to-line voltage, the DC capacitor voltage has to be 1.2-1.3 times more. Thus the DC voltage reference signal has to be equal to 14000 V.

It can be seen from the equation 4.1.1 that the converter has the high value inductance which comparable with the ASC. To avoid this MMC structure can be used. However, since the converter topology is already selected, the parallel connection technique can be applied. The n numbers of the converters operate with common DC link independently and connected in parallel at the output. The output converter inductance has the following dependence on the number of converters:

$$L_n \approx \frac{L}{n^2} \tag{4.1.3}$$

Figure 4.1.2 shows the converter connection structure. Every convertor has the filter inductance (equation 3.2.5) connected in parallel at the output.

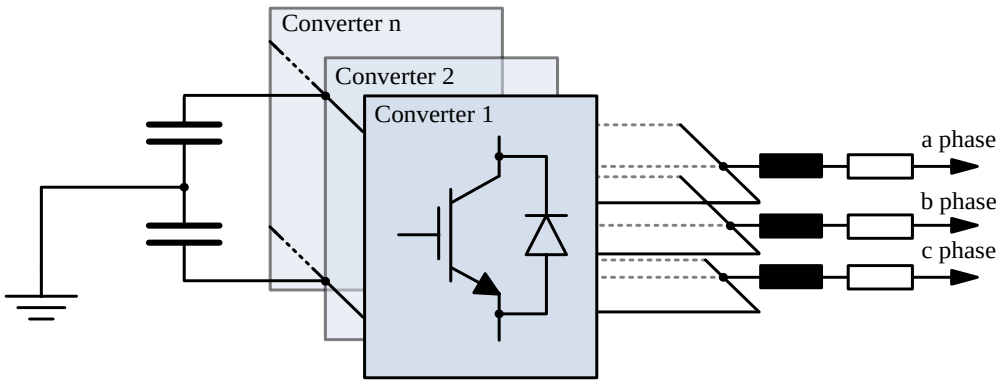

Figure 4.1.2 Parallel connection circuit

According to equations 4.1.1 and 4.1.3 5 converters are enough to decrease the output inductance. In practice 7 converters will be used to decrease the inductance to the value 6 mH.

The control system is common for all converters, but the carrier signals in PWM are shifted by $\frac{2 \cdot \pi}{n}$ relatively to the first converter.

It should be noted that the parallel connection can be replaced by the MMC structure (see Figure 1.11), which has the small filter inductance at the output [44]. But the MMC are advantageous to use with the power more than 10 MVA. Thus, the converter would have the additional functions. Using MMC the additional arm energy controllers are required [45].

4.2. Simulation results

Ground fault mode without converter

Figures 4.2.1 – 4.2.4 show the simulation results of the network without converter with the fault appearing at the time 0,7 s.

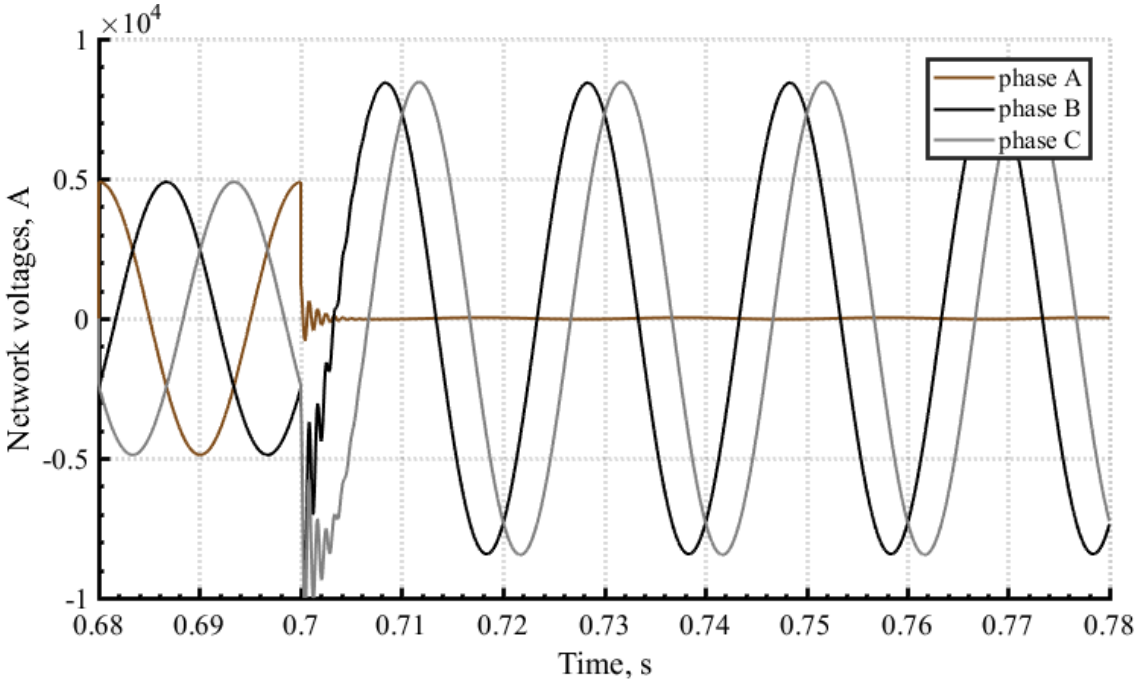

Figure 4.2.1 Network voltages after the GF without the compensation

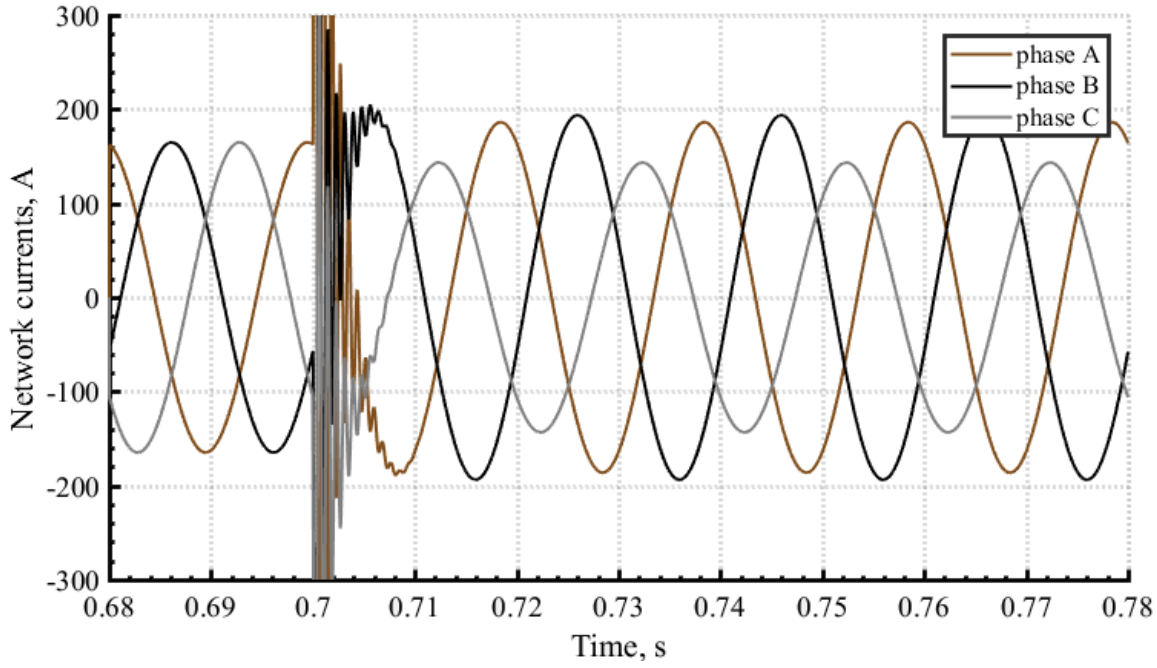

Figure 4.2.2 Network currents after the GF without the compensation

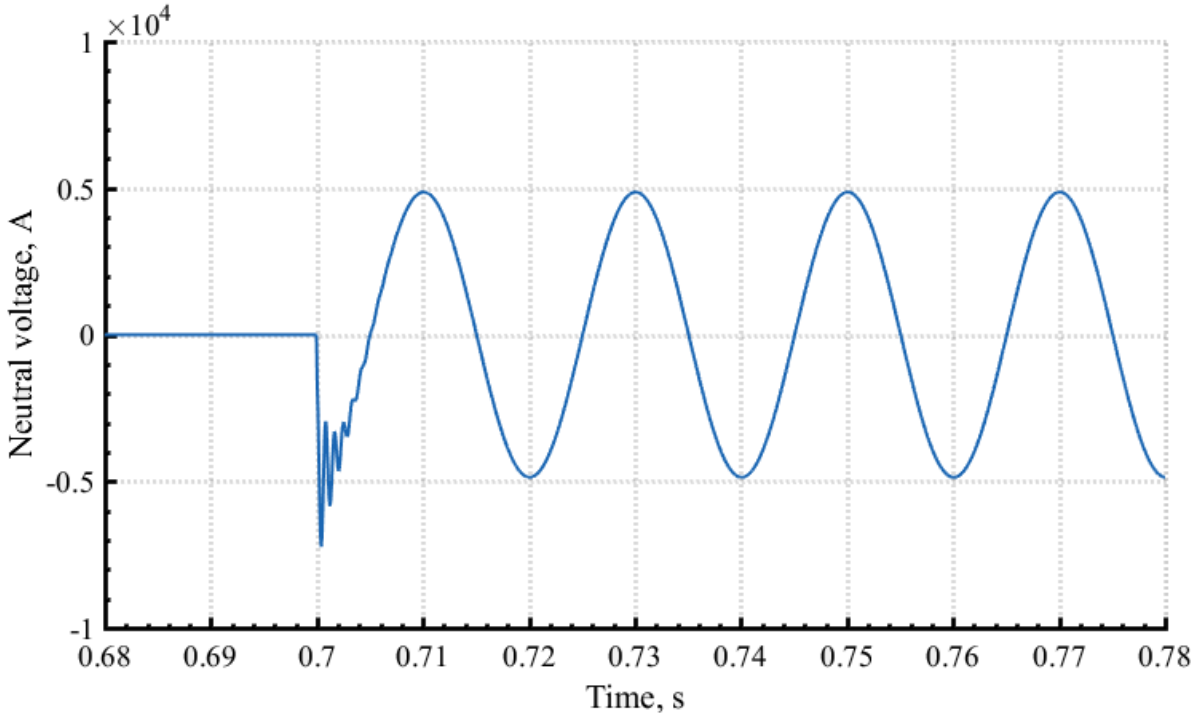

Figure 4.2.3 Neutral voltage after the GF without the compensation

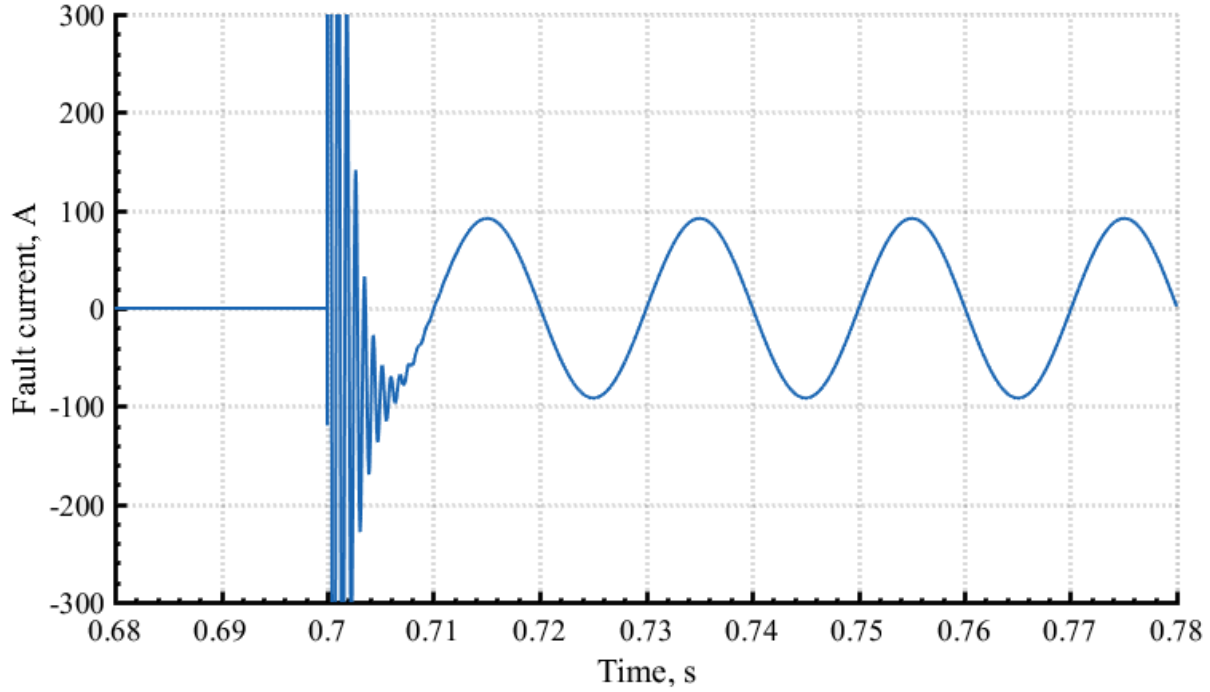

Figure 4.2.4 Fault current after the GF without the compensation

Measuring mode

Figures 4.2.5 – 4.2.7 show the simulation results of the capacitance measuring mode.

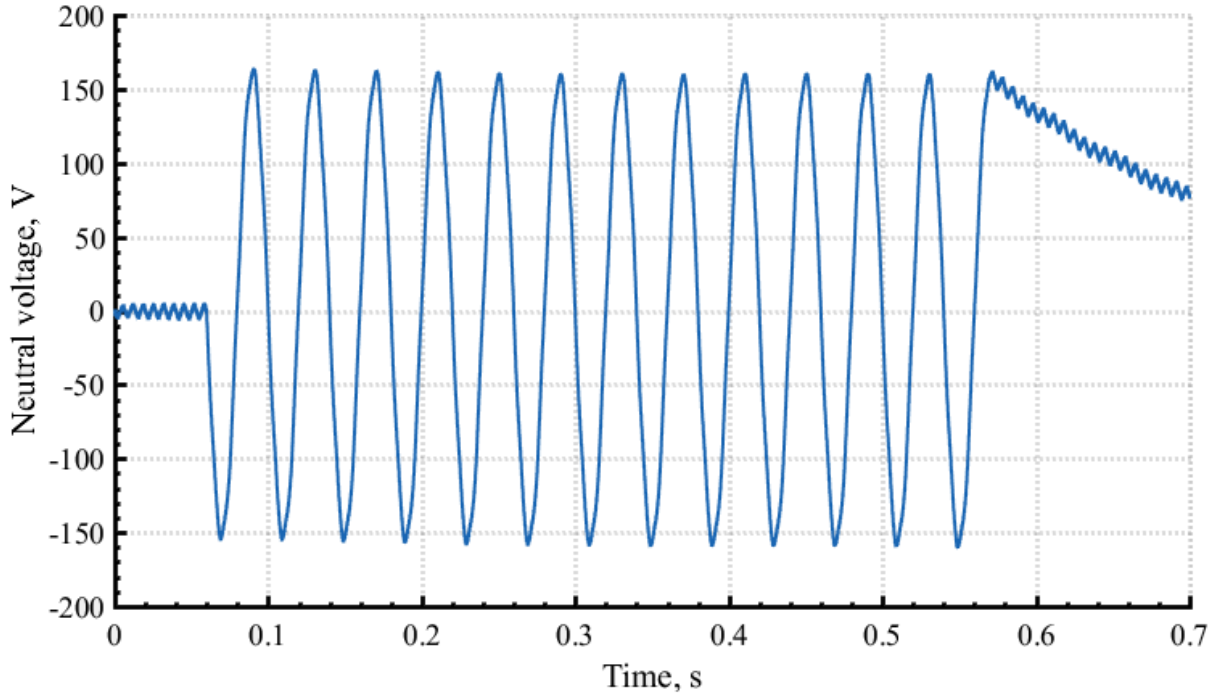

Figure 4.2.5 Neutral voltage in the measuring mode (25 Hz)

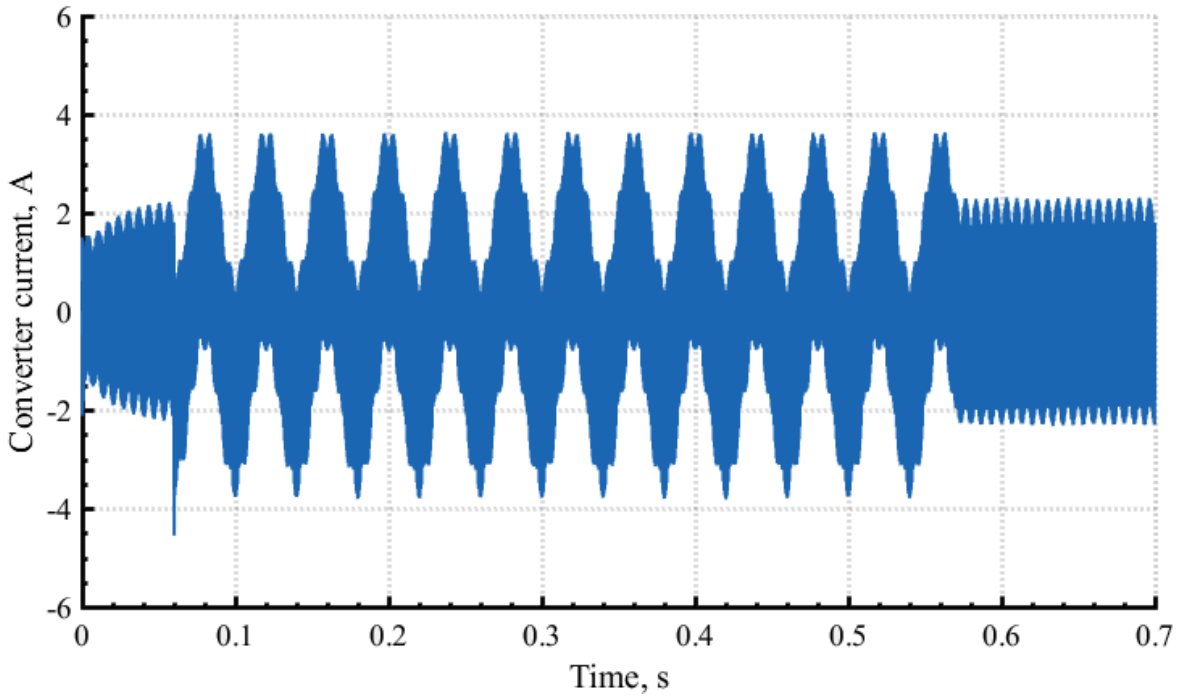

Figure 4.2.6 Converter current in the measuring mode (25 Hz)

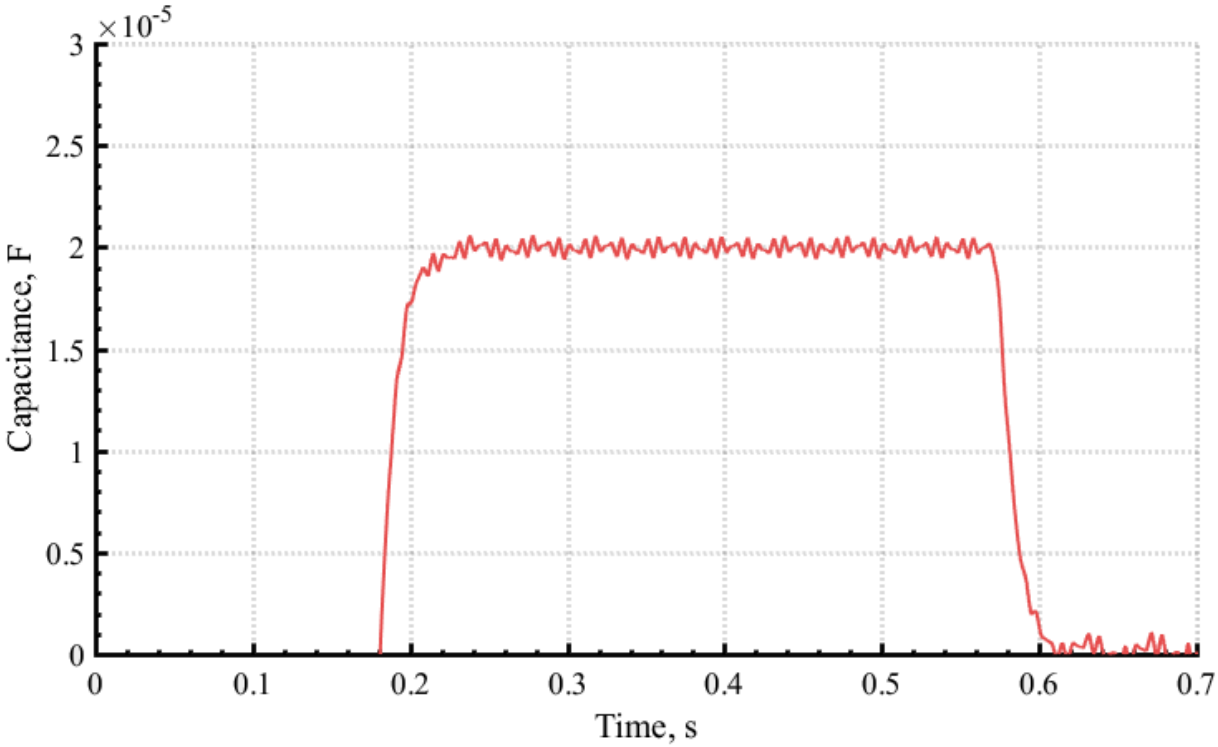

Figure 4.2.7 Measured network capacitance

As it can be seen from Fig.ure 4.1.1 the measured 25 Hz voltage is transformed into *dq* coordinates using the same principle as for the main harmonic (the Hilbert transform have been used). Using the equation 3.2.3 the network capacitance can be found. Recalling the network parameters from Table 4.1.1 one can see the accuracy of the measurement. To eliminate the HF components the low-pass filter has been used.

Compensation mode

Figures 4.2.8 – 4.2.11 show the simulation results of the fault compensation appearing at the time 0,7 s and self-extinguishing at 1,05 s.

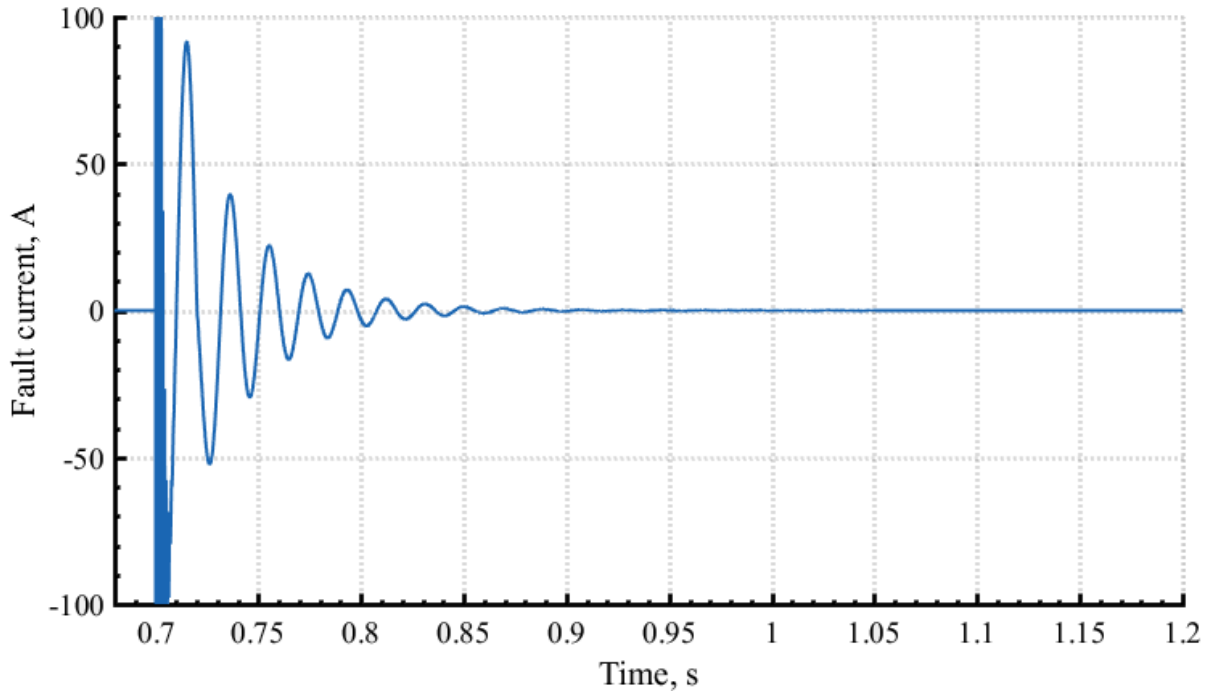

Figure 4.2.8 Fault current after the GF with the compensation

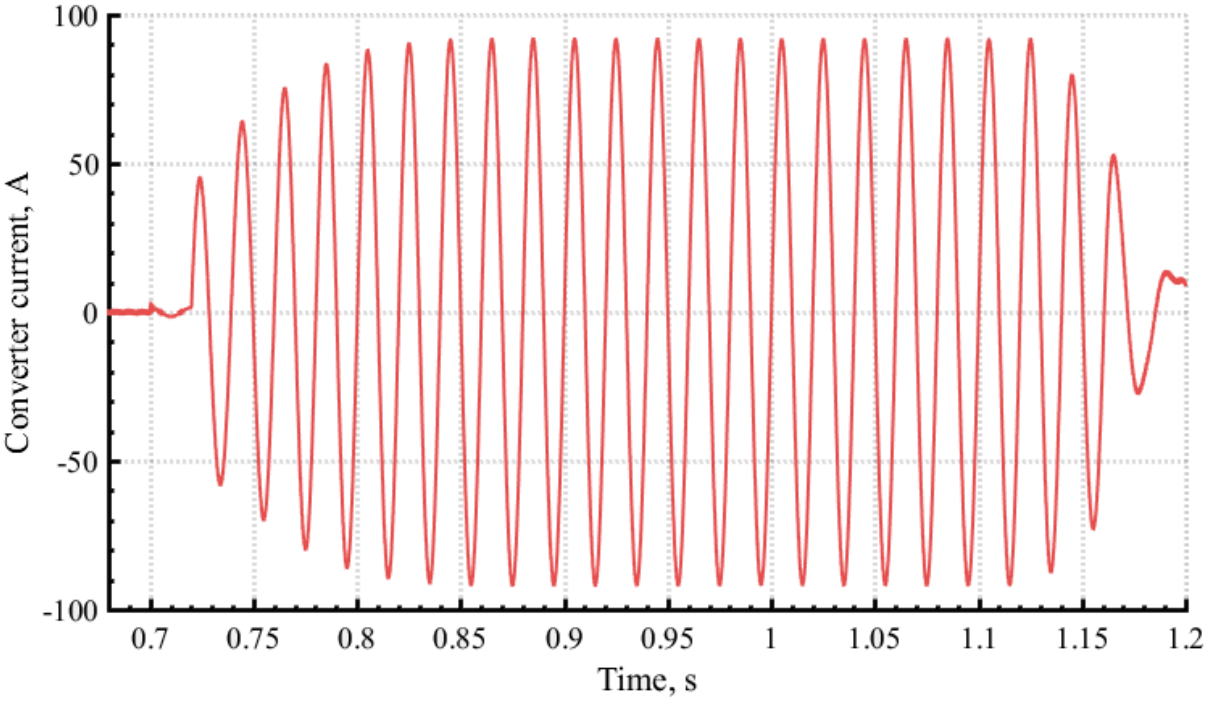

Figure 4.2.9 Converter compensation current

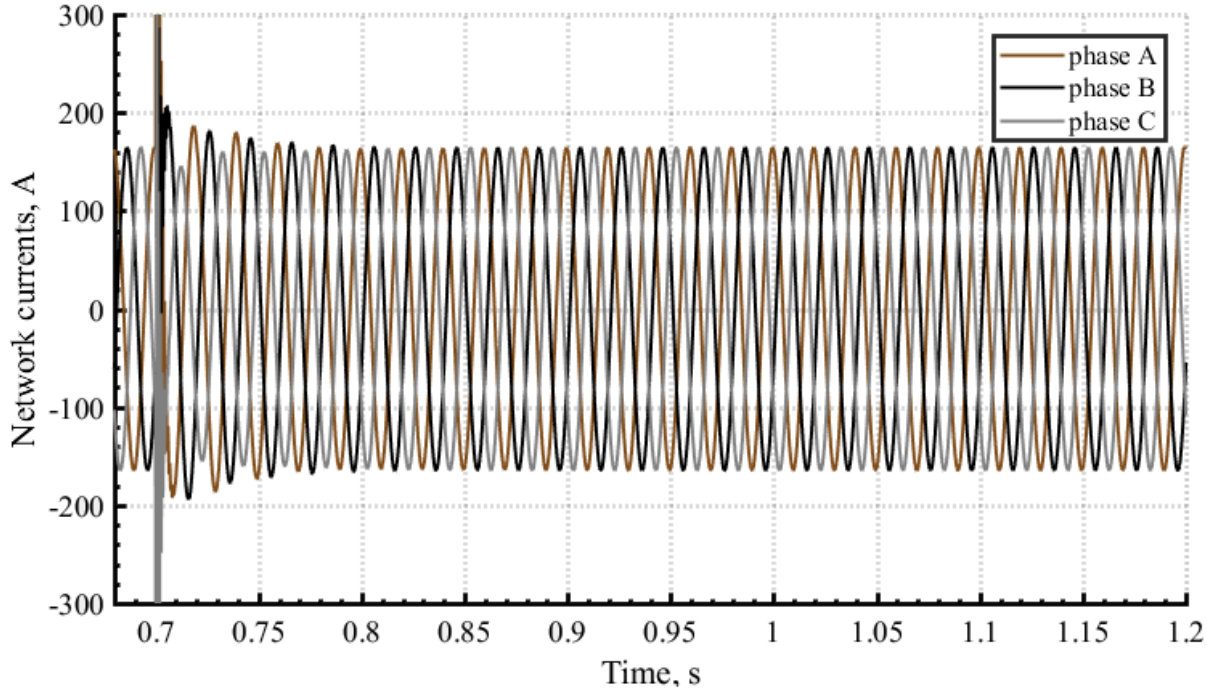

Figure 4.2.10 Network currents after the GF with the compensation

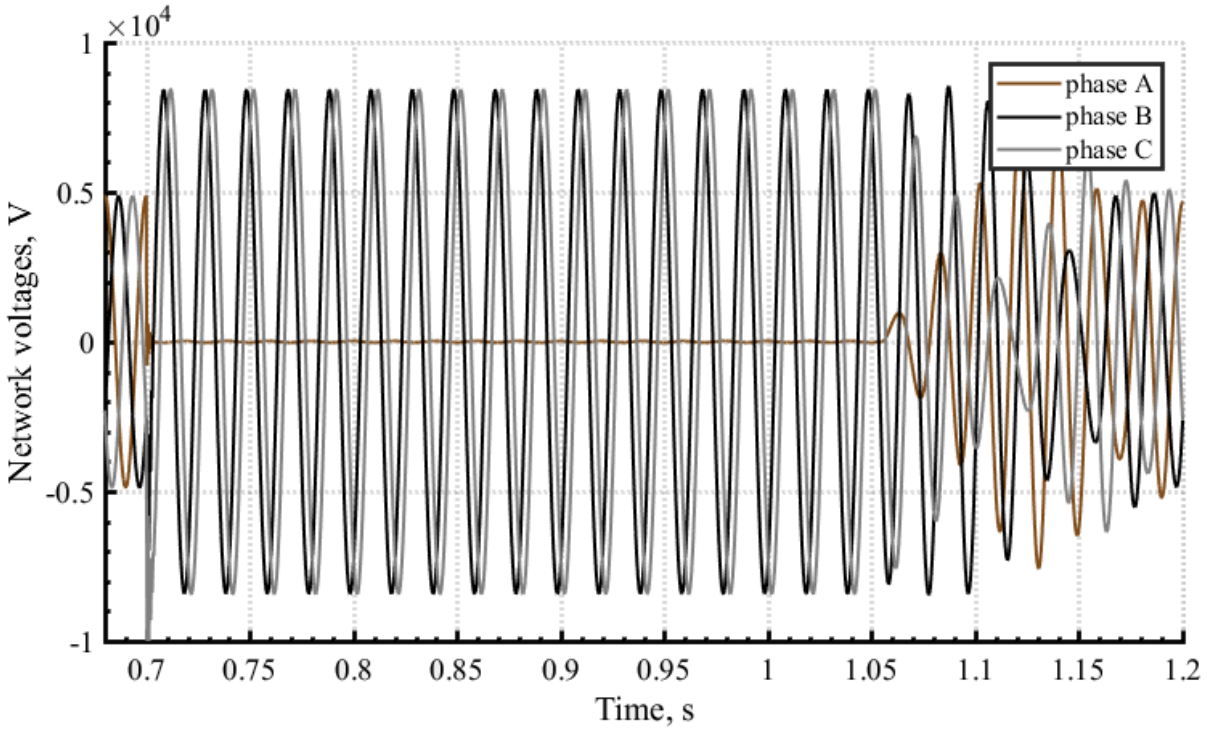

Figure 4.2.11 Network voltages after the GF fault with the compensation

After the compensation started the network currents become balanced and the GF current elimination can be seen in Figures 4.2.8 and 4.2.10. After the GF current self-extinguishing at time 1.05 s, the converter checked the fault presence and finished the compensation. The network voltages become balanced and the compensation current turns zero (Figures 4.2.9 and 4.2.11).

However, to confirm the GF elimination criteria (section 3.2) the fault time should be extended in the model. Figures 4.2.12 – 4.2.14 show the simulation results of the fault compensation appearing at time 0.7 s and self-extinguishing at 1.15 s. The period of check (see Figure 3.2.8) depend on the simulation step of the modes controller. Thus after a specified number of steps the GF presence is checked again at time 1.36 s, which is seen in Figure 4.2.14. After the positive response (there is no GF any more) the compensation is finished.

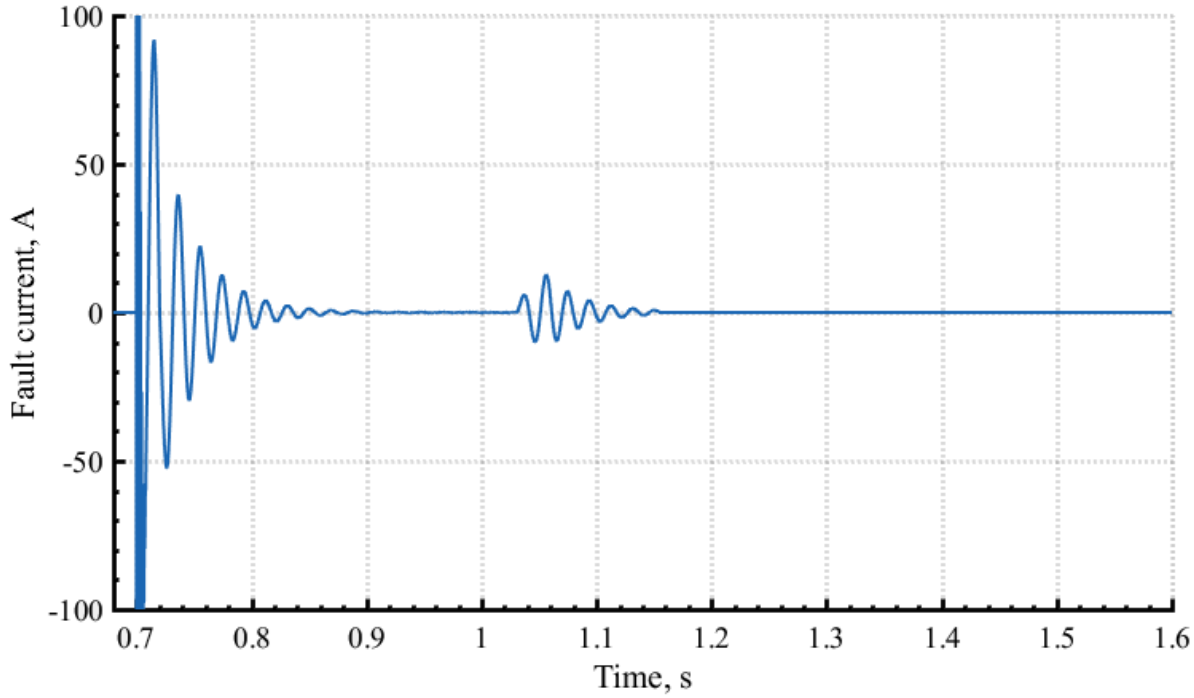

Figure 4.2.12 Fault current after the GF with the compensation

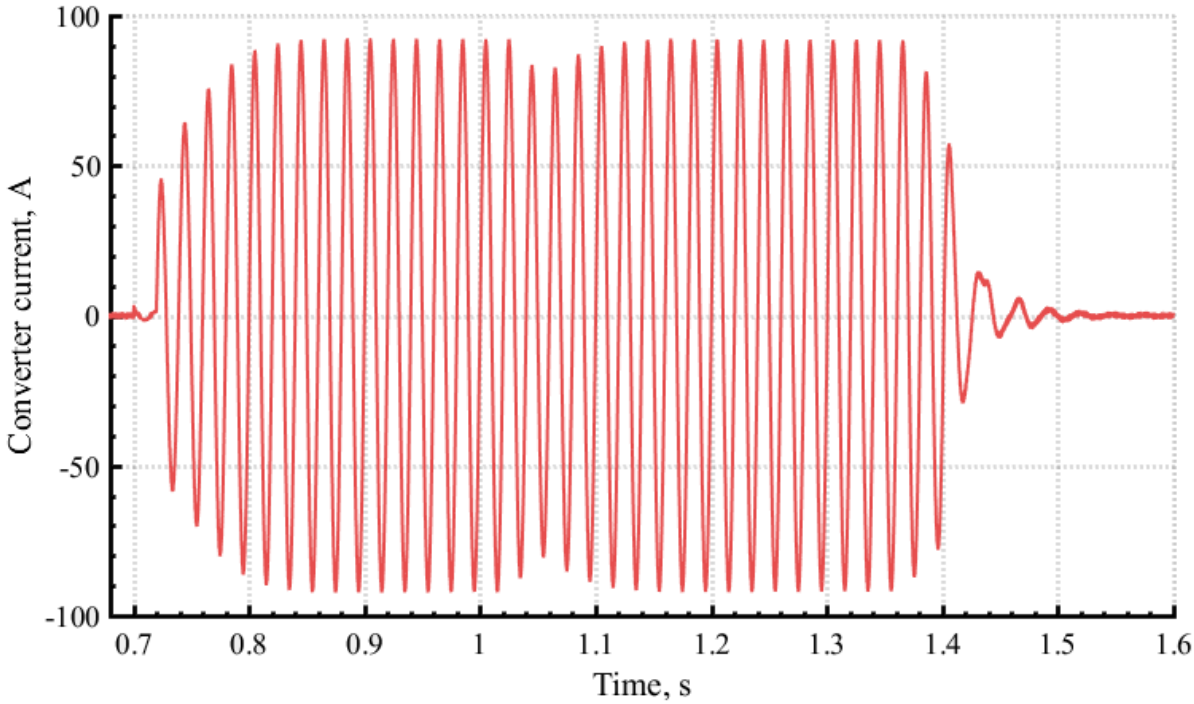

Figure 4.2.13 Converter compensation current

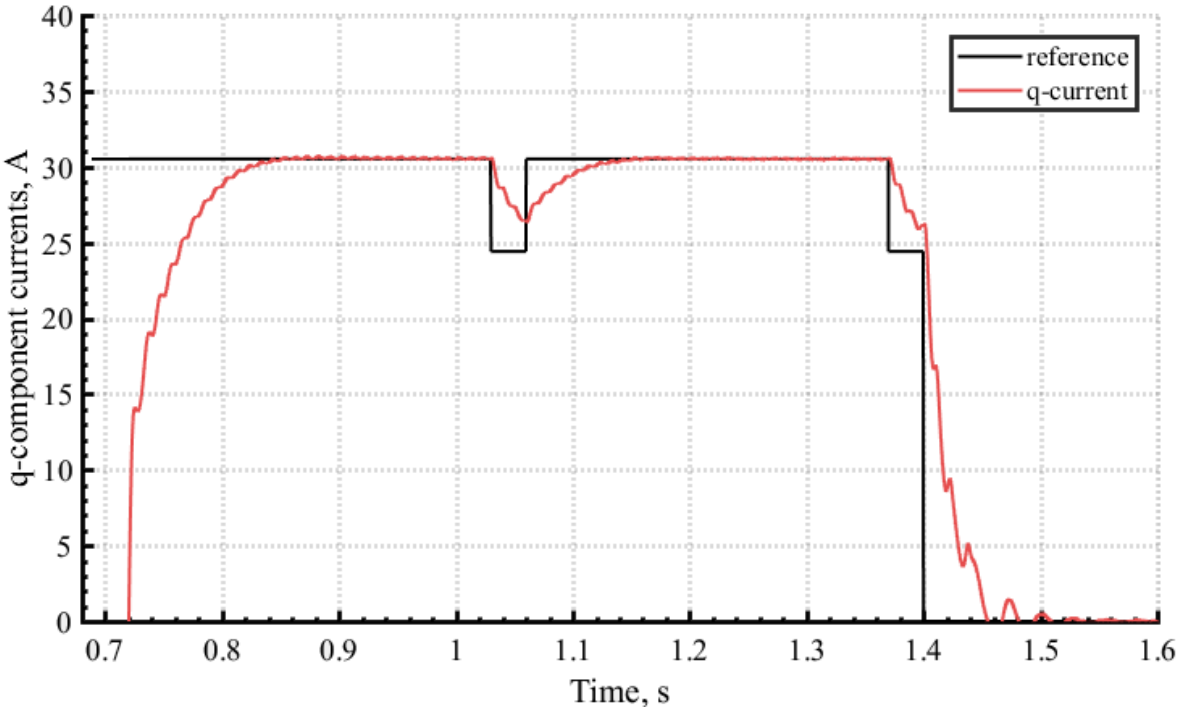

Figure 4.2.14 *q*-component controller

HF compensation mode

Figures 4.2.15 – 4.2.17 show the compensation mode with the absence of the HF (5 and 7) negative sequence voltages in the network with the fault appearing at the time 0,3 s. The HF compensation principle is demonstrated for 5th and 7th harmonic components.

As it can be seen from Figure 4.2.15 the high value HF fault current is still flowing with the exception of the fundamental harmonic component. The network voltages (Figure 4.2.16) are unsymmetrical as well. As it mentioned before one of the HF compensation techniques is based on the eliminating HF components before the fault.

Figures 4.2.18 - 4.2.21 show the processes with HF compensation. The HF compensation starts at the time 0,1s. Figure 4.2.18 show the elimination of the HF voltage components (after 0.1 s). After elimination of the HF voltages the GF current does not contain any HF components and the compensation process (see Figure 4.2.19) looks as in previous section (see Figure 4.2.8 or 4.2.12). However the converter currents contain the HF compensation components and are shown in Figures 4.2.20, 4.2.21. Examining Figures 4.2.15-4.2.21 one can conclude the efficiency of the proposed technique.

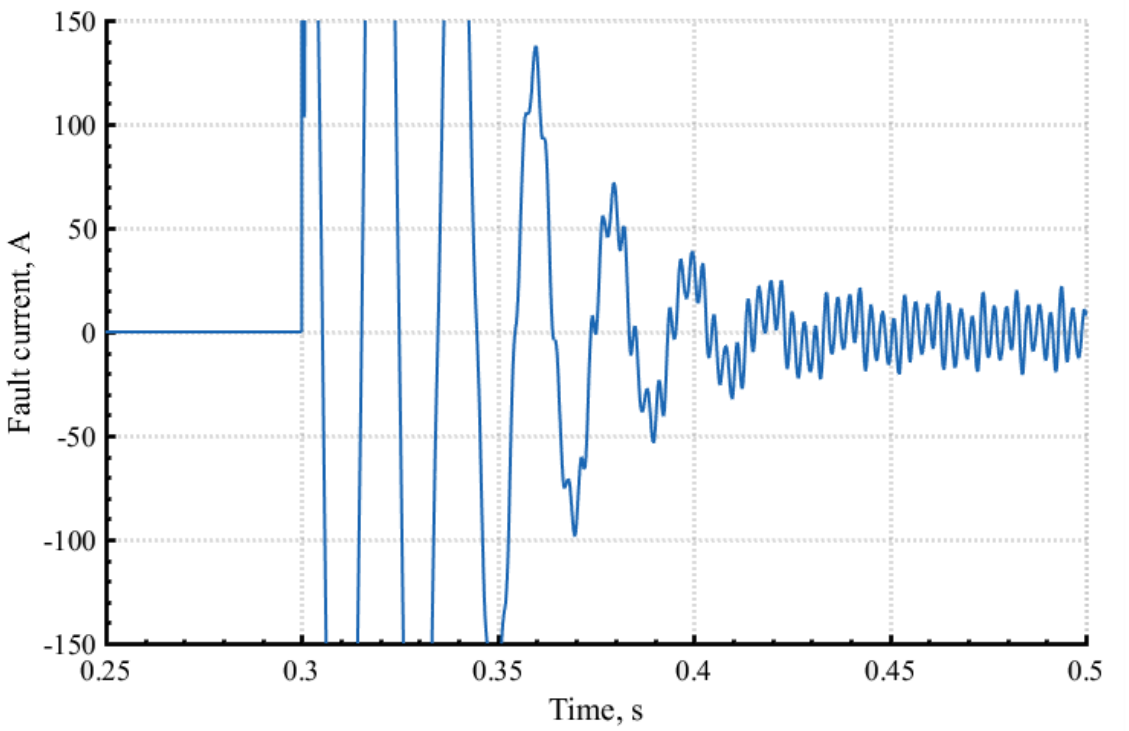

Figure 4.2.15 Fault current after the GF without the HF compensation

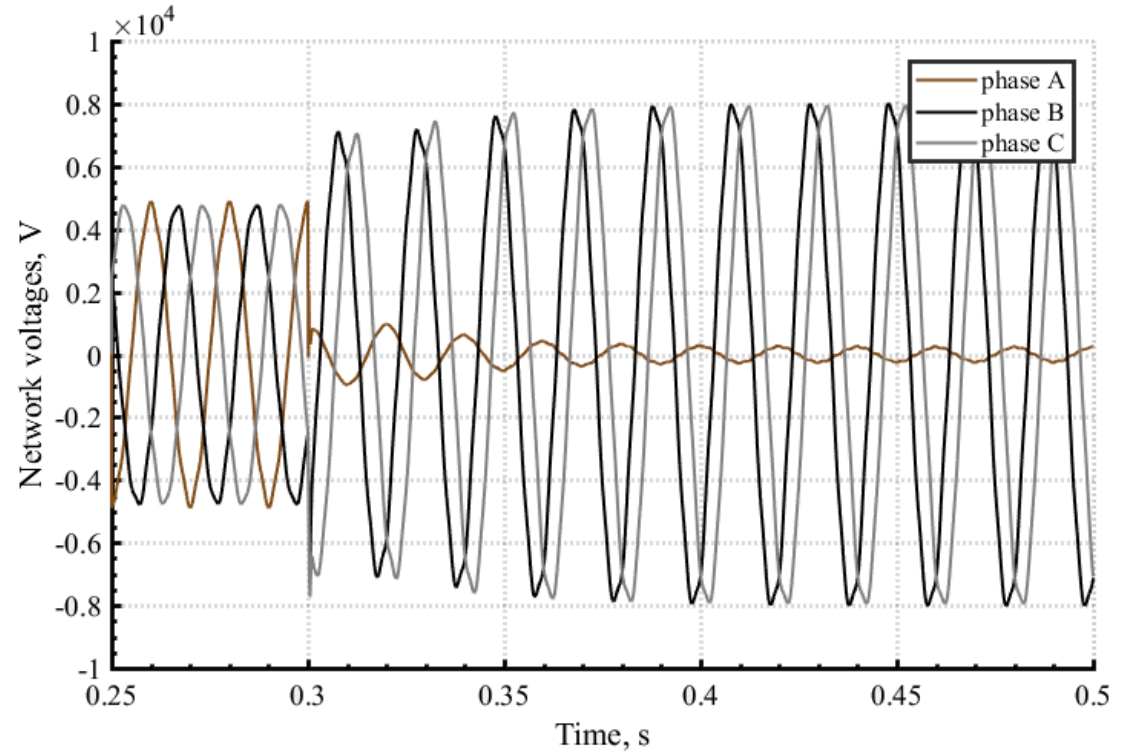

Figure 4.2.16 Network voltages after GF without the HF compensation

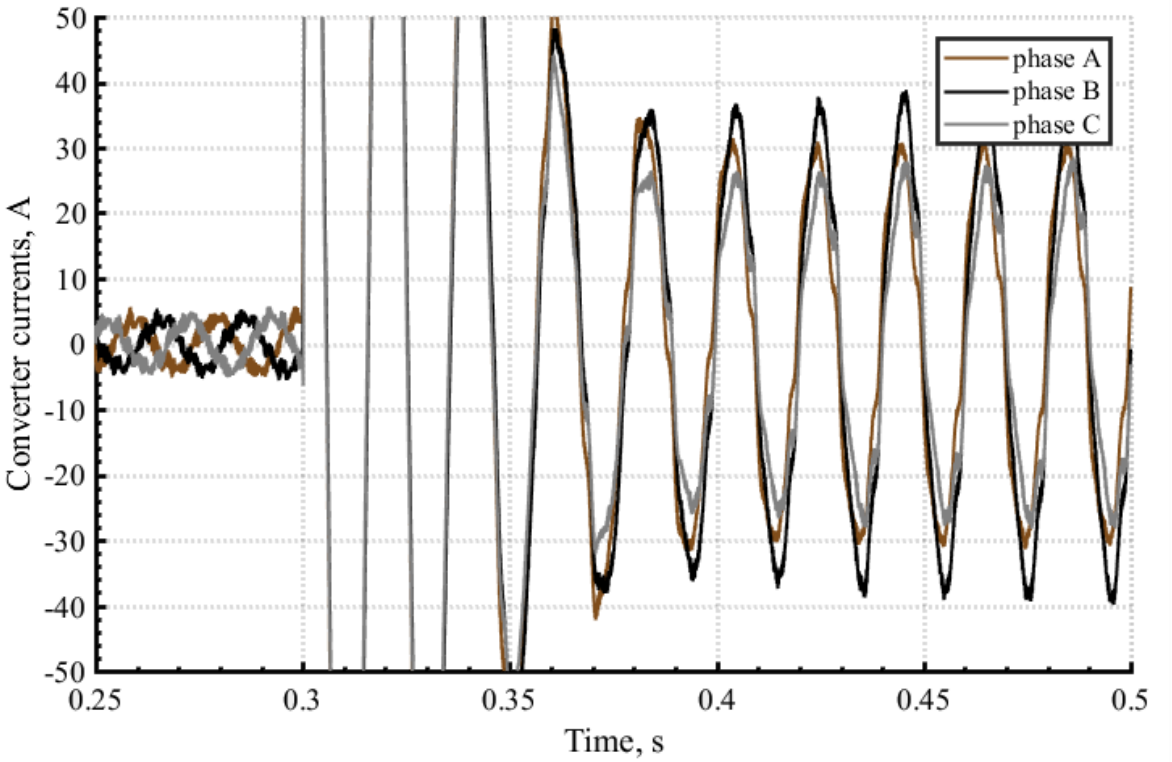

Figure 4.2.17 Converter currents without the HF compensation

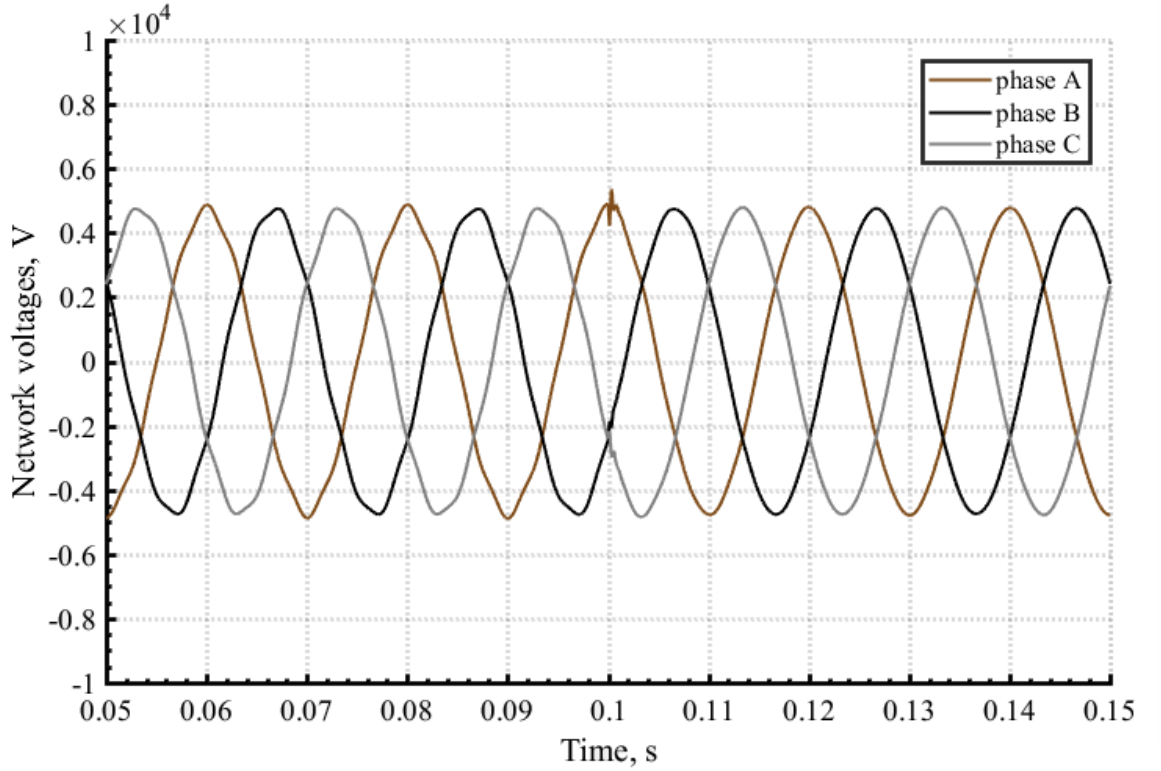

Figure 4.2.18 Network voltages after the HF compensation

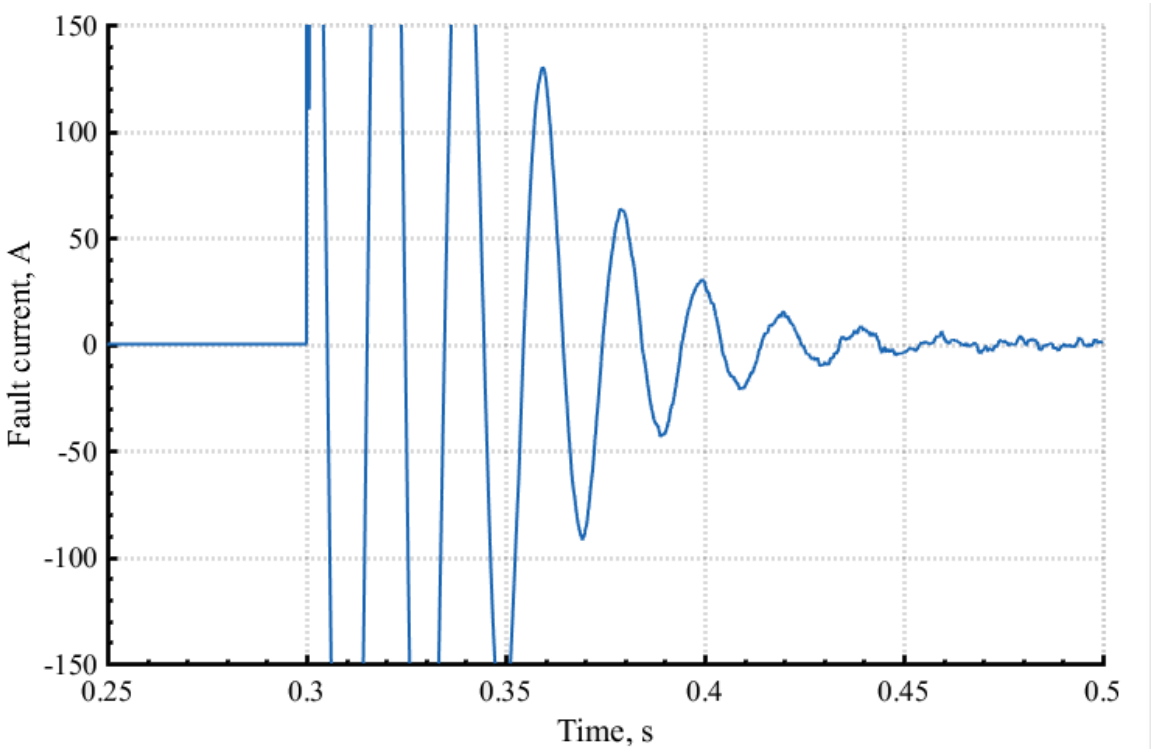

Figure 4.2.19 Fault current after the GF with the HF compensation

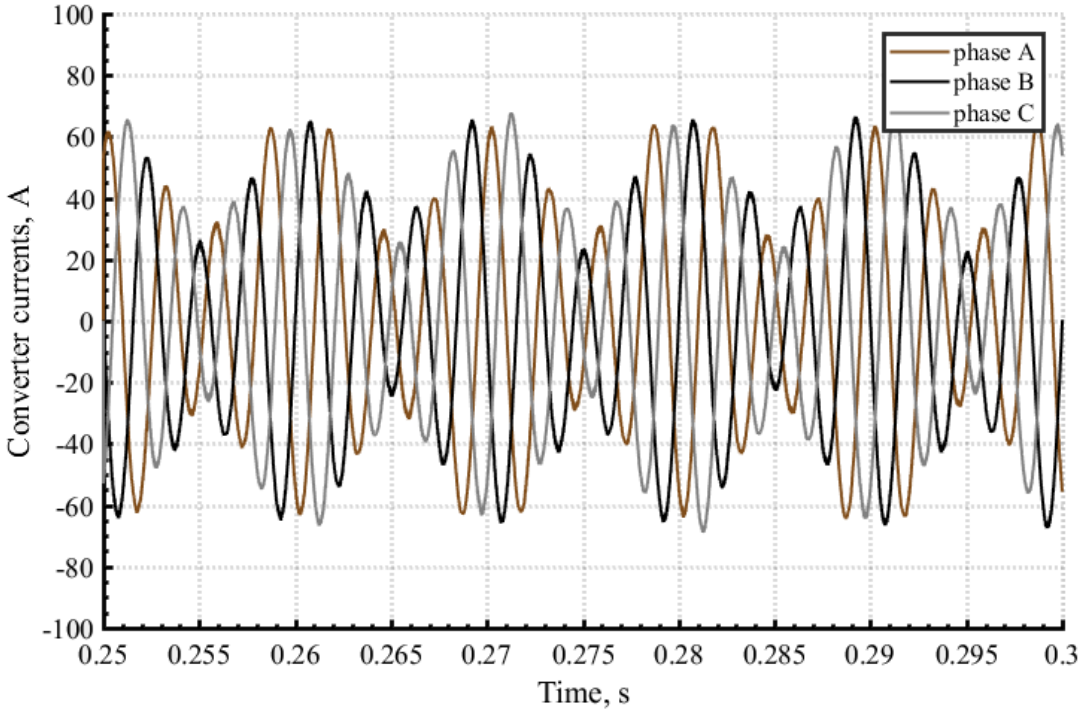

Figure 4.2.20 Converter steady-state HF compensation currents

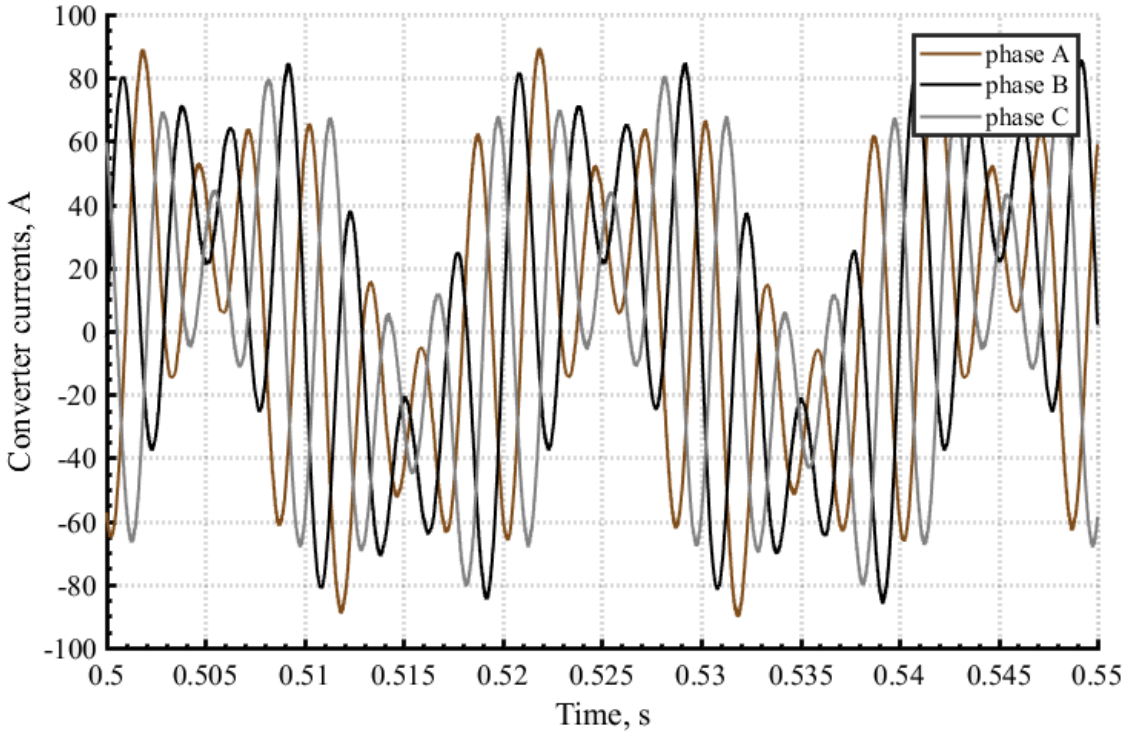

Figure 4.2.21 Converter steady-state HF and zero compensation currents

CONCLUSIONS AND OUTLOOK

In this thesis, the concept of the active ground fault current compensation converter has been demonstrated. Due to its advantages the power electronic device can change the arc suppression coils which are used now in medium voltage grids. The three-phase multilevel converter is chosen as most suitable converter topology. It offers the fast total ground fault current compensation as well as high frequency components, the ground fault current presence and elimination identification, the constant ground fault current value determination during the operation. Particularly, important for the ground fault compensation, the time response dynamic of the compensator.

The mathematical model of the network in modal coordinates to realize the compensation principle is described. Based on the model, the transient processes with the converter are considered and the converter influence on the ground fault current value is investigated. The converter current dependences on the network capacitance are obtained.

Two different symmetrical components decomposition approaches are investigated: the classical symmetrical components (CSC) method and the generalized symmetrical components (GSC) method. It is found that the CSC is more complex and can be used only at the main frequency of the input signals. The GSC is multipurpose in terms of the input harmonic composition due to the Hilbert filter using. While using the generalized components method a specific frequency range of interest to be decomposed can be selected. The different synthesis approaches of the Hilbert filter structures are investigated. The second-order IIR filter structure is chosen to be used in control algorithm.

In order to synthesize the converter control structure the mathematical model in *dq*-reference frame is used. Applying the direct synthesis method for DC-DC convertors, the converter control structure is obtained and the controller parameters can be calculated. It has three independent loops in parallel (main harmonic) to control the output converter current: positive, negative and zero sequence loop. The positive sequence loop is used to control the DC-link voltage as well.

The operation modes of the converter are considered. Analyzing the existing methods of the grid capacitance determination, the most suitable has been selected and examined. The ground fault presence and elimination criteria are investigated and selected. The ground fault presence is identified by the neutral voltage increasing more than 15% of the nominal voltage. The ground fault elimination is identified by the zero voltage dependency on the converter current (see Section 3.2).

The high frequency components compensation is investigated. Two different techniques are considered: the compensation of the source voltages before a fault and the compensation of zero currents after a fault. The voltage sources before the fault can be compensated only when there is sufficient ratio between the line impedances and the converter currents. The HF current compensation does not have any restrictions but requires more Hilbert filters to perform the *dq*-

transformation for each HF component. Finally, the complex long line is theoretically considered as well as the case of nonlinear loads. The effects of the complex long line need closer investigation in the future.

The final chapter is dedicated to the power circuit parameters and simulation. The simulations are performed in Matlab Simulink. The 7 3-level diode clamped converters, which are connected in parallel to decrease the output filter inductance, are used. The simulations prove all the synthesized algorithms for the main harmonics and for the HF components: the compensation principle (main and HF components), the ground fault presence and elimination, the grid capacitance measurement and the switching between the operation modes.

As the further investigation the circuit with the transformer can be considered as well as the complex grid. The hybrid compensation circuit which includes the one-phase converter for ground fault current compensation and the three phase active power filter can be the subject of the future research work as well.

Bibliography

1. Donald W. Zipse, Earthing – Grounding Methods – A Primer, IEEE's IAS' PCIC's Technical Conference, Sept 24, 2001, IAS/PCIC 01-02.
2. J. R. Dunki-Jacobs, "The historical development of neutral grounding practices,"IEEE Ind. Applicat. Mag., vol. 3, pp. 10–20, Mar./Apr. 1997.
3. Y. Hase. *Handbook of Power System Engineering*. John Wiley & Sons, Ltd, 2013. – 768 p.
4. T.A. Short. *Electric Power Distribution Handbook.* CRC PRESS, 2004 – 768 p.
5. CEA, CEA Distribution Planner's Manual, Canadian Electrical Association, 1982.
6. EPRI TR-109178, *Distribution Cost Structure — Methodology and Generic Data*, Electric Power Research Institute, Palo Alto, CA, 1998.
7. Power Quality Implications of Distribution Construction, EPRI, Palo Alto, CA: 2004. 1002188
8. L. Wang. The fault causes of overhead lines in distribution networks. APOP2016.
9. Dunki-Jacobs, J. R., The Escalating Arcing Ground-Fault Phenomenon, IEEE Trans. Ind. Appl. IA-22, p. 1156-1161 (1986).
10. F. A. Likhachev, "Ground faults in ungrounded and resonant grounded networks". Moscow: Energiya, 1971. (in russian) (Лихачев Ф.А. Замыкания на землю в сетях с изолированной нейтралью и с компенсацией емкостных токов. - М.: Энергия, 1971. - 152 с.)
11. Rules of technical operation of power plants and networks of the Russian Federation (in russian). Правила технической эксплуатации электрических станций и сетей Российской Федерации. СПб.: Изд-во «Деан», 2000. – 352 с.
12. Ayurzana E., Mambetzhanov A.D., Takyrbashev B.K., Dzhamagidze D., Petrov M.I., Kuzmin A.A. Assessment of the components of the current single-phase earth fault when conducting field experiments in the networks of the middle class voltage for various purposes.(in russian) (Оценка составляющих тока однофазного замыкания на землю при проведении натурных экспериментов в сетях среднего класса напряжения различного назначения).
13. DIN VDE 0101 (VDE 0101):2000-01 Starkstromanlagen mit Nennwechselspannungen über 1 kV. Berlin Offenbach: VDE VERLAG.
14. Stade, Dietrich; Schau, Holger. Influence of voltage harmonics on single-phase earth fault currents. First International Conference „Power Quality" Paris 15.10. – 18.10.1991 Session D2: Network-based quality improvements Report D-24
15. Petersen W. Neutralizing of ground fault current and suppression of ground fault arcs through the ground fault reactor. E.T.Z., 1919.
16. IEEE T STANDARD 142-2007— IEEE Recommended Practice for Grounding of Industrial and Commercial Power Systems (Green Book).

17. IEEE Std C57.32™-2015, IEEE Standard for Requirements, Terminology, and Test Procedures for Neutral Grounding Devices.

18. Standard instruction for compensation of capacitive earth fault current in electric networks of 6–35 kV (in Russian). (Типовая инструкция по компенсации емкостного тока замыкания на землю в электрических сетях 6–35 кВ (РД 34.20.179). Утверждена Главным научно-техническим управлением энергетики и электрификации 06.06.1987).

19. DIN VDE 0228, Maßnahmen zur Beeinflussung von Fernmeldeanlagen durch Starkstromanlagen, 1987.

20. Poll J., Löschung von Erdschlusslichtbögen, In: Elektrizitätswirtschaft, Jg.83 (1984 Heft 7, pp 322-327, VWEW-Verlag, Frankfurt am Main.

21. Wang Chonglin, Liang Rui, Liu Jianhua. Analysis on principle of operation of arc-suppression coil based on thristor controlled reactor. Proceedings of the 8th International Conference on Electrical Machines and Systems. ICEMS 2005, Sep. 2005, vol.2, pp: 1305-1308.

22. Druml G., Kugi A., Parr B., "Control of Petersen Coils", XI. International Symposium on Theoretical Electrical Engineering, 2001, Linz.

23. Han Xue, JiJiang Song. *Influence of the arc suppression coil with parallel resistance on single-phase arc grounding overvoltage*, Advanced Materials Research, Trans Tech Publications, Switzerland, 2013. p.284-288.

24. Zhanjun Qiao. Analysis and simulation on intermittent arc grounding overvoltage for neutral grounding via arc-suppression coil with shunt resistance in 35 kV urban distribution system, International Journal of Signal Processing, Vol.7, N. 5, 2014. p. 37 - 46.

25. Nasarichev A. N., Pugachev A.A., Titenkov S.S. Combined neutral grounding in networks 6–35 kV. Myths and Reality (in russian). Комбинированное заземление нейтрали в сетях 6–35 кВ. Мифы и реальность // Новости ЭлектроТехники. 2016. № 3(99).

26. Nasarichev A. N., Pugachev A.A., Titenkov S.S. Combined neutral grounding in networks 6–35 kV. Myths and Reality - 2 (in russian). Комбинированное заземление нейтрали в сетях 6–35 кВ. Мифы и реальность - 2 // Новости ЭлектроТехники. 2016. № 6(102).

27. Cerretti A. Practice of Conversion of Neutral Earthing Scheme and Experiences // 18th International Conference on Electricity Distribution (CIRED): Round Table Presentation. Turin, 2005.

28. Tomas Komrska, Zdenek Peroutka. A novel least norm-based PWM for a four-leg earth fault compensator, IECON 2014 - 40th Annual Conference of the IEEE Industrial Electronics Society 2014, Pages 1118 - 1123.

29. Device for compensation of earth fault current in three-phase electrical networks (versions): Pat. RU 2524347 (in russain). Устройство компенсации тока замыкания на землю в трехфазных электрических сетях (варианты): пат. RU 2524347 C2 Рос. Федерация: МПК H02J 3/26, H02M 7/44/ Мустафа Г.М.; заявитель и патентообладатель Мустафа Г.М.. – № 2012119729/07; заявл. 15.05.12; опубл. 20.11.13, Бюл. № 32.

30. W. Wang, L. Yan, X. Zeng, B. Fan and J. M. Guerrero, “Principle and Design of a Single-Phase Inverter Based Grounding System for Neutral-to-Ground Voltage Compensation in Distribution Networks”, *IEEE Trans. Ind. Electron.*, 2017, Volume: 64, Issue: 2, p. 1204 - 1213

31. W. Wang, L. Yan, X. Zeng, B. Fan and J. M. Guerrero, “Principle and Control Design of Active Ground-Fault Arc Suppression Device for Full Compensation of Ground Current”, *IEEE Trans. Ind. Electron.*, 2017, Volume: 64, Issue: 6, p. 4561 - 4570

32. Vagner K.F., Evans R.D. The method of symmetrical components (in russian). Метод симметричных составляющих. ОНТИ ККТП СССР, 1936. 408с.

33. C.L. Fortescue, “Method of Symmetrical Co-ordinates Applied to the Solution of Polyphase Networks”, *A.I.E.E. Trans.*, vol. 37, June 1918, pp. 1027-1140.

34. Kharitinov S.A., Djoraev T.U. Application of the Hilbert transform in power supply systems with semiconductor frequency converters (in russian). Харитонов С.А., Жораев Т.Ю. Применение преобразования Гильберта в системах электроснабжения с полупроводниковыми преобразователями частоты. Труды XXV Межрегиональной НТК «Проблемы эффективности и безопасности функционирования сложных технических и информационных систем», ч. 5. – Серпухов, 2006. - С. 109-115

35. Kharitinov S.A., Djoraev T.U. The generalized method of symmetrical components and the method of their separation using a digital phase-shift filter (in russian). Харитонов С.А., Жораев Т.Ю. Обобщенный метод симметричных составляющих и методика их выделения с помощью цифрового фазовращающего фильтра. Научный вестник НГТУ. -. - №1(34), Новосибирск, НГТУ, 2009, с. 191-203.

36. Kharitinov S.A. Geometric analogies in the analysis of energy characteristics in electrical circuits with semiconductor devices (in russian). Харитонов С.А. Геометрические аналогии при анализе энергетических характеристик в электрических цепях с вентилями. Научный вестник НГТУ. - Новосибирск: НГТУ, 1998. - С.77-111.

37. Frenks L. Signal Theory (in russian). Френкс Л. Теория сигналов. - М., «Сов.радио», 1974. – 344 с. с ил.

38. Alan V. Oppenheim, Ronald W. Shafer. Digital signal processing. – Prentice Hall, INC, Englewood cliffs, New Jersey. 1975. – 416 p.

39. Lawrence R. Rabiner, Bernard Gold. Theory and application of digital signal processing. – PrenticeHall, INC, Englewoodcliffs, NewJersey. 1975. – 848 p.

40. Katsikis. V.N. MATLAB - A Fundamental Tool for Scientific Computing and Engineering Applications – Volume 1, 2012.

41. Igor O. Bessonov, Sergey A. Kharitonov, Denis V. Makarov, Maksim A. Zharkov: Synthesis of Circuit Regulation of Current for Buck DC-DC Converter. Methodical Aspect, 16th International Conference on Micro/Nanotechnologies and Electron Devices EDM 2015, June 30 2014-July 4 2014, Pages 391 – 396.

42. H. Akagi, E. H. Watanabe, and M Aredes, Instantaneous Power Theory and Applications to Power Conditioning. Piscataway, NJ: IEEE Press, 2007.

43. Crastan V. *Elektrische Energieversorgung 1*. Springer Vieweg, 2015. – 668 p.

44. F. Zhang and G. Joos, “A predictive nearest level control of modular multilevel converter,” in Proc. IEEE Appl. Power Electron. Conf. Expo. (APEC), Mar. 2015, pp. 2846–2851.

45. G. Bergna, E. Berne, P. Lefranc, and M. Molinas, “Modular multilevel converter leg-energy controller in rotating reference frame for voltage oscillations reduction,” in Proc. IEEE PEDG, Jun. 2012, pp. 698–703.

Glossary

AC	alternating current
GF	ground fault
MVAC	medium voltage alternating current
HVAC	high voltage alternating current
ASC	arc suppression coil
HV	high voltage
MV	medium voltage
AEFCC	active earth fault current compensator
MMC	modular multilevel converter
HF	high frequency
FFT	fast Fourier transformation
SO	symmetrical optimum
MO	modulus optimum
IIR	infinite impulse response
FIR	finite impulse response
STATCOM	static synchronous compensator
NPC	neutral-point clamped
PI	proportional-integral
PWM	pulse-width modulation

Style of writing

Variables:

e, i	small letter: time variables
$\boldsymbol{e, i}$	bold letter: matrix, column matrix or vector
r, L, C	resistance, inductance and capacitance
$\underline{I}$	complex variables
X	complex inductive and capacitive reactance
$\underline{Z}$	complex impedance
$\hat{I}$	amplitude values
b_0, a	coefficients
$h(n), w(n)$	impulse responses
$\vec{\underline{u}}$	complex vectors
$\dot{i}$	derivative
γ	gamma
T_μ	time constants

Indexes:

s	source variable
n	network variable (resistance, reactance)
a, b, c	phase indexes
C	capacitance variables(currents and voltages)
$L1 ... Lm$	load variables
$i,\ k\ , f$	cross-sections
n	neutral variable (voltage, current)
$\alpha\beta 0$	Clarke domain components
α	α circuit components
β	β circuit components
0	zero circuit components (lower)
0	zero circuit d and q (DC signals) components (upper)
f	fault cross-section components
$+$	positive circuit components
$-$	negative circuit components
h	Hilbert transformations
$+-$	components without zero sequence

d	d circuit components
q	q circuit components
$*$	reference signals
c	current loop components
v	voltage loop components
LP	low pass filter
m	modulation signals
$'$	filtered variables
t	test signal
(n)	harmonic variables

List of Figures

APPENDIX

The network currents can be determined as follows:

$$\mathbf{i^i = i^i_{\alpha\beta 0}} \cdot \left[\mathbf{T_{\alpha\beta 0}}\right]^{-1} = \begin{bmatrix} \mathrm{i}^{\mathrm{i}}_{\alpha} \\ \mathrm{i}^{\mathrm{i}}_{\beta} \\ \mathrm{i}^{\mathrm{i}}_{0} \end{bmatrix} \cdot \begin{bmatrix} 1 & 0 & 1 \\ -1/2 & \sqrt{3}/2 & 1 \\ -1/2 & -\sqrt{3}/2 & 1 \end{bmatrix} = \begin{bmatrix} i_a^i + i_0^i \\ -\frac{1}{2}\cdot i_a^i + \frac{\sqrt{3}}{2}\cdot i_b^i + i_0^i \\ -\frac{1}{2}\cdot i_a^i - \frac{\sqrt{3}}{2}\cdot i_b^i + i_0^i \end{bmatrix} \tag{5.1.1}$$

Considering the fault conditions (2.1.11) and (2.1.17 – 2.1.18):

$$\begin{aligned}
&\underline{I_a^i} = \underline{I_a^i} + \frac{\underline{I_0^i}}{2} = \frac{\underline{E_a^s} + j\cdot\frac{X_a^{nC}}{3}\left(\underline{I_0} - \underline{I_a^k}\right)}{(R_a^s + j\cdot X_a^{sL} + R_a^n + j\cdot X_a^{nL} - j\cdot\frac{X_a^{nC}}{3})} + \frac{\underline{I_0}}{2};\\
&\underline{I_b^i} = -\frac{1}{2}\cdot\underline{I_a^i} + \frac{\sqrt{3}}{2}\cdot\underline{I_b^i} + \frac{\underline{I_0^i}}{2} = -\frac{\underline{E_a^s} + j\cdot\frac{X_a^{nC}}{3}\left(\underline{I_0} - \underline{I_a^k}\right)}{2\times(R_a^s + j\cdot X_a^{sL} + R_a^n + j\cdot X_a^{nL} - j\cdot\frac{X_a^{nC}}{3})} +\\
&+\frac{\sqrt{3}}{2}\cdot\frac{\underline{E_b^s} - j\cdot X_b^{nC}\cdot I_b^k}{(R_b^s + j\cdot X_b^{sL} + R_b^n + j\cdot X_b^{nL} - j\cdot X_b^{nC})} + \frac{\underline{I_0}}{2}\\
&\underline{I_c^i} = -\frac{1}{2}\cdot\underline{I_a^i} + \frac{\sqrt{3}}{2}\cdot\underline{I_b^i} + \frac{\underline{I_0^i}}{2} = -\frac{\underline{E_a^s} + j\cdot\frac{X_a^{nC}}{3}\left(\underline{I_0} - \underline{I_a^k}\right)}{2\cdot(R_a^s + j\cdot X_a^{sL} + R_a^n + j\cdot X_a^{nL} - j\cdot\frac{X_a^{nC}}{3})} +\\
&-\frac{\sqrt{3}}{2}\cdot\frac{\underline{E_b^s} - j\cdot X_b^{nC}\times I_b^k}{(R_b^s + j\cdot X_b^{sL} + R_b^n + j\cdot X_b^{nL} - j\cdot X_b^{nC})} + \frac{\underline{I_0}}{2}
\end{aligned} \tag{5.1.2}$$

The capacitor currents can be found from three phase circuit (Fig.2.1.6):

$$\underline{I_a^C} = \underline{I_a^i} - \underline{I_a^k} - \underline{I^f} = \frac{\underline{E_a^s} + j \cdot \frac{X_a^{nC}}{3}\left(\underline{I_0} - \underline{I_a^k}\right)}{(R_a^s + j \cdot X_a^{sL} + R_a^n + j \cdot X_a^{nL} - j \cdot \frac{X_a^{nC}}{3})} + \frac{\underline{I_0}}{2} - \underline{I_a^k} - \frac{\underline{E_a^s}}{\left(-j \cdot \frac{X_a^{nC}}{3}\right)} - \frac{3}{2}\underline{I_0};$$

$$\underline{I_b^C} = \underline{I_b^i} - \underline{I_b^k} = -\frac{\underline{E_a^s} + j \cdot \frac{X_a^{nC}}{3}\left(\underline{I_0} - \underline{I_a^k}\right)}{2 \cdot (R_a^s + j \cdot X_a^{sL} + R_a^n + j \cdot X_a^{nL} - j \cdot \frac{X_a^{nC}}{3})} +$$

$$+ \frac{\sqrt{3}}{2} \cdot \frac{\underline{E_b^s} - j \cdot X_b^{nC} \cdot I_b^k}{(R_b^s + j \cdot X_b^{sL} + R_b^n + j \cdot X_b^{nL} - j \cdot X_b^{nC})} + \frac{\underline{I_0}}{2} - \underline{I_b^k} \qquad (5.1.3)$$

$$\underline{I_c^C} = \underline{I_c^i} - \underline{I_c^k} = -\frac{\underline{E_a^s} + j \cdot \frac{X_a^{nC}}{3}\left(\underline{I_0} - \underline{I_a^k}\right)}{2 \times (R_a^s + j \cdot X_a^{sL} + R_a^n + j \cdot X_a^{nL} - j \cdot \frac{X_a^{nC}}{3})} +$$

$$- \frac{\sqrt{3}}{2} \cdot \frac{\underline{E_b^s} - j \cdot X_b^{nC} \cdot I_b^k}{(R_b^s + j \cdot X_b^{sL} + R_b^n + j \cdot X_b^{nL} - j \cdot X_b^{nC})} + \frac{\underline{I_0}}{2} - \underline{I_c^k}$$

As it mentioned before, to obtain the transient process the equation system (2.1.1) should be solved analytically using for example operational method. The system should be modified considering the fault conditions (2.1.10, 2.1.11). To solve the system the following assumptions have been used:

- the system parameters are balanced and linear ($C_a^n = C_b^n = C_c^n, L_a^n = L_b^n = L_c^n$

$R_a^n = R_b^n = R_c^n, L_a^s = L_b^s = L_c^s,\ R_a^s = R_b^s = R_c^s$);

- to reduce number of state variables the system idling operation mode is considered;

- voltage sources are balanced and ideal;

Using Mathcad the following Laplace equations can be obtained

$$i_a^i(s) = i^f(s) = \frac{6 \cdot \pi \cdot C^n \cdot f \cdot \hat{E}^s \cdot s}{\left(4 \cdot \pi^2 \cdot f^2 + s^2\right) \cdot \left(3 \cdot C^n \cdot L \cdot s^2 + 3 \cdot C^n \cdot R \cdot s + 1\right)}$$

$$L = \left(L^n + L^s\right) \qquad (5.1.4)$$

$$R = \left(R^n + R^s\right)$$

$$i_b^i(s) = -\frac{\pi \cdot C^n \cdot \hat{E}^s \cdot f \cdot \left(3 \cdot s + 3 \cdot C^n \cdot L \cdot s^3 + 3 \cdot C^n \cdot R \cdot s^3 - 2 \cdot \pi \cdot \sqrt{3} \cdot f\right)}{\left(4 \cdot \pi^2 \cdot f^2 + s^2\right) \cdot \left(3 \cdot C^n \cdot L \cdot s^2 + 3 \cdot C^n \cdot R \cdot s + 1\right) \cdot \left(C^n \cdot L \cdot s^2 + C^n \cdot R \cdot s + 1\right)} -$$

$$- \frac{\pi \cdot C^n \cdot \hat{E}^s \cdot f \cdot \left(6 \cdot \pi \cdot \sqrt{3} \cdot C^n \cdot L \cdot f \cdot s^2 + 6 \cdot \pi \cdot \sqrt{3} \cdot C^n \cdot R \cdot f \cdot s\right)}{\left(4 \cdot \pi^2 \cdot f^2 + s^2\right) \cdot \left(3 \cdot C^n \cdot L \cdot s^2 + 3 \cdot C^n \cdot R \cdot s + 1\right) \cdot \left(C^n \cdot L \cdot s^2 + C^n \cdot R \cdot s + 1\right)} \qquad (5.1.5)$$

$$i_c^i(s) = -\frac{\pi \cdot C^n \cdot \hat{E}^s \cdot f \cdot \left(3 \cdot s + 3 \cdot C^n \cdot L \cdot s^3 + 3 \cdot C^n \cdot R \cdot s^3 - 2 \cdot \pi \cdot \sqrt{3} \cdot f\right)}{\left(4 \cdot \pi^2 \cdot f^2 + s^2\right) \cdot \left(3 \cdot C^n \cdot L \cdot s^2 + 3 \cdot C^n \cdot R \cdot s + 1\right) \cdot \left(C^n \cdot L \cdot s^2 + C^n \cdot R \cdot s + 1\right)} - \\ + \frac{\pi \cdot C^n \cdot \hat{E}^s \cdot f \cdot \left(6 \cdot \pi \cdot \sqrt{3} \cdot C^n \cdot L \cdot f \cdot s^2 + 6 \cdot \pi \cdot \sqrt{3} \cdot C^n \cdot R \cdot f \cdot s\right)}{\left(4 \cdot \pi^2 \cdot f^2 + s^2\right) \cdot \left(3 \cdot C^n \cdot L \cdot s^2 + 3 \cdot C^n \cdot R \cdot s + 1\right) \cdot \left(C^n \cdot L \cdot s^2 + C^n \cdot R \cdot s + 1\right)} \tag{5.1.6}$$

The time diagrams of the Laplace inverse transformation are shown in Figure 2.1.11.

Solving the equation system based on Figure 2.1.6 the following current equations can be obtained:

$$i_a^i(s) = i^f(s) = \frac{2 \cdot s \cdot \left(\hat{I}_0 - 9 \cdot \pi \cdot C^n \cdot f \cdot \hat{E}^s\right)}{3 \cdot \left(4 \cdot \pi^2 \cdot f^2 + s^2\right) \cdot \left(3 \cdot C^n \cdot L \cdot s^2 + 3 \cdot C^n \cdot R \cdot s + 1\right)} \tag{5.1.7}$$

$$i_b^i(s) = -\frac{3 \cdot \left(2 \cdot \sqrt{3} \cdot \pi^2 \cdot L \cdot \hat{E}^s \cdot C^{n2} \cdot f^2 \cdot s^2 + 2 \cdot \sqrt{3} \cdot \pi^2 \cdot R \cdot \hat{E}^s \cdot C^{n2} \cdot f^2 \cdot s - \pi \cdot L \cdot \hat{E}^s \cdot C^{n2} \cdot f \cdot s^3\right)}{\left(4 \cdot \pi^2 \cdot f^2 + s^2\right) \cdot \left(3 \cdot C^n \cdot L \cdot s^2 + 3 \cdot C^n \cdot R \cdot s + 1\right) \cdot \left(C^n \cdot L \cdot s^2 + C^n \cdot R \cdot s + 1\right)} + \\ + \frac{-3 \cdot \pi \cdot C^{n2} \cdot \hat{E}^s \cdot f \cdot s^2 + 2 \cdot \sqrt{3} \cdot \pi^2 \cdot \hat{E}^s \cdot C^n \cdot f^2 - 3 \cdot \pi \cdot \hat{E}^s \cdot C^n \cdot f \cdot s}{\left(4 \cdot \pi^2 \cdot f^2 + s^2\right) \cdot \left(3 \cdot C^n \cdot L \cdot s^2 + 3 \cdot C^n \cdot R \cdot s + 1\right) \cdot \left(C^n \cdot L \cdot s^2 + C^n \cdot R \cdot s + 1\right)} + \\ + \frac{\hat{I}_0 \cdot L \cdot C^n \cdot s^3 + \hat{I}_0 \cdot R \cdot C^n \cdot s^2 + \hat{I}_0 \cdot s}{3 \cdot \left(4 \cdot \pi^2 \cdot f^2 + s^2\right) \cdot \left(3 \cdot C^n \cdot L \cdot s^2 + 3 \cdot C^n \cdot R \cdot s + 1\right) \cdot \left(C^n \cdot L \cdot s^2 + C^n \cdot R \cdot s + 1\right)} \tag{5.1.8}$$

$$i_b^i(s) = -\frac{3 \cdot \left(2 \cdot \sqrt{3} \cdot \pi^2 \cdot L \cdot \hat{E}^s \cdot C^{n^2} \cdot f^2 \cdot s^2 + 2 \cdot \sqrt{3} \cdot \pi^2 \cdot R \cdot \hat{E}^s \cdot C^{n^2} \cdot f^2 \cdot s + \pi \cdot L \cdot \hat{E}^s \cdot C^{n^2} \cdot f \cdot s^3\right)}{\left(4 \cdot \pi^2 \cdot f^2 + s^2\right) \cdot \left(3 \cdot C^n \cdot L \cdot s^2 + 3 \cdot C^n \cdot R \cdot s + 1\right) \cdot \left(C^n \cdot L \cdot s^2 + C^n \cdot R \cdot s + 1\right)} + \\ + \frac{3 \cdot \pi \cdot C^{n^2} \cdot \hat{E}^s \cdot f \cdot s^2 + 2 \cdot \sqrt{3} \cdot \pi^2 \cdot \hat{E}^s \cdot C^n \cdot f^2 + 3 \cdot \pi \cdot \hat{E}^s \cdot C^n \cdot f \cdot s}{\left(4 \cdot \pi^2 \cdot f^2 + s^2\right) \cdot \left(3 \cdot C^n \cdot L \cdot s^2 + 3 \cdot C^n \cdot R \cdot s + 1\right) \cdot \left(C^n \cdot L \cdot s^2 + C^n \cdot R \cdot s + 1\right)} \\ - \frac{\hat{I}_0 \cdot L \cdot C^n \cdot s^3 + \hat{I}_0 \cdot R \cdot C^n \cdot s^2 + \hat{I}_0 \cdot s}{3 \cdot \left(4 \cdot \pi^2 \cdot f^2 + s^2\right) \cdot \left(3 \cdot C^n \cdot L \cdot s^2 + 3 \cdot C^n \cdot R \cdot s + 1\right) \cdot \left(C^n \cdot L \cdot s^2 + C^n \cdot R \cdot s + 1\right)}$$

(5.1.9)

The time diagrams of the Laplace inverse transformation are shown in Figure 2.1.12, 13 (from time 0.55 s).